SINGLE MOLECULE STUDIES ON DNA COMPACTION & GENE REGULATION IN BACTERIA CELLS

LIM CI JI

NATIONAL UNIVERSITY OF SINGAPORE

2014

SINGLE MOLECULE STUDIES ON DNA COMPACTION & GENE REGULATION IN BACTERIA CELLS

LIM CI JI

(B. Sci. (Hons.), NTU)

A THESIS SUBMITTED

FOR THE DEGREE OF DOCTOR OF PHILOSOPHY

NUS GRADUATE SCHOOL FOR INTEGRATIVE SCIENCES AND ENGINEERING

NATIONAL UNIVERSITY OF SINGAPORE

2014

DECLARATION

I hereby declare that the thesis is my original work and it has been written by me in its entirety. I have duly acknowledged all the sources of information which have been used in the thesis.

This thesis has also not been submitted for any degree in any university previously.

Lim Ci Ji

6 April 2014

Acknowledgements

I would like to thank my PhD supervisor, Professor Yan Jie, for the enormous support he provided me throughout my four years of PhD research study. Professor Yan Jie is one of the most down-to-earth professors I have met. He discusses science with his students or colleagues like how friends would do, and I feel this helps to remove the "hierarchy barrier" for a constructive open discussion. I benefited a lot from working with Professor Yan Jie and this has helped built up my belief and confidence in becoming an independent scientist. He is also generous in giving opportunities to help me to excel and develop attributes that are important to becoming an independent scientist. I greatly appreciate all that he has done for me during my PhD study.

I believe to enjoy "playing" science, one would need to work among colleagues that are collaborative, fun-loving and vibrant. Fortunately throughout my PhD study, I had been working with an amazing bunch of colleagues/friends. They provided me numerous joys and laughter and most importantly, support during difficult times in research. The constant support and encourage among us are what make our research more tolerable and enjoyable. For this, I wish to thank several students who I have mentored for their final-year project (FYP) in NUS. Eventually some of them went on to become my colleagues. I would like to thank Sin Yi, Keyi, Wei Juan and Zibo for entrusting their FYP with me as their mentor. They provide great stimuli in doing science and I hope they would go on and do great for their respective

careers. I would like to also thank Hongxia, Chen Hu, Xinghua, Xiaodan, Ryo, Rus, Ricksen, Li You, Yuanyuan, Saranya, Ranjit, Xu Yue, Lin Jie, Wenbo, Carmen, Yanan, Mingxi, Yuan Xin, Wenwen, Huijuan, Shimin, Chen Jin, Taishi, Peiwen, Shuangru, Durgarao, Nirmalya, Anand and Chee San for sharing numerous happy times with me. There are many others I would like to thank and I am sorry if I missed out anyone.

I would like to thank Mr. Teo, Sin Yin, Bee Ling, and Michael for their administrative support during my PhD. They have been very helpful in getting my purchases arrived in time. For this, I also wish to thank Saranya for her enormous help in buying stuff for my research. I also wish to thank NGS for being supportive and providing an excellent PhD program, this includes the excellent administrative support by Ms. Irene Chuan and Ms. Wendy Lee. I wish to thank Professor Linda J. Kenney for her helpful discussion and advice, which strongly shape my scientific career. I also wish to thank Professor Phan Anh Tuan for his helpful advice and guidance during my PhD lab search and my subsequent postdoctoral job hunt. Last but not least, I would like to thank my wife, Xiuhua, my mum and brother for their constant support and understanding. I had a fantastic time doing my PhD, thank you everyone once again.

Table of Contents

Summary

The understanding of how bacteria perform their chromosomal DNA packaging and gene regulation has direct implications to understanding bacterial pathogenesis and this requires immediate attention given the recent emergence of deadly antibiotics resistance bacteria strains. One of the key mediating factors in bacterial chromosomal DNA compaction and gene regulation is the bacterial nucleoid-associated proteins (NAPs). How these bacteria nucleoid-associated proteins mediate their biological functions are not clear and have proven elusive. The answer may be in the NAPs DNA architectural properties, which is the alteration of DNA topology upon DNA-binding. By using highly sensitive single-molecule techniques, we showed that the rigid nucleoprotein filaments formed by NAPs is a conserved DNA-protein structure important for bacterial NAPs gene silencing functions. We further showed that the nucleoid-associated proteins are able to use their distinct DNA-binding mode(s) to regulate DNA supercoiling. These findings provide a mechanistic and novel platform for microbiologists to understand how NAPs may perform their chromosomal DNA organization and gene regulatory functions *in vivo*.

List of Tables

List of Figures

Chapter 1

Background

1.1. Bacterial cell & its organization

The biology cell is classified into two types of cells, eukaryotes and prokaryotes. The prokaryotic cells are single-cell organisms and are the simpler structured cell among the two; for example, the prokaryotic cells are not compartmentalized like the eukaryotic cells. The bacteria are the major domain classified under the prokaryotes kingdom and are of fundamental importance to nature and human. They are small in size, typically a few micrometers in length and have a wide range of shapes, from rods to spheres. Bacteria are highly adaptable to environmental conditions, with some bacteria species found in extreme conditions such as hot springs and radioactive waste. The bacteria cell structure is simple, composing of a cell membrane encasing its cytoplasmic contents (**Fig. 1.1**).

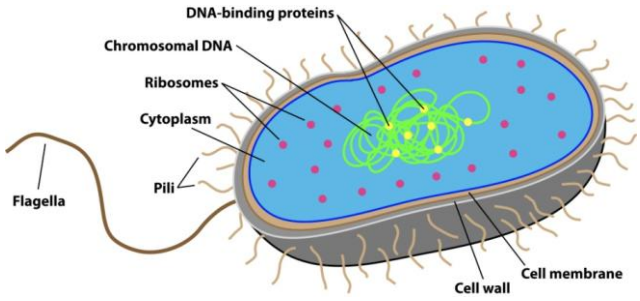

Figure 1.1 The cellular structure of the prokaryotic cell, in this case, is the bacteria cell. It is basically a package of cytoplasmic contents (including the DNA, RNA, ribosomes and proteins) enclosed by a cell membrane and cell wall.

The major cellular components are the water-soluble deoxyribonucleic acid (DNA), proteins and metabolites. An important biomolecule is the bacteria chromosomal DNA. The chromosomal DNA is the principle genetic information carrier of the bacteria and is the template and starting point of the central dogma processes in bacteria.

1.2. The Nucleoid

The bacteria chromosome is typically a single circular DNA, several megabases in length. At its full elongated form, the bacteria chromosome is more than 1 millimeters in length. As the bacteria cell dimension is only about several micrometers in length, the bacteria chromosome has to be highly condensed to fit into the cell. This is not to say that the bacteria is required to condense an extended chromosome into its eventual compacted state but a significant amount of pressure or interactions would be required to keep the chromosome highly compressed inside the cell. The condensed chromosomal DNA is one of the visible large structures observable under a microscope, and it is termed as the nucleoid given its functional similarity to the eukaryotic cell nucleus. Its topology consists of numerous discrete domains that are topologically disconnected from each other (1). An electron microscope image of the *Escherichia coli* (*E. coli*) nucleoid revealed the chromosome has a central core that has DNA loops radiating out from it, akin to a rosette shape (2, 3). These suggest that the nucleoid may be functionally divided into two topological domains, the central core and the peripheral DNA loops. This has been proposed previously, suggesting most of the DNA-related processes may occur at the exterior DNA loops due to the easier access of DNA at peripheral regions (4).

The complicated topology of bacteria nucleoid, coupled with its involvement in numerous fundamental biological processes, suggest the nucleoid topology to be highly dynamic. For example, supercoiling has been extensively linked to regulating transcription processes (5), a well-studied supercoiling-sensitive operon would be the S.enterica and *E.coli* proU operon (6). This is invariantly related to how the nucleoid is organized and mediated by which factors. The compaction of chromosomal DNA is primarily driven through supercoiling of DNA - the *E. coli* chromosomal DNA is negatively supercoiled. The DNA loop domains emanating from the nucleoid core are the result of branched DNA plectonemes formed from DNA supercoiling. Biochemistry studies have shown these DNA plectoneme domains are of ~ 10-15 kb in size and every cell has about 200-400 of them (7). The biochemistry studies derived size of the DNA plectoneme domains is consistent with that obtained from electron microscope imaging analysis.

Supercoiling is heavily regulated by the actions of topoisomerases proteins. An important *E.coli* topoisomerase is the DNA gyrase which introduces negative DNA supercoiling while topoisomerases I relaxes the supercoiled DNA (8, 9). However, DNA supercoiling alone cannot account for the degree of DNA compaction and organization seen in bacteria cell. A class of protein complex, known as the structural maintenance of chromosome (SMC) condensin protein complex, is found to be a key factor in maintaining the bacteria nucleoid structure (10). The *E. coli* analog, MukB, MukF and MukE complex is important for condensing nucleoid as it has been shown that cells lacking this complex exhibited decondensed nucleoid and defective chromosome segregation (11). Henceforth, the SMC protein complex is proposed to be the best candidate responsible for constraining DNA plectoneme formations and also function as a nucleoid scaffold (12, 13).

1.3. Nucleoid-Associated Proteins

Other than DNA supercoiling and SMC protein complex, another class of protein, the nucleoid-associated proteins (NAPs), are also found to be important to nucleoid organization and other nucleoid-related DNA transactions, such as regulation of gene expression (14). NAPs are small, abundant DNA-binding proteins associated with the nucleoid. In E. *coli*, a dozen of NAPs has been identified and they typically bind to DNA in nanomolar concentration range (15). Their population (also copy number) depends on the bacteria growth phase and environmental conditions (16). The major NAPs in *E. coli* are H-NS (Histone-like nucleoid structuring) protein, HU (Heat unstable) protein, IHF (Integration host factor) protein, FIS (Factor for inversion stimulation) protein, DPS (DNA-binding proteins from starved cells) and StpA (Suppressor of td phenotype A). For a more complete list, one may refer to a review article (14). The average number of each major NAP (~12 members) in *E.coli* was measured to be around 18,000 to 200,000 per cell (17). Taking an average NAP copy number of 50,000, 12 major NAPs would result in 600,000 DNA-binding NAPs per cell. Given the *E.coli* chromosome is 4.6 million bp in length and an average NAP binds to 10 bp of DNA, the *E.coli* chromosome would be fully bound with NAPs. It would be expected that DNA occupancy by NAPs would be a dynamical process, heavily competed by NAPs with inter-regulation between them.

NAPs are also known as architectural proteins as they are able to alter DNA topology upon binding to DNA. Depending on the NAP, they are able to bridge DNA, locally bend or stiffen the DNA (14, 18). Here, these alterations of DNA topology are termed as the DNA-binding modes; DNA-bridging, DNA-bending, DNA-condensation, DNA-cross-linking, and DNA-stiffening mode. DNA-bridging and DNA-bending mode are intuitive to understand but DNA-stiffening mode may be mediated by several mediating mechanism. For example, a NAP may form a rigid

protein filament along DNA, resulting in an apparent increase in DNA stiffness. **Figure 1.2** is a cartoon illustration of the various NAPs DNA-binding modes.

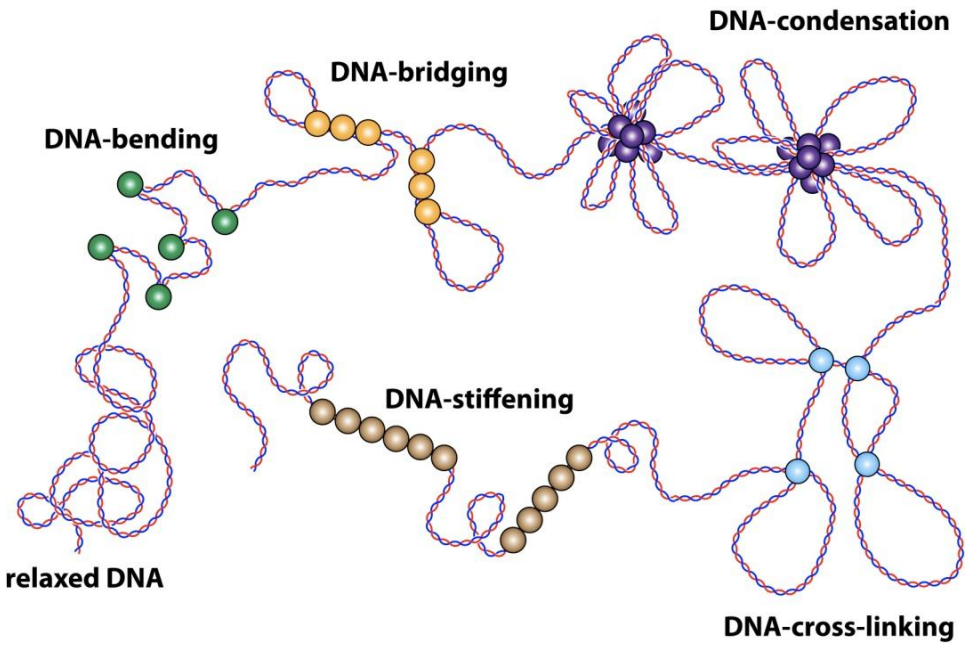

Figure 1.2 The various DNA-binding modes of nucleoid-associated proteins.

NAPs are not restricted to a single DNA-binding mode. Most, if not all NAPs, possess at least two distinct DNA-binding modes which are regulated by numerous environmental factors. In the case of the *E. coli* H-NS, it possesses two distinct DNA-binding modes that are regulated by the presence of magnesium ions - DNA-stiffening mode at low magnesium concentration and DNA-bridging mode at high magnesium concentration (19). Similarly, the *E. coli* HU protein possesses two distinct DNA-binding modes that are regulated by its own concentration – DNA-bending mode at low HU protein concentration and DNA-stiffening mode at high HU protein concentration (20). The *E. coli* IHF protein is basically a DNA-bending protein (21) but exhibits DNA-bridging mode at high IHF protein or magnesium concentration (22). *E. coli* H-NS paralogue, StpA, is also able to stiffen DNA while causing higher-ordered DNA-bridging at high magnesium concentration (23). DPS

and FIS proteins are simpler; current studies suggest they are only able to bridge DNA, causing DNA condensation (24, 25). In general, the plethora of DNA-binding modes exhibited by NAPs provided them the mediating mechanism in performing their respective roles in nucleoid organization and gene expression regulations.

1.3.1. H-NS and H-NS-like proteins in gene silencing

NAPs are heavily involved in controlling gene expression in bacteria at a global scale, mainly serving as a negative regulator (14, 18). This is not surprising given the abundance of NAPs and DNA-binding ability. An important *E. coli* NAP involved in gene silencing is the H-NS protein. In the absence of H-NS, about 5% of *E. coli* genes had a change in gene expression level, of which 80% experienced an increase in gene expression (26). H-NS also plays regulatory roles in gene expression regions that are responsive to environmental condition changes such as temperature and osmolarity (27, 28). H-NS is also responsible in silencing laterally-acquired genes (29). Laterally-acquired genes (or horizontally transferred genes) are genes that are acquired from another organism, and H-NS preferential binding to AT-rich sequences allow them to silence the laterally-acquired genes in *Salmonella* that are often AT-rich (30).

H-NS performs its gene silencing function through binding to DNA but its mediating mechanism is still unclear. It has been demonstrated that H-NS preferentially binds to AT-rich curved DNA sequences and this is important for its gene silencing mechanism (31). However, it has been shown that DNA binding alone is not sufficient for H-NS silencing of the osmolarity sensitive proU expression (32). These results are in conflict with each other in trying to explain how H-NS selects genes for silencing. More recently, it has been proposed that H-NS does indeed binds to specific sequences and then cooperatively extends to form a nucleoprotein (DNA-

protein) complex (33). This model is then able to explain previous findings, as other than specific sequences, H-NS still requires a specific nucleoprotein structure to mediate gene silencing. This is also supported by a previous study that showed a cis-spreading nucleoprotein filament is responsible for H-NS gene silencing (34).

To understand the structure of H-NS nucleoprotein complex, one needs to first know the structure of H-NS protein. It is well accepted that the H-NS structure can be broken down into 3 parts; N-terminus domain (NTD), C-terminus domain (CTD), and a flexible unstructured linker in between. The H-NS NTD is largely responsible for protein-protein interactions – dimerization and also important for its gene silencing functions (35-37). For the H-NS CTD, it is responsible for its DNA-binding ability (38). A full H-NS nucleoprotein structure is not obtained due to the flexible linker region. However, an interpolated model prediction has proposed H-NS forms a helical scaffold with DNA (39), although this model has not be experimentally verified as of now.

Despite the lack of a full structure, single-molecule and biochemistry studies have revealed more clues to how H-NS may mediate gene silencing. This can be broadly classified by H-NS two distinct DNA-binding modes – DNA-bridging and DNA-stiffening. Using atomic force microscopy imaging, H-NS was first shown to mediate DNA compaction through DNA bridging (40). Another study using single-DNA stretching, instead showed H-NS caused an increase in DNA-stiffening rather than DNA compaction (41). This study further shows the DNA-stiffening mode of H-NS is sensitive to temperature and osmolarity, environmental conditions that regulates H-NS gene regulatory functions. This conflict in observations was reconciled in a study (19), where it was shown that H-NS actually possesses two distinct DNA-binding modes regulated by magnesium ions - DNA-stiffening mode at low magnesium conditions and DNA-bridging mode at high magnesium.

H-NS DNA-stiffening can be described as a structural consequent of the cooperative nature of H-NS DNA-binding, where presumably, H-NS polymerizes along DNA to form a rigid protein scaffold or filament. This idea is based on the extensive nature of DNA protection by H-NS in DNA-stiffening mode (41), H-NS DNA-binding cooperativity (33) and images of H-NS rigid nucleoprotein filament islands formed discretely along a large piece of DNA (19). Due to the higher bending rigidity of H-NS nucleoprotein filament, single-DNA stretching experiments are able to detect H-NS nucleoprotein filament formation through an apparent increase in DNA bending rigidity upon H-NS polymerization. However, the dynamics of H-NS nucleoprotein filament assembly or disassembly on DNA are still not known and have proved elusive due to the complexicity of H-NS DNA-binding properties and small molecular size.

Both DNA-binding modes provide a platform to understand how H-NS mediates gene silencing. H-NS was proposed to trap *E. coli* RNA polymerase (RNAP) in a DNA loop formed by H-NS DNA bridging near the promoter region, thus causing *E. coli* RNAP to stall at open complex stage (42). This model is further refined by including the polymerization of H-NS along two distal patches of H-NS-binding specific sequences, before H-NS mediate bridging between these two sites (43). The cause of H-NS DNA-stiffening is due to H-NS polymerizing along DNA, forming a rigid nucleoprotein filament complex. This is most evidently shown by atomic force microscopy imaging (19). The extensive nature of H-NS rigid nucleoprotein filament provides a tantalizing prospect of alternative gene silencing models - the filament occlusion of *E. coli* RNAP binding to promoter sites or blockage of RNAP from elongation (19). In addition, the study (19) that showed H-NS nucleoprotein filament stability is sensitive to temperature and osmolarity and not H-NS DNA-bridging mode lent weight to the filament-based model as a primary mechanism in H-NS gene silencing. The H-NS filament gene silencing model is

further supported by another study that showed H-NS silencing can only be relieved by anti-silencing protein SsrB when H-NS is in nucleoprotein filament mode (44).

H-NS structure and function are highly conserved across bacteria species. By definition, proteins that are of similar sequence, structure or gene silencing function with *E. coli* H-NS are referred to as H-NS-like proteins (27, 45). To date, there are more than 50 H-NS-like proteins are identified, mainly through their sequence similarity or gene silencing functions (27). The *E. coli* H-NS paralogue, StpA, shares 58 % amino acid sequence similarity with H-NS (46), shares similar gene silencing functions with H-NS and also constrains DNA supercoiling like H-NS (47). In addition to their similarities, H-NS and StpA also shares an intricate relationship. Both H-NS and StpA are able to suppress the expression of each other genes (48), and StpA is able to complement H-NS functions *in vivo* (49, 50).

In terms of DNA organization, StpA is shown to be able to mediate DNA bridging (51), similar to H-NS (19, 40). Interestingly, the *Pseudomonas Aeruginosa* gene silencing H-NS-like protein, MvaT protein (52), is also able to mediate DNA bridging (51). This led to a proposal that DNA-bridging is a shared property conserved in H-NS-like family proteins and is important to their gene silencing functions. This idea is supported by another study that showed the gram-positive Mycobacterium bacteria H-NS-like protein, Lsr2, a gene silencer (53), is also able to mediate DNA bridging (54). Since DNA-bridging is highly conserved in H-NS-like proteins, the newly discovered rigid nucleoprotein filament formation by *E. coli* H-NS (19), which provides an alternative platform for H-NS to silence genes, may be also a conserved transcription repressing structure.

1.3.2. Nucleoid-associated proteins in chromosomal DNA organization

In addition to their gene regulation function, NAPs is heavily involved in bacteria chromosomal DNA packaging (55). This is not surprising given NAPs possess a plethora of different DNA-binding modes which can organize the bacterial chromosomal DNA into a dynamic super-structure. Indeed, this is most evidence by a series of experiments that showed a strong correlation between the nucleoid structure and NAPs.

Electron microscopy imaging has shown that HU can compact circular DNA into nucleosome-like nucleoprotein structures (56). The over-expression of an *E. coli* HU with a variant HU_{α} had resulted in a more compacted nucleoid (57). In addition, HU preferentially bind to negative supercoiled DNA (58) and is able to constrain negative supercoiling *in vitro* (56). Given the importance of DNA supercoiling state to nucleoid organization, it is therefore clear that HU play a role in organizing the nucleoid structure. However, which HU DNA-binding mode – DNA-bending or stiffening – is responsible for the perceived effect on nucleoid is still unclear. IHF, the specific sequence homologue of HU, is able to compact DNA through its DNA-bending capability (21, 22, 59). AFM imaging showed deletion of IHF resulted in an increase in "thin nucleoprotein fibers", which is postulated to be the fundamental nucleoid structure modulated by NAPs (60). The effect of IHF on nucleoid organization might not be as crucial as HU given the IHF copy number *in vivo* is 5 times lesser than HU (15). In IHF case, unlike HU's, its mediating DNA compaction mechanism is straight forward since it was shown to exhibit predominate DNA-bending properties (22) and DNA condensation at high magnesium conditions (22)

H-NS DNA-bridging properties provide a more convincing proposal in terms of DNA compaction. Over-expression of H-NS in *E. coli* has resulted in heavily

condensed nucleoid (61) and led to induction of artificial stationary phase (62). H-NS is also intertwined with the bacterial chromosomal DNA supercoiling state. H-NS deletion has led to a change in plasmid and chromosomal DNA supercoiling level – an increase in negative supercoiling (63). This is consistent with a previous study that showed H-NS can constrain plasmid DNA supercoiling *in vitro* (64). In addition, H-NS has been proposed to be a domainin, a protein that can segregate chromosomal DNA into topologically isolated supercoiled domains (65). All of these H-NS findings can be explained by the H-NS DNA-bridging capability, first revealed in an AFM imaging study (40). However, the emergence of the H-NS alternative DNA-binding mode; DNA-stiffening mode, prompts a question on which DNA-binding mode H-NS use to perform its chromosomal DNA organization function and how it regulate *in vivo* DNA supercoiling level.

The other major NAP involved in bacterial chromosomal DNA organization is the DPS protein. Its copy number follows the growth phase of the bacteria, reaching maximum copies at stationary phase (16). From crystal X-ray structural studies, DPS is able to form a dodecameric protein complex that is able to condense and protect DNA from digestion (66). This is confirmed by an AFM imaging study that revealed DPS can condense plasmid DNA *in vitro* and the DPS-DNA interaction can be regulated by environmental pH and magnesium changes (24). In terms of how DPS impact nucleoid structure, AFM imaging of lysed nucleoid after DPS deletion suggests DPS is required to form a compacted nucleoid (67). Henceforth, DPS is important in nucleoid structuring. Considering the importance of DNA supercoiling in nucleoid organization, how DPS affects DNA supercoiling is not well-understood and requires further address.

In summary, bacteria NAPs are heavily involved in nucleoid organization. It is reasonable to speculate that the nucleoid organization state is dependent on the population of individual NAP which in turn, is known to be dependent on cellular

growth phase (16). Sequentially, the NAPs distinctive DNA-binding modes are expected to provide them the mediating mechanism to perform their nucleoid structuring role.

1.4. Single-molecule perspective

Before the intervention of single-molecule measurements, we have been looking at biological processes at a bulk level. Bulk measurements provide an average and often static observation of individual molecules and neglect numerous other details available at a single-molecule level. For an ideal situation for bulk measurements, the molecular population of the sample should be homogeneous so that the measurement corresponds to a single species of sample. In addition, the initiated bulk reaction should be ideally synchronized such that the result represents a coherent picture of dynamics instead of being derived from numerous overlaps of non-synchronized reactions.

However, in most situations, most samples do not offer a homogeneous population or well-synchronized reactions or both. In this case, single-molecule measurements would provide a way to decouple the collective signals and elucidate individual information from each molecule/reaction, regardless of the samples' homogeneity and reaction synchronization. As such, single-molecule can provide the distribution of species in a heterogeneous sample, and it can measure a single-molecule reaction in a poorly-synchronized sample pool. Despite the numerous advantages of single-molecule in peering into individual molecule reaction, it is not as direct as bulk experiments in harnessing collective information, it is also often technically challenging to perform long time-scale experiments as compared to most bulk experiments and it also provides much technical difficulties in probing into *in vivo* samples than bulk experimental techniques.

Nonetheless, looking at one molecule at a time provides a new and exciting perspective that can yield many important details that are often obscured in bulk measurements. For example, if a bio-molecule property is rapidly changing with time, single-molecule measurements can provide time-trajectory data (kinetics) which reveals the bio-molecule individual states it went through and its corresponding kinetics. One classic example is the case of the kinesin motor protein. Prior to single-molecule measurements, kinesin is thought to move along the microtubule tracks in a constant velocity manner (68). With the use of single-molecule measurement technique – optical trapping, it was revealed that kinesin moves along microtubule in 8 nm step-size (69, 70). Subsequently, the energy requirement for each step of kinesin and its force generation are elucidated (71-73). Henceforth, introduction of single-molecule techniques opens up a new field in kinesin molecular mechanism and provides the long elusive model in how kinesin moves along the microtubule.

Another example on the impact of single-molecule studies on a particular research field is the RNA polymerase (RNAP). The RNA polymerase is a multi-subunits protein complex responsible in transcribing DNA to mRNA; the first step in protein expression. Structural studies (X-ray) provide important atomic-resolution structural details on how RNAP performs its transcription function, akin to providing 'frozen' images of RNAP at work. However, the kinetics linking these 'frozen' images describing how the RNAP-DNA complex evolves structurally remains elusive, until the intervention of single-molecule techniques. A myriad of single-molecule studies have been done to elucidate the kinetics between various transcription stages and these provide a platform to study how transcription is regulated at every stage. Perhaps, the most beneficial area is the RNAP elongation kinetics. It has been shown that RNAP has been shown to either exhibit a bimodal or homogeneous elongation velocity distribution (74, 75). Often the transcription runs are punctuated with pauses of various lengths, which is sequence dependent (74). Most recently, a single-

molecule study has elucidated the mechanical torque limit the RNAP can withstand during transcription elongation, which provides us insights to how much DNA supercoiling is needed to stop transcription (76).

In summary, the application of single-molecule techniques to old problems has opened up many new undiscovered phenomena. Single-molecule techniques have also allowed us to study bio-molecules reaction kinetics and thermodynamics pathway which were previously impossible using traditional bulk measurement methods. Single-molecule techniques may be classified into two broad categories – single-molecule manipulation and single-molecule imaging. The next two subsections describe the various types of single-molecule manipulation and imaging techniques.

1.4.1. Single-molecule manipulation techniques

The term manipulation means the capabilities of moving a single molecule, applying force to the molecule, and measuring the deformation of the molecule at high spatial and temporal resolution. It is a generic method to study molecular structure, stability, and interaction. Recently it has been often used to study how force regulates mechano-sensitive bio-molecules. Force is terribly overlooked among the several parameters (i.e. temperature, salt, etc.) that govern bio-molecules reactions. Force plays an important role in numerous biological processes that typically involves motion at various scales such as DNA replication, DNA segregation, cell adhesion and motion. In terms of molecular interactions, the folding of proteins typically uses salt bridges and formation of bonds to compete against thermal fluctuations to maintain a certain functional protein structure. Most proteins bind to specific ligand through surface-bonds recognition, which are docked by transient chemical bonds (i.e. salt bridges, Van Der Waals) and covalent bonds (disulphide-bridges).

The force range in biological systems typically ranges from pico-Newton to nano-Newton. The force required to melt a double-stranded DNA or RNA hairpin structure, which is mainly stabilized by hydrogen bonds, is measured to be 5-15 pN depending on hairpin length, sequence and temperature (77). For covalent bond, the disruption force required is measured to be 1-2 nN (78). Force manipulation of bio-molecules often requires highly-sensitive detection scheme which can measure length ranging from angstrom (Å, 10^{-10}) to millimeters (10^{-3}). The elongation of RNA polymerase along the DNA template read one base pair (3.4 Å) at a time (79) while kinesin moves with 8 nm step-size (69). Henceforth, single-molecule manipulation techniques allow one to manipulate force in the orders of pN and measure length change in the orders of nm.

The most widely-used single-molecule manipulation techniques are the optical tweezers, magnetic tweezers and atomic force microscopy (AFM) (**Fig. 1.3**). All three of these techniques offer force application to a single bio-molecule with high spatial and time resolution. The force application may be classified into two categories –force clamp and force ramp. Force clamp application is self-explanatory – constant force load on a bio-molecule. Force ramp refers to a controlled rate in increasing the force load on a bio-molecule with time. The intrinsic nature of the magnetic tweezers allows one to perform constant force studies (80). The optical tweezers (81) and AFM (82) are more suitable to perform force ramp studies although high-speed feedback systems have been incorporated to enable optical tweezers (70, 83) and AFM (84, 85) to perform constant average force studies with some feedback noise.

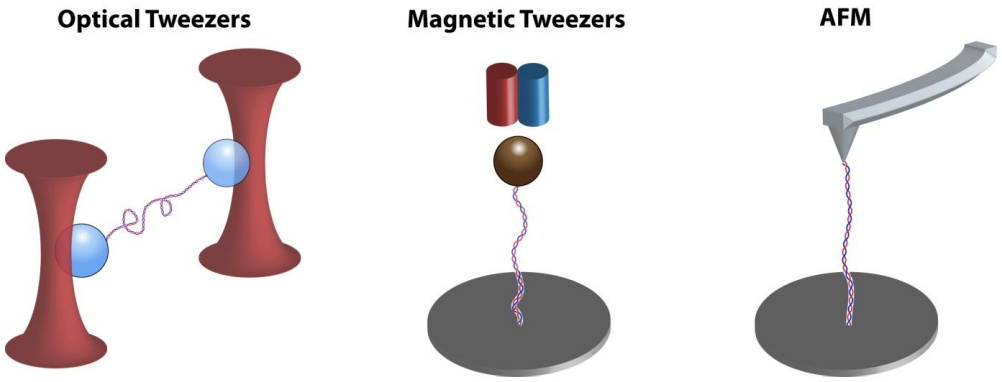

Figure 1.3 Various single-molecule manipulation techniques depicting stretching of a single DNA molecule.

The application of force clamp allows one to extract useful biochemical information from bio-molecules reaction. For example, by plotting the measured extension of a single double-stranded DNA (dsDNA) at various constant force (Force-extension plot), we can extract the intrinsic elastic property of the dsDNA (dsDNA bending rigidity) by fitting the data with a well-established polymer model – Worm-like chain (WLC) model (81, 86) (**Fig. 1.4**). The WLC model is further extended to allow one to study the effects of DNA-distorting proteins through force-extension curve measurement (19, 87), since protein binding must modify the DNA polymer elasticity. This makes single-DNA stretching a novel generic method to detect protein binding. Another example is using an optical tweezers force clamp to study the kinetics of RNA or DNA hairpin folding and unfolding, which revealed the folding/unfolding energy landscape and intermediate structures (88, 89). This method versatility is demonstrated by its application to protein folding/unfolding studies (90, 91). The force clamp method has also been used to study motor protein translocating activities such as the bacterial RNA polymerase (74, 92, 93), eukaryotic RNA polymerase II (94, 95) and virus helicase (96-98).

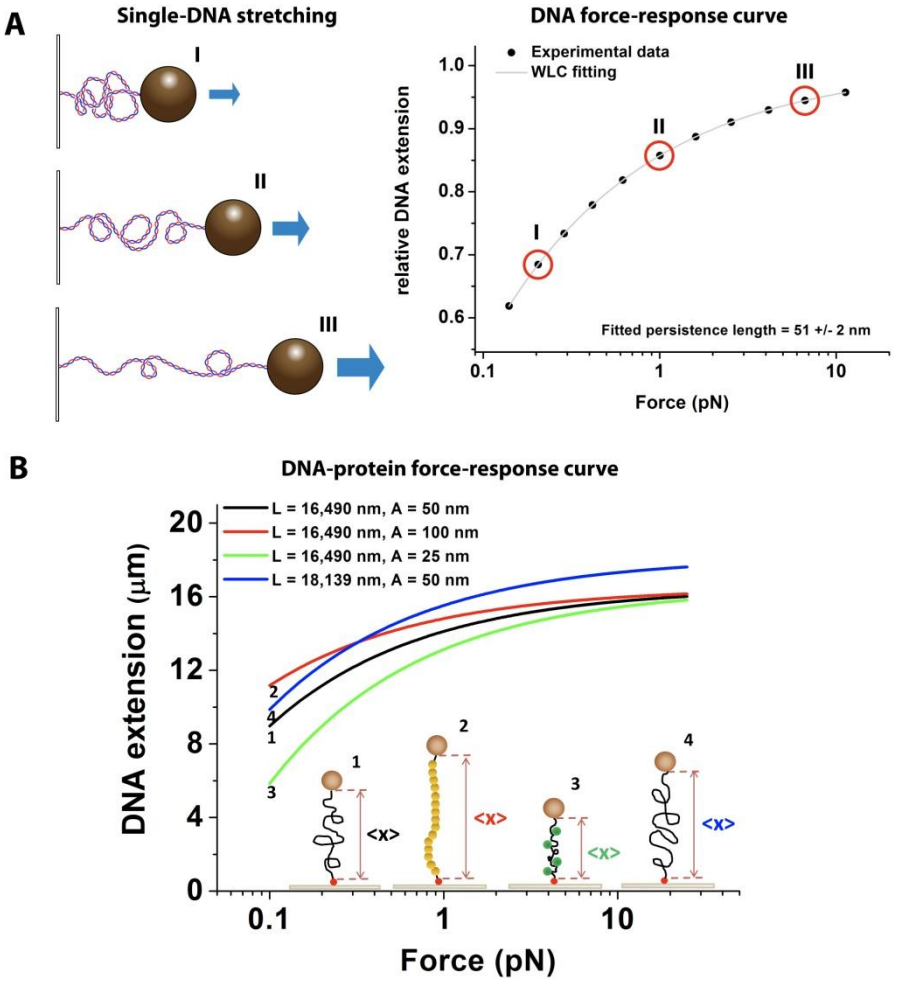

Figure 1.4 Single-DNA stretching experiments. (A) Cartoon schematic showing the change in DNA extension as the DNA stretching force changes. A typical force-extension curve is shown at the right panel. The relative DNA extension (defined as DNA extension divided by its contour length) as a response to imposed DNA stretching force. The circular black symbols represent the experimental data which are fitted with the WLC model (solid grey line). (B) The DNA force-extension curve can be used to detect a change in DNA's physical property, such as the DNA bending rigidity, A, (otherwise known as persistence length) and its contour length, L. DNA-distorting proteins that changes will hence be detected through a change in the behaviour of the DNA force-extension curves. For example, DNA-stiffening proteins would cause an apparent increase in DNA bending rigidity (red curve, no. 2 inset cartoon) while DNA-bending proteins would cause an apparent decrease (green curve, no. 3 inset cartoon).

Other than stretching a single DNA (X, Y, Z manipulations), the DNA may be twisted (θ manipulation) to control the DNA twists (referred to as linking number), and hence DNA supercoiling (99, 100). As mentioned, DNA supercoiling is an important factor in numerous DNA transactions, and thus studying DNA supercoiling

at a single-molecule level provides valuable kinetic information and processes. The magnetic tweezers is a natural candidate to perform single DNA supercoiling studies since a torque is imposed on the paramagnetic bead by the dipole-magnetic field interactions (**Fig. 1.5**). By rotating the magnet, the paramagnetic bead will rotate accordingly, and with a torsion-constrained DNA tether, twist may be introduced or removed readily.

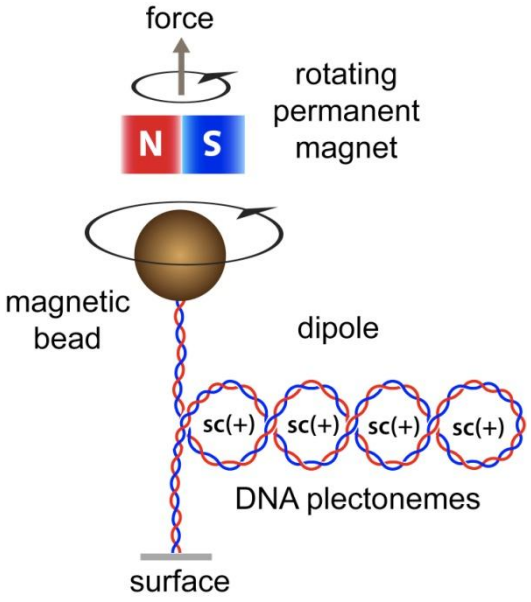

Figure 1.5 Magnetic tweezers to stretch and twist torsion-constrain DNA tether. The permanent magnet's magnetic field causes a magnetic dipole to form in the paramagnetic bead. Rotation of the permanent magnet would then cause the paramagnetic bead to rotate in the same orientation. In this case, twisting the DNA tether in an anti-clockwise orientation would cause formation of positive DNA supercoiling (plectoneme formations).

In summary, single-molecule manipulation techniques provide a new perspective in understanding old and new biological problems. By tuning the imposed force on a single bio-molecule, it allows one to elucidate many biochemical and physical chemical properties that are previously unattainable using traditional bulk measurements.

1.4.2. Single-molecule imaging

The previous section describes using force to manipulate single bio-molecules. This is akin to "touch and feel" experiments. In this section, we describe the "see" type of single-molecule techniques. The potential of visualizing single-molecule localization is huge. For example, it can tell you where a specific bio-molecule is localized in a cell, how many of them are located at a particular region and its conformation and structure. Single-molecule imaging may be broadly classified into two categories – non-fluorescence and fluorescence imaging.

The most common adopted non-fluorescence single-molecule imaging technique is based on atomic force microscopy (AFM). AFM imaging provides user with topological information of the bio-molecules that are adhered on a flat surface (**Fig. 1.6**). AFM imaging provides spatial resolution up to sub-nanometer and has been used to image single bio-molecules such as the dsDNA molecule (101, 102). As the dsDNA conformation and the number of proteins bound on the dsDNA can be easily visualized, AFM imaging has been used to study DNA-protein interaction. For example, AFM imaging showed *E. coli* H-NS mediate DNA compaction through DNA-bridging (40) while *E. coli* IHF compacts DNA through DNA-bending (103). Critically, AFM imaging only provides 'frozen' images of single bio-molecules on a surface and does not provide kinetics information. However, recently, high-speed AFM imaging of single bio-molecules has been achieved using AFM incorporated with a high-speed scanner (104). Using this technique, single myosin walking on actin (105) and ATPase catalysis reaction (106) have been visualized.

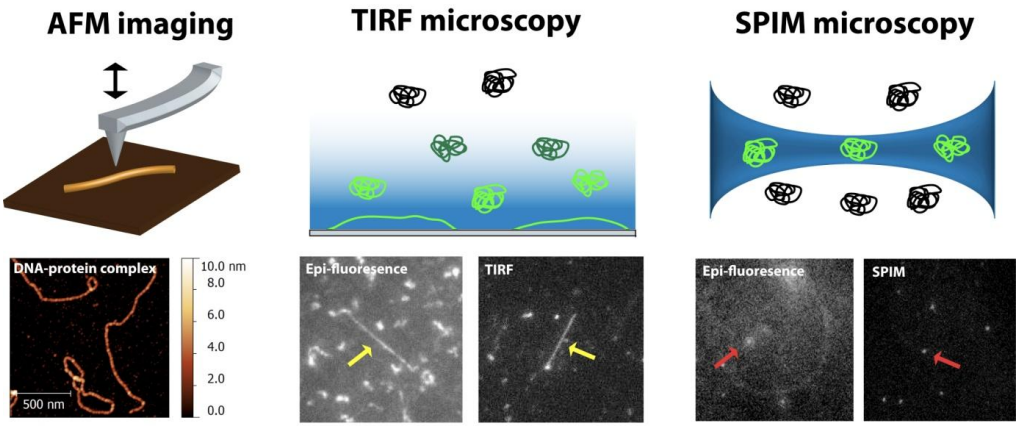

Figure 1.6 Single-molecule imaging using Atomic force microscopy (AFM) or fluorescent optical sectioning microscopes. AFM imaging allows one to image single biomolecule conformation on a flat surface through topography measurements. Image of a DNA-protein complex is shown below the AFM schematic. Optical sectioning fluorescence microscopes allow one to reduce background/out of focus fluorophores contribution and imaging single fluorophore. TIRF microscopy excites only a thin layer (100-150 nm thickness) near the surface thus reducing background contribution. Images of a stretched YOYO-1 stained λ-DNA (yellow arrows) in TIRF showed higher signal-to-noise ratio than epi-fluorescence microscopy (wide-field). SPIM microscopy utilizes a single-sheet light plane (1 μm thick at thinnest segment) to excite solution fluorophores. Images of relaxed YOYO-1 stained λ-DNA (condensed spots, red arrows) showed higher signal-to-noise ratio than epi-fluorescence microscopy.

Fluorescence singe-molecule imaging uses specific fluorescence labeling, to detect and localize the bio-molecules of interest. To obtain imaging of single fluorophores, the density of the fluorophores has to be in the order of pico- to nanomolar (107). Optical sectioning microscopy such as the total internal reflection fluorescence (TIRF) and single-plane illumination (SPIM, also known as light sheet) microscopes provide alternative methods to image single fluorophores by minimizing the fluorescence excitation volume (**Fig. 1.6**). Optical sectioning helps reduces the background contribution of non-focal plane fluorophores to improve the signal-noise ratio (SNR).

Upon the rapid development of single-molecule fluorescence microscopy, they have been used to tackle various biological problems. Confocal microscopy has been used to analyze nucleotide excision repair complexes at a single-molecule level

(108). It has also been widely used to track single fluorescence-labeled protein mobility in live cells (109, 110) and determine protein-protein networks (111, 112). TIRF microscopy is used to observe and study DNA replication machinery working on a flow-stretched single-DNA molecule near the glass surface (113, 114). It is also been used to study single kinesin processivity and its dependent on ATP (115). Single-molecule colocalization technique using multi-color fluorescence TIRF microscopy has been used to study the bacterial RNA polymerase interaction with transcription factors during transcription (116, 117) and also provided insights to spliceosome mechanism (118, 119). As described above, single-molecule imaging applications have provided many insights to biological problems and have proved to be a powerful tool in tackling biological questions.

1.5. Research motivations & hypotheses

The bacterial NAPs play numerous important roles in biological processes; mainly chromosomal DNA packaging and gene regulations. The unique property of the NAPs is that most of them possess one or more distinct DNA-binding mode(s). Since the NAPs must bind to chromosomal DNA to mediate their cellular functions, they must use their distinctive DNA-binding mode(s) to perform their functions. This raises a question on how each distinct NAP DNA-binding mode is used to mediate the biological functions. Single-molecule manipulation and imaging experiments, coupled with systematic functional mutations of NAP, provide the best and clearest approach to study the effect of NAP DNA-binding mode on chromosomal DNA packaging and gene transcription.

1.5.1. Is nucleoprotein filament a conserved structure of H-NS-like family proteins

The formations of rigid protein filament on DNA were observed in two major *E.coli* NAP, H-NS (19) and HU (20), both are involved in global gene regulation in bacteria (20, 120, 121). Intuitively, the formation of a protein filament on DNA suggests it may serves as a physical barrier to block promoter site access from RNA polymerase or even impede RNA polymerase elongation. This can explain how bacteria uses NAPs to silence genes expression. If this is true, nucleoprotein filament formation should be universal or conserved across H-NS-like family proteins (or global gene silencing) proteins. It is also expected that NAPs that are involved in chromosomal DNA protection may also have the capability to form the protective nucleoprotein filaments; one such possible NAP is the *E. coli* Dan protein which is highly-expressed during anaerobic stress (122). The *E. coli* StpA will be an important NAP to investigate if it forms rigid filament on DNA due to its paralogous relationship with H-NS (123) and its gene silencing functions (124, 125). Similar study can be done in parallel on other gene silencing NAPs such as the H-NS-like *Pseudomonas Aeruginosa* MvaT (52) and *Mycobacterium Tuberculosis* Lsr2 (126).

1.5.2. Elucidating H-NS gene silencing mechanism

To understand how H-NS mediate its gene silencing functions, the missing link between H-NS gene silencing *in vivo* studies and its DNA-binding modes has to be elucidated. Foremost, it is important to investigate whether which H-NS DNA-binding mode (nucleoprotein filament or DNA-bridging) is used for gene silencing or both DNA-binding modes are involved. To address this question, we seek to identify which H-NS DNA-binding mode is affected in gene silencing defective H-NS

mutants. This will allow us to connect the defective gene silencing observations *in vivo* to *in vitro* H-NS DNA-binding mode(s).

1.5.3. Effects of distinctive NAPs DNA-binding modes on DNA supercoiling

The bacterial NAPs play a major role in chromosomal DNA organization. It is believed that they perform their roles by directly condensing linear DNA through either bending DNA or bridging DNA (55). However, how NAPs influence DNA supercoiling, which is another DNA organization factor, is not studied, presumably due to the assumption that NAPs and supercoiling independently regulate chromosomal DNA organization. Supported by evidences that NAPs can affect DNA supercoiling levels (63, 127, 128), the effect of distinctive NAP DNA-binding mode on DNA supercoiling should be investigated. The effects of NAPs on DNA supercoiling are likely non-trivial, and may prove to be fundamental to how NAPs organizes chromosomal DNA and performs gene regulatory functions.

Chapter 2

Rigid nucleoprotein filament is a conserved structure formed by H-NS-like family proteins

2.1. Introduction

The H-NS-like family proteins are classified as bacterial NAPs involved in gene silencing (27, 52). In *E.coli*, H-NS has a paralogue known as StpA. StpA has a 58% similarity in amino acid sequence to H-NS (123). Due to this similarity, it was initially believed to be a multi-copy gene silencer that serves as H-NS backup in H-NS deficient or depleted cells (129). Both StpA and H-NS exhibit negative autoregulation and is also able to suppress the promoter of each other thus demonstrating certain symmetry between them (124, 125). Interestingly, expression of StpA is enhanced by higher temperature and osmolarity during cell growth which means H-NS gene silencing could be compromised at such growth conditions (130). Other than their common ability in gene silencing, they also both share preferences in binding curved DNA (49). Despite the similarity, StpA and H-NS do have distinct functions. Compared to H-NS, StpA has a higher affinity to DNA which suggests that their heterogeneous gene regulation profiles are likely mediated by direct DNA binding (49).

Based on H-NS and StpA paralogous relationship, it will be interesting to determine StpA DNA-binding mechanism and compare it to H-NS. StpA was previously reported to bridge DNA like H-NS (51). However, H-NS is able to form

rigid protein filament along DNA in low divalent ions solution conditions (19, 41). Intuitively, rigid protein filaments formed on DNA can serve as a physical blockage of DNA from RNA polymerase for gene transcription. If this is true, H-NS-like family of proteins should show similar capability in forming rigid protein filaments on DNA to cause gene silencing. As such, it will be interesting to study H-NS-like proteins DNA-binding mechanism and determine if they have a common property in forming protein filaments along DNA. Hence, StpA is an important protein to study given its paralogous relationship with H-NS and also its ability to silence genes in *E.coli*.

H-NS-like family of proteins was previously identified only in gram-negative bacteria proteins. Recently, a NAP from the gram-positive mycobacteria tuberculosis named Lsr2, was found to be H-NS-like (54). Lsr2 was shown to bridge DNA like H-NS and also able to complement H-NS in H-NS deficient *E.coli cells*. In addition, Lsr2 was able to silence genes and also preferentially binds to AT-rich DNA sequences similar to H-NS (43, 53, 131). All of these suggest Lsr2 is a functional paralogue of H-NS although sequence similarity is low. Similar to H-NS *E.coli* paralogue StpA, Lsr2 was shown to bridge DNA using atomic force microscope (AFM) imaging (54, 132). However these information presented might be incomplete as the high concentration of divalent ions involved in their AFM imaging can conceal for example, the formation of rigid filament on DNA which is only dominant at low divalent ions buffer conditions as seen in H-NS (19). Since Lsr2 shares numerous similarities to H-NS and is also the first identified H-NS-like protein in gram-positive bacteria, it will thus be interesting to determine if Lsr2 is able to form a rigid protein filament on DNA like H-NS. This will add further prove that gene silencing in bacteria is facilitated by NAPs forming a physical coating on DNA promoter sites thus blocking DNA accessibility.

To further prove the importance of protein filament formation on DNA caused by gene silencing NAPs, it will be important to show the universality of this trait, i.e. across bacteria families (gram-positive and gram-negative bacteria) or NAPs expressed only in stressful conditions. In the case of anoxia stress response in *E. coli*, a novel NAP named Dan is highly expressed and was shown to be able to mediate DNA bridging like H-NS (122). Due to its novelty, Dan gene silencing capability in anoxia condition is poorly understood and further biochemistry characterization needs to be done. Dan is shown to be involved in metabolic pathway regulation, mainly acting as a transcription factor (133). This suggests that Dan may be involved in gene silencing activities and especially so during anoxia conditions. This warrants a detailed study on Dan and determines if it has the ability to form a protein filament on DNA like H-NS. In this chapter, we will use single-molecule manipulation (Magnetic tweezers) and imaging (AFM) techniques to study H-NS *E. coli* paralogue StpA DNA organization properties and their response to environmental factors that are known to affect StpA *in vivo* gene silencing functions.

2.2. Materials & Methods

StpA over-expression and purification

The *stpa* gene was inserted into the pET-14b expression vector to induce over-expression of N-terminal 6XHis-tagged StpA. The expression construct was transformed into the BL21 (DE3) *E. coli* expression strain using standard heat-shock method. Successful transformed cells were selected on ampicillin agar-plate and used to initiate a 8 Litres growth culture using LB media containing ampicillin. The culture was grown at 37 °C to OD600 0.6-0.7 before IPTG was added to induce over-expression of StpA. The cells were collected via centrifugation and lysed using sonication. Dnase I (RQ1 Dnase, Promega, U.S.A.) was then added into the cell

lysate and allowed to incubate on ice for three hours to digest the chromosomal DNA to reduce the lysate viscosity. The lysate was then centrifuged to sediment the debris while the supernatant was collected. The supernatant was then adjusted to a final concentration of 1 M NaCl and 20 mM immidazole.

Gravity-assisted immobilized metal affinity flow column Nickel-charged resin (Ni-NTA Agarose, Qiagen, Singapore) was used to purify the 6XHis-tagged StpA from the lysate supernatant. The lysate supernatant was added into a gravity-flow column with bedded nickel-charged resin and washed with 10 ml of washing buffer (20 mM immidazole in a 50 mM phosphate, 500 mM NaCl buffer) and followed by 1 ml of pre-elution buffer (100 mM immidazole) to remove any unbound non-specific proteins. The 6XHis-tagged StpA protein was then eluted with 2.5 ml of elution buffer (containing 250 mM immidazole) in volumes of 500 µl. The eluted protein was run with SDS-PAGE to determine the purity and molecular weight of the protein for verification purpose. The 6XHis-tagged StpA protein concentration was measured with Nanodrop ND1000 (Wilmington, U.S.A.) using known StpA absorbance extinction coefficient. Mass spectroscopy was done to further verify the protein identity. Glycerol was added to the protein to 50% v/v for cryo-protection before storing in -20 °C. StpA isoelectric point was calculated using the pI/MW tool from the Expasy website.

AFM imaging method and analysis

Two different length of DNA were used in the AFM imaging: a 5,386 bp linearized φX174 dsDNA (New England Biolabs) and a 576 bp dsDNA obtained through PCR method (134). Long DNA such as the λ-DNA (16.490 µm) is not preferred in AFM imaging due to its length, which typically exceeds the scanning area size of the AFM experiments (up to 4 µm) that is required to achieve high-quality images. Glutaraldehyde-coated mica surface was used for the AFM imaging experiments as

this surface allows DNA-protein complexes to be deposited on the surface in any buffer condition and have shown to preserve the conformation of DNA-protein complexes such as nucleosome arrays and other bacterial DNA-protein complexes (19, 103, 135, 136). To prepare the glutaraldehyde-coated mica, 0.1 % APTES solution was added onto a 0.5 cm x 0.5 cm piece of freshly-peeled mica and allowed to incubate for 15 minutes at room temperature. The APTES-modified mica was then rinsed with deionised water to remove unbound APTES before it was dried with nitrogen gas and incubated in a desiccator for at least two hours to allow APTES cross-linking to take place. After this, 1 % glutaraldehyde solution was deposited onto the APTES-modified mica and allowed to incubate for 15 minutes at room temperature before rinsing and drying as described before. At this stage, the glutaraldehyde molecules are covalent bonded onto the mica surface and should not diffuse into the added sample solution to cause non-specific protein-DNA cross-linking.

Linearized φX174 DNA (0.2 ng/µl) was mixed with StpA at specified protein to DNA base pair molar ratio (i.e. 1:1 ratio is 300 nM of protein with 0.2 ng/µl of 5,386 bp DNA molecules) and allowed to incubate for 20 minutes. The protein-DNA mixture was then added on a glutaraldehyde –modified mica (hereafter glu-mica) surface for 20 minutes before rinsing extensively with 3 ml of deionised water and then finally dried gently with clean nitrogen gas. In the case where 576 bp DNA molecules are used, the same protocol was used except that the DNA-protein mixture was diluted twice with the experimental buffer immediately before depositing on the glu-mica.

AFM imaging experiments in acoustic AC mode were performed using the Agilent 5500 AFM. AFM scanning was done at various scan square sizes of 1-4 µm with spatial resolution of 512 by 512 or 1024 by 1024 points. The scanning speed was typically fixed at 1 Hz to obtain images with sufficient signal-noise ratio. The raw

AFM images were processed with the Gwyddion software (http://gwyddion.net/) which allows the images to be converted to jpeg format. Data analysis of the DNA contour length and end-to-end distance were done using DIY software written with Matlab (MathWorks, Natick, M.A.). To digitize the DNA conformation, the processed image was first filtered by an averaging filter before converting to a binary image based on a user-defined threshold value. The DNA is then digitized by skeletonizing the binary image into a curved line with single pixel width which depicts the DNA conformation backbone (see **Figure 2.1**). This is based on a previously described method (137).

The digitized DNA conformation is a series of eight connected chaincode. The contour length can be determined by calculating how many even and odd transitions and then using an estimator to obtain the contour length value. In the algorithm, the corner chain estimator was used (138). This estimator includes an additional corner count which is defined by every consecutive odd-even or even-odd transition. Mathematically, the contour length of the digitized DNA is expressed as

$$L_{DNA} = L_{pixel}(0.980n_e + 1.406n_o - 0.091n_c) \qquad (2.1)$$

Where L_{pixel} is the calibrated pixel dimension, n_e is the number of even transition, n_o is the number of odd transition and n_c is the number of corner. The DNA end-to-end distance is defined by the distance between the ends of the polymer (the distance between the first and last pixel of the digitized DNA).

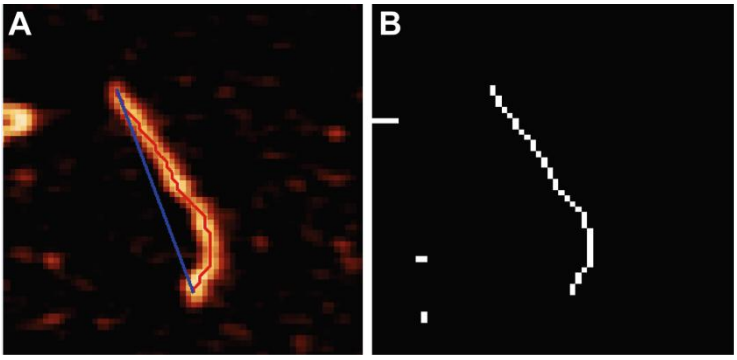

Figure 2.1 DNA conformation analysis algorithm. (A) The original image overlaid with the measured DNA contour length (red line) and end-to-end distance (blue line). (B) The digitized DNA backbone from the left panel. This is the image that was used to measure DNA contour length and end-to-end distance. The scale bar represents 150 nm.

Transverse Magnetic Tweezers Experiment Setup

The transverse magnetic tweezers was setup as described previously (19, 139), see **Figure 2.2**. The longer edge of a No. 0 coverslip was polished extensively to achieve a visibly flat and thin edge to minimize the diffraction shadow size under high magnification observation (under microscope). The polished edge was functionalized with streptavidin to allow specific tethering of single DNA that is labelled with biotin at both ends. Briefly, a flow cell was constructed such that the polished edge is well extended into the centre of the flow cell. This allows us to distinguish the polished edge where the DNA tethers will reside. A long DNA tether (> 4 µm) is required for the transverse magnetic tweezers experiment as there is typically a diffraction shadow size of 1-2 µm along the polished edge under objective magnification. Hence in this work, the λ-DNA, which is ~ 16 µm (48,502 bp) in length, was used. A longer DNA tether will reduce the error in estimating the actual DNA extension due to the diffraction shadow.

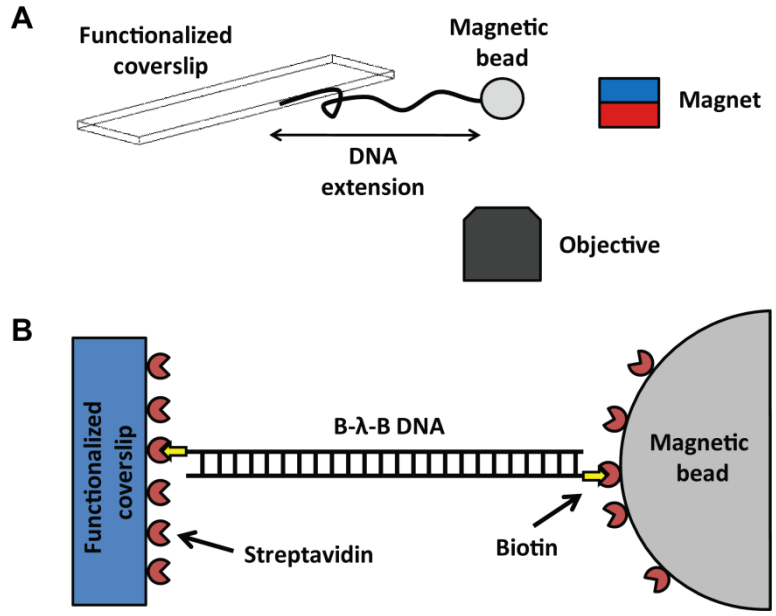

Figure 2.2 Transverse magnetic tweezers setup. (A) The schematic representation of the transverse magnetic tweezers with the DNA tether in an inverted microscope setup. (B) The DNA was tethered at both ends using the strong biotin-streptavidin conjugation with the streptavidin-functionalized edge and magnetic bead.

The both ends of the λ-DNA were labelled with biotin using polymerase method to form the B-λ-B DNA construct. A low concentration (5 ng/µl) of the B-λ-B DNA was added into the flow cell and allowed to incubate for 10 minutes to allow one end of the DNA to bind to the streptavidin edge and also to achieve a low DNA tether density such that the tethers are fairly spaced apart. The remaining unbound B-λ-B DNA was washed away with PBS buffer before adding 2.8 µm sized streptavidin-coated magnetic beads (Dynabeads M-280 Streptavidin, Invitrogen, Singapore) and then incubated for 10 minutes to allow the other end of the tether DNA to bind the beads to form a DNA tether. To manipulate the DNA tether, a permanent magnet (5 mm diameter) was brought close to the flow cell to impose a magnetic force on the bead, in parallel geometry with the DNA tether. A long working distance 50X microscope objective was used to image the DNA tether onto a CCD camera (Pike F-032, Allied Vision Technologies, Germany) which allows us to record the images at 100 frames per second. To measure and record the DNA tether

extension in real-time, a program written using LabVIEW (National Instruments, US) was used. The sub-pixel localization of the magnetic bead was obtained in real-time using centroid tracking method, and subtracted with the coverslip edge to obtain the DNA tether extension. The applied magnetic force was calculated using the following equation (100, 140):

$$F = \frac{k_B T z}{\langle \delta x^2 \rangle} \qquad (\mathbf{2.2})$$

Where k_B is the Boltzmann constant, T is temperature, z is the DNA extension and $<\delta x^2>$ is the transverse fluctuation along a direction perpendicular to the force direction. The force acting on the DNA tether through the magnetic bead can be modulated by changing the distance between the flow cell and the permanent magnet, which was remotely controlled by the LabVIEW program. The force-extension curve of the DNA tether was then obtained by measuring the DNA tether extension at various magnet position and thus at various pulling force.

To determine if the DNA is singly tethered or multiply tethered, the measured force-extension curve was fitted with the Marko-Siggia worm-like-chain model. The fitted parameters yield the estimated DNA contour length and persistence length. A single DNA tether should have a persistence length value of $\approx 50 \pm 5$ nm in a buffer condition of 150 mM KCl and pH 7.5 (i.e. in PBS buffer) (81, 86). The fitted DNA contour length should also be near the value of the theoretical contour length of the DNA used in the experiment (for λ-DNA, it is 16,490 nm). After a single DNA tether was confirmed, we can then add the proteins or change the buffer using a mechanical syringe pump (NE-1000, New Era Pump Systems, Farmingdale, N.Y.) which minimizes mechanical perturbations to the sensitive measurements. The force-extension curves of the DNA or DNA-StpA co-filament were fitted with the high-

force regime approximation of the Marko-Siggia WLC model (See equation below) to calculate the apparent persistence length, A of the DNA-protein complex. For naked DNA, this equation is valid for imposed force as low as ≈ 0.08 pN (86). The fitting will yield two parameters; apparent persistence length, A and DNA contour length, L.

$$\frac{z}{L} = 1 - \sqrt{\frac{K_B T}{4FA}} \qquad \textbf{(2.3)}$$

High-throughput Magnetic Tweezers Experiment Setup

For the investigation of DNA tethers digestion rate by DNase I, approximately 10 DNA tethers were monitored simultaneously. To observe 10 or more DNA tethers in the transverse magnetic tweezers setup, a bigger field of view was needed and thus a 10X objective was used. As the DNA tethers were pulled with a constant force of ~ 3-5 pN, a single cleavage anywhere along the DNA would result in the magnetic bead to detach and move rapidly towards the magnet, out of the observation field. Hence the disappearance of bead would suggest the DNA tether is digested by DNase I. A ROI (region of interest) was drawn for every bead that were tethered and recorded in real-time. The numbers of DNA tethers tracked were determined by the number of ROIs with a bead inside. As the tethers were digested with time upon introduction of DNase I, tracked beads that moved out of the ROI were recorded as digested (**Figure 2.3A, blue arrow**). If the bead is multiply tethered, a single cleavage would result in the bead moving out of the ROI but still remained tethered due to other remaining un-cleaved DNA molecules (**Figure 2.3A, red arrow**). This is recorded as a single cleavage event.

To determine repeatability of the experiment, all high-throughput magnetic tweezers DNase I assays were repeated at least twice and this allowed a rough estimation of the DNA tether lifetime (defined as the time taken for 50% of DNA tethers being digested divided by the total initial DNA tethers) in various experimental conditions. For naked DNA, the values were: 3 ± 1 seconds in 50 mM KCl and 320 nM Dnase I, 8 ± 1 seconds in 500 mM KCl and 1280 nM Dnase I, 6 ± 5 seconds in 50 mM KCl, 10 mM MgCl2 and 32 nM Dnase I.

Figure 2.3 High-throughput magnetic tweezers experiment (A) Time-lapsed screenshots of DNA tethers that are cleaved in the presence of 1,280 nM DNase I in 500 mM KCl buffer condition. The green boxes were the ROIs enclosing the beads that were tethered. The blue arrows follow the process of a single DNA tether being cut by DNase I which resulted in the bead disappearing from the screen at frame 5. The red arrows follow the process of a multi-DNA tethered bead where the first DNase I cleaving event resulted in the bead moving out of the ROI at frame 2 but not disappearing from the screen. This was recorded as a single DNA breakage event. This bead was not traced after frame 2. (B) The cartoon schematic of the experimental setup which is shown in panel A. Due to the geometry of the magnet (a single cylindrical magnet was used), stacked magnetic beads that are parallel to the force will be observed occasionally. Some of the beads will be attached directly onto the edge due to excessive multi-DNA tethering.

2.3. Results

StpA organizes DNA into various distinct conformations depending on StpA coverage along DNA

Major bacterial NAPs such as the *E.coli* H-NS and HU were shown to exhibit multiple DNA-binding modes depending on buffer conditions or protein coverage along the DNA (19, 20, 141). The *E. coli* StpA DNA-binding mode has not been fully tested in different buffer conditions or binding coverage along DNA other than a previous AFM study which showed StpA bridges DNA at low protein coverage (51). Here, we used atomic force microscopy (AFM) to image StpA-DNA complexes at various protein to DNA base pair (bp) ratios (hence at different StpA coverage along DNA). Glu-mica (see Methods) was used as the deposition surface to preserve the complex integrity and conformation since the same experimental buffer used for reaction can be used for deposition (19, 136, 142). **Figure 2.4** shows the AFM image of linearized DNA molecules incubated at 1:1 StpA:DNA ratio. We observed that the majority of complexes (> 80%) are a mixture of two distinct conformations; which are elongated filaments and large homogenous loop structures (> 250 nm in contour length) at the ends of the filaments.

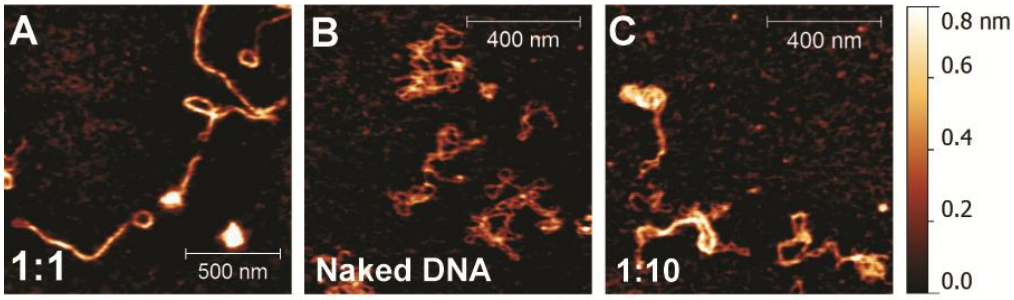

Figure 2.4 StpA binding resulted in simultaneous DNA stiffening and bridging. (A) AFM images of linearized φX174 dsDNA incubated at 1 StpA per 1 bp ratio (1:1 StpA:DNA ratio, 300 nM StpA) showed homogenous large StpA-coated DNA hairpins. (B) Naked φX174 DNA in same experimental condition. Comparing with (A), the naked DNA assumed random coiled/relaxed conformations with much

thinner complex width. (C) DNA-StpA complexes at 1:10 StpA:DNA (30 nM StpA) ratio showed localized DNA condensation amongst random coiled conformations.

The observed conformations are distinct from that observed with DNA in the absence of StpA (Fig. **2.4B**). In addition, we also observed a small sub-population of the StpA-DNA complexes that were condensed, although it may be debris (**Fig. 2.5A, arrows**). Nonetheless, the majority of the StpA-DNA complexes were of elongated conformation, which from the mechanical perspective, would suggest the DNA became stiffer upon StpA binding. The height homogeneity along the backbone of the StpA-DNA complexes suggests that the DNA were evenly coated by StpA. Taking the above two observations together, we interpreted that StpA likely form a rigid filament along DNA, thus resulting in an apparent increase in DNA stiffness. When the StpA DNA coverage ratio was reduced to 1 StpA to 10 bp (**Fig. 2.4C**), localized regions of the DNA molecules were observed to have a higher height, which suggests StpA binding/ or recruitment to DNA may be cooperative in nature rather than through random binding. At a much lower StpA DNA coverage of 1:100 StpA:DNA ratio, we saw that StpA caused DNA bridging (**Fig. 2.5C-D**), in contrast to the filamentous conformation at higher StpA coverage. Both the 1:10 and 1:100 StpA:DNA ratio data are consistent with previous StpA AFM studies which showed StpA caused DNA bridging (132).

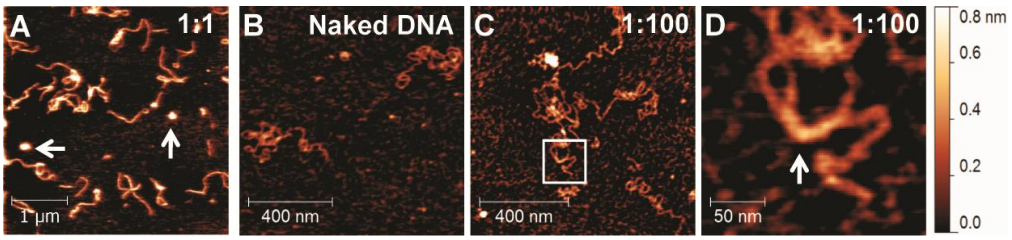

Figure 2.5 AFM images of StpA DNA-bridging capability and that the StpA-DNA filamentous complexes were unable to self-interact. The experimental conditions were similar as those done in Figure 3.4. The StpA/DNA bp ratio is indicated at the top right corner of each subpanel. (A) A typical large area scan of the StpA-DNA conformations on glu-mica surface. One can see that the majority of the complexes

are elongated complexes. The white arrows indicate highly-condensed conformations that are a small sub-population of the entire sample. (B) Naked linearized φX174 DNA substrates. (C) At 1:100 StpA:DNA ratio (3 nM StpA), some StpA binding were observed. (D) A zoom-in of the white box in panel C revealed StpA bridging of DNA, as indicated by the white arrow.

From the AFM imaging data, it is obvious that DNA was organized into multiple conformations depending on StpA coverage along the DNA; at low StpA coverage, StpA caused DNA localized condensation while at high or saturated StpA coverage, StpA simultaneously organized DNA into elongated nucleoprotein filaments and large DNA loops. The filaments are likely due to the formation of StpA protein filament along DNA.

StpA DNA-bridging results from StpA nucleoprotein filament and DNA interaction

The co-existence of rigid filaments and loop structures at high StpA DNA coverage are of peculiar interest, given both conformations antagonizes one another from energetic perspective (i.e., a rigid filament makes it harder to form highly curved loop). Hence, we proposed two models that can explain this observation. The first model is the StpA nucleoprotein filament may interact with itself or similar complexes to form long tracts of DNA bridges (**Figure 2.6A)**. The second model is the StpA nucleoprotein filament may instead interact with DNA segment to form long tracts of DNA bridges (**Figure 2.6B)**. So we performed further experiments to resolve the two models, and we showed that the co-existence of rigid filaments and DNA loops was due to the second model (see below).

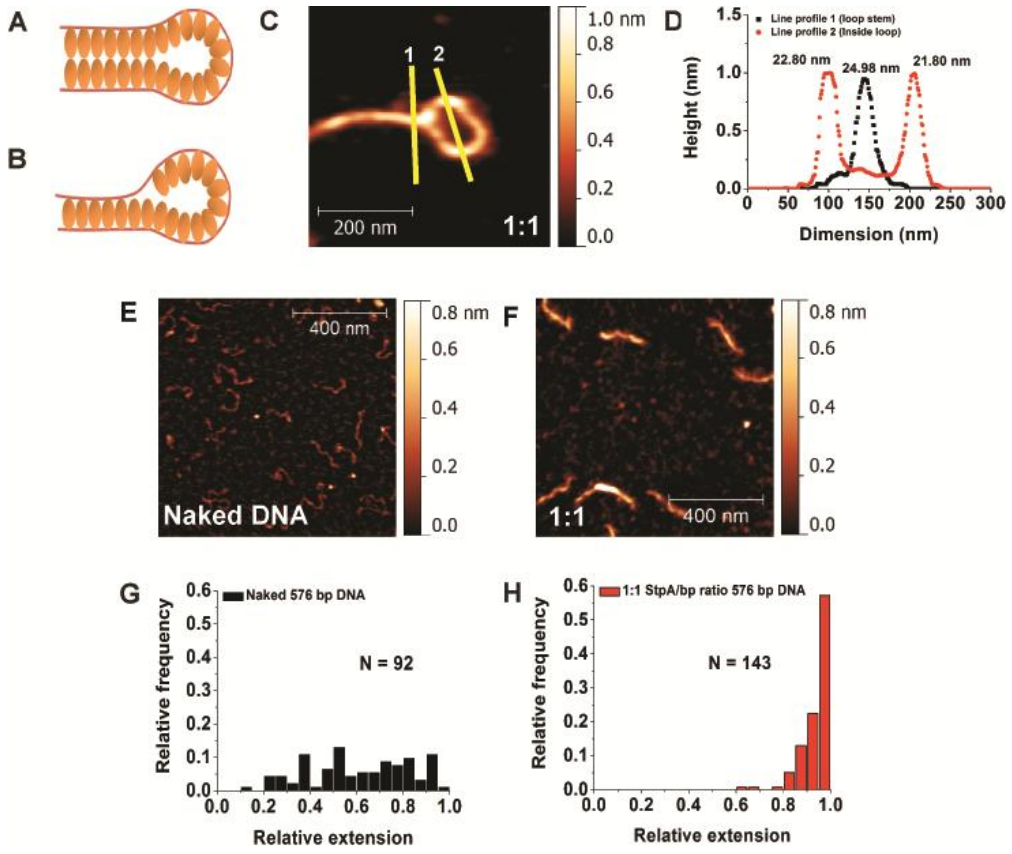

Figure 2.6 DNA-StpA nucleoprotein filament interacts with DNA to form DNA bridges. (A & B) Hypothetical models which illustrate how StpA may form rigid filaments and large DNA loop structures. (C) An AFM image of the DNA loop structure at high StpA coverage. The yellow lines are drawn where the width are measured in panel D. (D) Line profile analysis showed the widths of StpA coated DNA in the loop and at the loop stem are the same. The width values are indicated at the top of the peaks. (E) An AFM image (1 x 1 µm in size) of linear 576 bp DNA represented with height scale (z-axis) of 0-0.8 nm. (F) The same 576 bp DNA incubated at 1:1 StpA:DNA ratio (high StpA DNA coverage) showed that the DNA width was visibly thicker and straighter. The population of the StpA-DNA complex were almost homogeneous with majority being monomeric StpA nucleoprotein filament. (G) A histogram of 576 bp DNA relative extension (or DNA extension divided by its contour length). The histogram distribution is widely spread which suggests DNA itself adopts random conformations. (H) Similar histogram of 576 bp DNA incubated in 1:1 StpA:DNA ratio. The distribution showed that majority of the DNA was almost fully extended to its contour length which suggests DNA stiffening by StpA. The above analysis is in good agreement with the second model in panel B.

Our AFM experiment with φX174 DNA incubated at 1:1 StpA:DNA ratio and allowed to interact for 5 hours showed no DNA condensation caused by StpA (**Fig. 2.7A**). This is in disagreement with what the first model would have predicted which is the accumulation of StpA-DNA condensates that are mediated by StpA

nucleoprotein filament self-interactions. The first model was further disproved when we measured the width of the StpA nucleoprotein filament at various segments of a StpA-DNA loop structure, and found that the width in the loop and at the loop stem were of similar size (**Fig. 2.6C & D**). This is because the model would have predicted that the width at the stem would be twice as large as the width inside the loop head due to the presence of two StpA nucleoprotein filaments at the loop stem (**Fig. 2.6A**).

The second model also provides testable predictions which we can use experiments to verify. It predicts that if we were to allow StpA to fully coat the entire DNA before the DNA is allowed to form StpA-mediated loops, we would obtain a fully elongated StpA nucleoprotein filament. This was tested and proved true when we incubated shorter 576 bp DNA at high StpA DNA coverage and observed majority of the StpA-DNA complexes are monomeric elongated filaments (**Fig. 2.6E & F**). A shorter DNA was used to reduce the probability of DNA looping and thus favours the outcome of elongated filaments. A high StpA:DNA ratio was used to facilitate rapid coverage of DNA by StpA before any DNA looping event occurs. The monomeric population also suggests that once StpA fully coated the DNA, the StpA nucleoprotein filaments are unable to interact with one another, which is consistent with the second model.

Relative extension analysis histograms are shown in **Figures 2.6G & H**. In the absence of StpA, the relative extension of short DNA was well distributed while at 1:1 StpA:DNA ratio, distribution was localized near 1, which suggests the StpA-DNA complexes were extended nearly to its contour length. The width analysis also showed the StpA nucleoprotein filament had a thickness of up to ~ 10-15 nm (after subtracting AFM tip widening effect of ~ 12 nm, **Fig. 2.7B**) and has only a slight reduction in the DNA contour length (**2.7C**). The upper estimation of StpA nucleoprotein filament width is due to the potential change in interaction energy between AFM tip and sample.

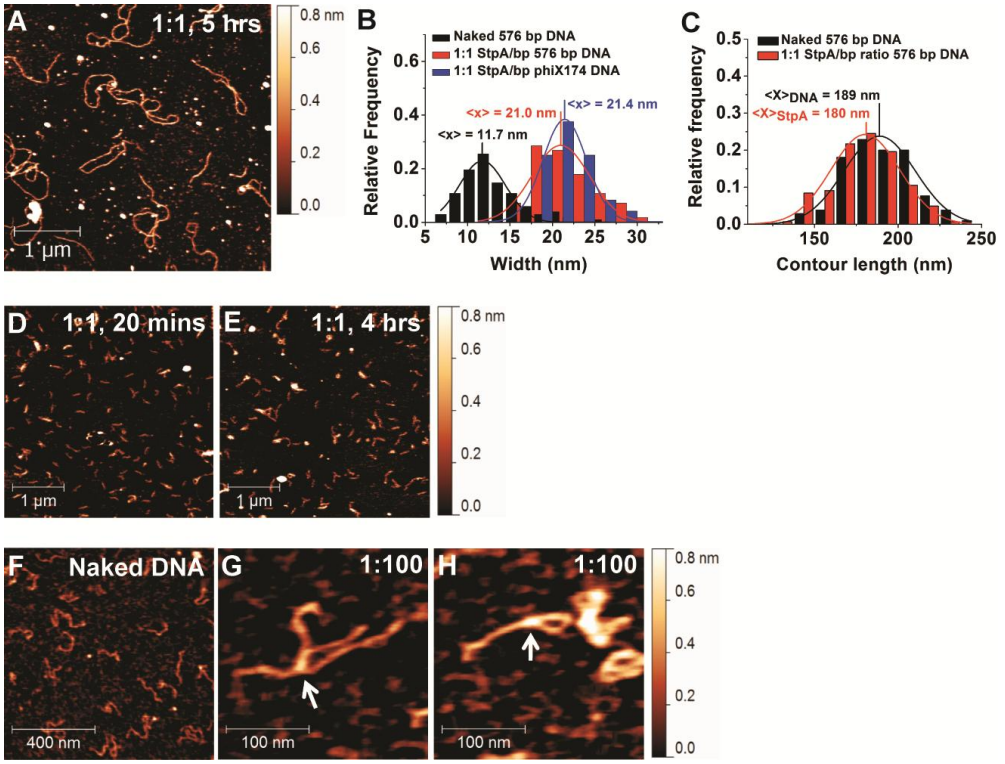

Figure 2.7 AFM images and dimension analysis of StpA nucleoprotein filament DNA bridging. (A) φX174 DNA incubated at 1:1 StpA:DNA ratio for 5 hrs showed no DNA condensation that is otherwise predicted by the model in Figure 3.6A. (B) Width analysis showed StpA nucleoprotein filament formation resulted in a ~10 nm increase in DNA thickness as compared to DNA. (C) Contour length analysis of 576 bp DNA incubated with/without 1:1 StpA:DNA ratio conditions showed there was only a slight reduction in DNA contour length upon filament formation. (D-E) Long time incubation (between 20 minutes and 4 hours) of 576 bp DNA with 1:1 StpA:DNA ratio showed no significant change in StpA-DNA complex conformation population. This suggests that StpA nucleoprotein filaments do not interact with each other. Large 4 x 4 µm images were used to better compare the complex population distribution. (F-H) The same 576 bp DNA incubated at 1:100 StpA:DNA ratio (low StpA DNA coverage) showed StpA can still mediate DNA bridging with short DNA (indicated by the white arrows).

For further confirmation of our results, we showed that the monomeric 576bp StpA nucleoprotein filaments did not aggregate when allowed to interact for up to 4 hours (**Fig. 2.7D-E**). At a lower StpA DNA coverage of 1:100 StpA:DNA ratio, StpA DNA bridging can still be observed using the short 576 bp DNA (**Fig. 2.7F-H**). At low StpA DNA coverage, the coated StpA DNA regions can interact with other uncoated DNA segments. Putting all of these analyses together, we showed that at

high StpA DNA coverage, StpA form rigid nucleoprotein filaments and these filaments can mediate DNA bridging by interacting with naked DNA segments. In other words, the StpA nucleoprotein filament can bind two naked DNA segments simultaneously but just requires one DNA to form a nucleoprotein filament (**Fig. 2.6B**).

StpA DNA stiffening and bridging kinetically competes with each other

Our AFM experiments showed that StpA form a rigid nucleoprotein filament with DNA at high StpA DNA coverage (**Fig. 2.4A & 2.6F**). To further verify these findings, we performed single-molecule manipulation experiments to investigate the elastic response of a single DNA after StpA binding (87). The transverse magnetic tweezers setup was used to perform the measurements (139). A single λ-DNA was pulled at ≈ 11 pN (pico-newton) before StpA were introduced into the flow cell (**Fig. 2.2B**). The high force stretched the DNA and provided sufficient tension to prevent DNA folding by StpA and allowed StpA to instead form rigid filament along the DNA. After adding the proteins, force-extension curve measurements were performed by gradually reducing the pulling force in a step-wise manner until it was at ~0.08 pN before reversing the process (increasing the pulling force). At every pulling force, the DNA extension was recorded for 60 seconds and a final "steady-state" DNA extension value was calculated by averaging the data in the last 30 seconds. The forward and reverse force scans were compared to see if there was any hysteresis, which would indicate the presence of protein-induced DNA bridging/folding.

Forward and reverse force-extension measurements of a single λ-DNA tether were performed in the presence of 6, 25, 100, 300 and 600 nM StpA were (**Fig. 2.9A**). To reduce visual complexity, only the curves at 6, 25, and 600 nM StpA are shown in **Figure 2.8A.** Large hysteresis between the force and reverse force scans was observed at 6 nM StpA (compare the forward scan red filled circle with the reverse

curve blue filled up-triangle). This can be seen from the shorter DNA extension in the presence of 6 nM StpA as compared to the naked DNA extension (see DNA folding and unfolding time courses in **Fig. 2.9B-D**). The observed folding of DNA at 6 nM StpA concentration can be explained by StpA DNA bridging as seen in **Figure 2.6B**.

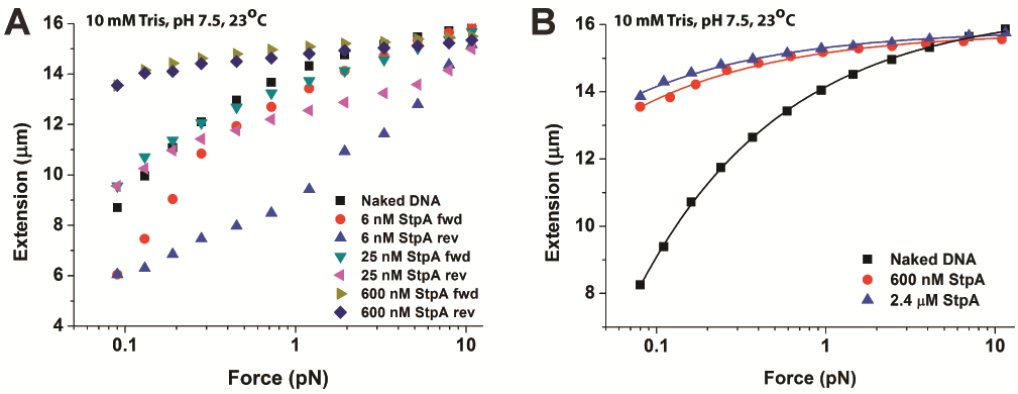

Figure 2.8 Magnetic tweezers experiments revealed the kinetic competition between StpA rigid nucleoprotein filament formation and nucleoprotein filament mediated DNA bridging. (A) Forward and reverse force-extension curves of λ-DNA (48,502 bp) in 50 mM KCl, 10 mM Tris, pH 7.4 at the indicated StpA concentrations. At low StpA concentration of 6 nM, significant hysteresis was observed which implies DNA is being condensed by StpA DNA bridging. At higher StpA concentration of 600 nM, the DNA extension became higher due to DNA stiffening and no hysteresis was observed. This is due to the domination of StpA nucleoprotein filament formation. At 25 nM StpA, a mixture of StpA DNA bridging and nucleoprotein filament was observed. This is indicated by the presences of both DNA extension hysteresis and stiffening. (B) Force-extension curves of λ-DNA at higher StpA concentration of 2,400 nM showed that DNA stiffening effect was saturated beginning at 600 nM StpA concentration. Only the forward curves are shown due as the reverse curves are similar. The lines represent fitting using the DNA WLC model. The fitting parameters gave a persistence length value with fitting error of 639.67 ± 34.80 nm and 909.50 ± 48.56 nm for 600 nM and 2,400 nM StpA concentrations respectively. The fitted contour length with fitting error is 15,794.54 ± 32.27 nm and 15,851.05 ± 27.05 nm for 600 nM and 2,400 nM StpA concentrations respectively.

At 25 nM StpA concentration, the level of hysteresis and DNA folding were reduced as compared to that observed in 6 nM StpA. In addition, the DNA extension was higher as compared to naked DNA's at low force (~ 0.1 pN). This can be explained by DNA stiffening effect caused by DNA-binding proteins, and the effect is more obvious at lower DNA pulling force. Hence it implies that at 25 nM StpA concentration, a significant portion of DNA is covered by rigid StpA filaments which results in an increase in the apparent DNA rigidity as determined by WLC model

fitting with the force-extension curve (87). The naked DNA portions can be further depleted by increasing the StpA concentrations, which would lead to a completely StpA covered-DNA. The StpA DNA bridging will also not have a chance to happen and thus DNA extension hysteresis should be minimal or none at all. As expected at higher StpA concentration of 600 nM, the DNA was significantly stiffened and no hysteresis was observed. This is also in agreement with the AFM imaging experiments data (**Fig. 2.4A & 2.6F**), which showed StpA formed rigid nucleoprotein filaments at high StpA concentrations.

The StpA nucleoprotein filament (DNA stiffening) and the filament interaction with naked DNA (DNA bridging) are mutually exclusive as in terms of conformation, they antagonizes each other (i.e. formation of StpA nucleoprotein filaments deplete naked DNA that are required for StpA DNA bridging. Hence this predicted a kinetic competition between the two processes. To prove this prediction, we performed a magnetic tweezers experiment whereby a single DNA tether was initially held at high DNA tension (~ 6 pN) to prevent StpA mediated condensation, then 600 nM StpA was quickly added into the flow cell (< 15-20 seconds) before the DNA pulling force was immediately reduced to ~ 0.1 pN (< 1 seconds) so that we can observe the kinetics of StpA DAN stiffening before it becomes saturated (**Fig. 2.9E**). We observed the DNA extension increased ~ 1.5 μm gradually after the DNA pulling force was reduce to ~ 0.1 pN before it abruptly dropped to 6.5 μm (shorter than original value). The observation is what we expected; the initial increase in DNA extension is due to the gradual formation of rigid StpA nucleoprotein filaments which caused DNA stiffening, and before it could fully coat the entire DNA, the lower DNA pulling force (~ 0.1 pN) allowed DNA looping to happen and thus caused StpA bridging to occur and a drop in DNA extension (StpA nucleoprotein filament bridging with naked DNA segments). It should be drawn to attention that at similar StpA concentration (600 nM) and buffer condition, saturated DNA stiffening was

observed when the DNA was prevented from StpA bridging by holding it at a large force (~6-8 pN) for a significantly longer time, which caused the naked DNA segments to be depleted by full coverage of StpA filaments (**Fig. 2.8A**).

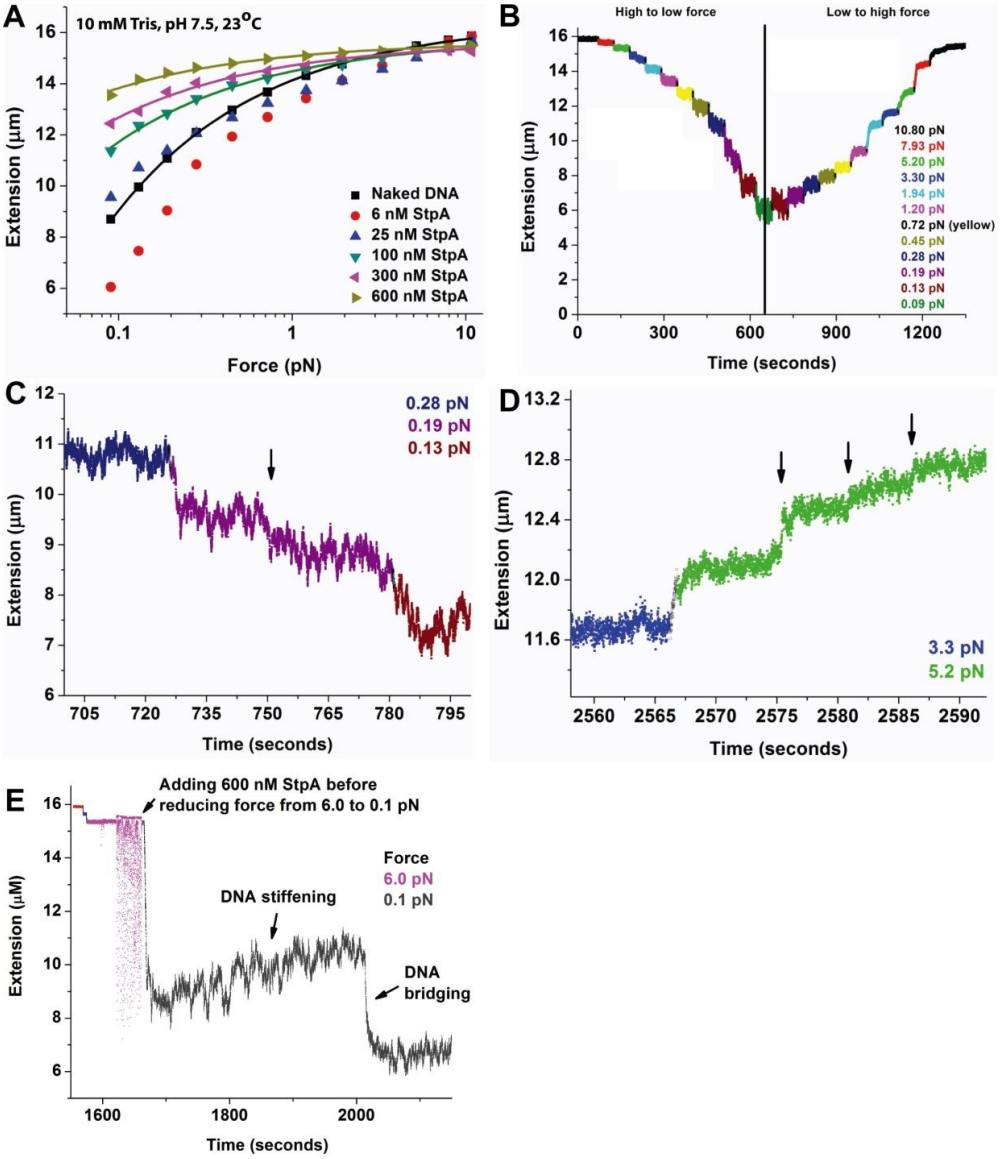

Figure 2.9 Magnetic tweezers λ-DNA force-extension curves (FECs) at different StpA concentrations. (A) FEC of the same λ-DNA recorded in 6, 25, 100, 300 and 600 nM StpA concentrations. The forward curves are shown only and only 6 and 25 nM StpA experiments had hysteresis which is shown in figure 3.8A. Marko-Siggia WLC model was fitted to the 100, 300 and 600 nM StpA concentration data and the fitting curves are represented by the solid lines of the respective symbols colour. (B) The DNA extension time-course of λ-DNA in 6 nM StpA during forward force scan (reducing force) and the subsequent reverse force scan (increasing force). (C) The folding time course at 6 nM StpA showing a StpA folding event (indicated by arrow). (D) The unfolding time course of the same experiment revealed several unfolding

events as indicated by the arrows. (E) The kinetic competition between StpA DNA stiffening and bridging are shown by magnetic tweezers experiment. 600 nM StpA was exchanged into the flow cell before the pulling force was reduced from 6 to 0.1 pN to better observe the DNA extension increment due to StpA DNA stiffening. The increase in extension was followed by an abrupt reduction. This can be explained by the occurrence of StpA DNA bridging before the DNA is fully coated by StpA filament.

StpA nucleoprotein filament increased the DNA bending rigidity more than ten-fold

We have demonstrated that StpA forms a rigid nucleoprotein filament with DNA at high StpA DNA coverage. The copy number of StpA *in vivo* was estimated to be 25,000 copies per cell (16) which translate to a *in vivo* concentration of ~ 10 μM. This estimated concentration is of much higher quantity than the tested StpA concentration in our study here (up to 2.4 μm). Hence we suggest the StpA nucleoprotein filament is likely physiologically relevant (see discussion) which prompts us to investigate its biophysical properties. To quantify the stiffness or specifically, the bending rigidity of the StpA nucleoprotein filament, we fitted the Marko-Siggia WLC model (86) to the λ-DNA force-extension curves that were done at high StpA concentrations (600 and 2,400 nM) (**Figure 2.8B)**. The data usage from high StpA concentration data is to ensure saturated coverage of DNA by StpA and thus an entire StpA nucleoprotein filament.

We observed that at 600 nM StpA concentration, the StpA DNA stiffening effect was saturated, and this was derived from the observed similarity in the level of DNA stiffening at a higher 2,400 nM (2.4 μM) StpA concentration. Quantitatively, the Marko-Siggia WLC model fitting yielded an apparent persistence length (bending rigidity) of 442.82 ± 161.28 nm (N = 9), which is about ten-fold higher than the naked DNA persistence length value of ~ 50 nm. Since the DNA original persistence length (~ 50 nm) is negligible as compared to the StpA nucleoprotein filament's value (~ 443 nm), we conclude that the StpA protein filament itself has a much higher

persistence length than naked DNA. In addition, the WLC model fittings showed the λ-DNA contour length had a slight decrease from original length of 16,490 nm to 15,915.03 ± 183.41 nm (N = 9) which is consistent with our AFM contour length analysis (**Fig. 2.7C**).

High salt disrupted the stability of StpA nucleoprotein filament

StpA expression in cells is up-regulated by osmotic shock and temperature (130). The sensitivity of the *E. coli* H-NS DNA-binding properties to environmental factors is demonstrated in single-molecule studies that showed H-NS nucleoprotein filaments are disrupted at high salt, temperature or acidic pH (19, 41). Hence, we think it will be important to investigate the response of StpA nucleoprotein filament stability to similar environmental changes. We performed magnetic tweezers force-extension measurements on single StpA nucleoprotein filament while changing environmental conditions. We found that the StpA nucleoprotein filament was insensitive to ionic strength (in terms of KCl) changes in the range of 5-300 mM, temperature in the range of 23^{o}C-37^{o}C, and pH in the range 6.6-8.8 (**Fig. 2.10A-C**). In contrast, we found that the StpA DNA bridging was sensitive to KCl and temperature but not pH changes (**Fig. 2.10D-F**).

As the stability of the StpA nucleoprotein filament was not affected by KCl concentration up to 300 mM KCl (which is also confirmed with AFM imaging experiments (**Fig. 2.10G & H**)), we wish to investigate at what ionic strength the StpA nucleoprotein filament will be disrupted. Hence we performed force-extension curves measurements of λ-DNA with 600 nM StpA in 5-500 mM KCl, whereby each KCl concentration measurement was done in independent experiments to eliminate any possible history dependence behaviour. Consistent with our previous data with 5-300 mM KCl, StpA caused saturated DNA stiffening (**Fig. 2.11A**). However, at 500 mM KCl, we observed no significant change in DNA force-response, and the force-

extension curve with and without presence of StpA overlapped. We attributed this to a reduction in StpA DNA-binding affinity at 500 mM KCl condition, which resulted in minimal or no binding of StpA on the DNA tether. However, we do not exclude the possibility that only the structural integrity of the StpA filament was disrupted (i.e. StpA filament becomes weaker or softer) while StpA still remain bound on the DNA.

To determine if StpA remain bound on the DNA at high ionic conditions, we first measured the force-extension curve of a λ-DNA in the presence of 600 nM StpA in 500 mM KCl buffer condition (which showed no significant DNA stiffening), then exchanged the flow cell buffer with 50 mM KCl buffer (which previously promoted strong DNA stiffening) in the absence of StpA and measured the force-extension curve again (**Fig. 2.11B**). We observed that the λ-DNA became strongly stiffened, similar to that in the presence of high StpA concentrations. Re-addition of 600 nM StpA in the same buffer had no change in the DNA stiffness, which indicated the StpA DNA stiffening or StpA binding was saturated in the previous condition. Exchanging the flow cell buffer with 600 nM StpA in 500 mM KCl caused the StpA DNA stiffening effect to disappear again. The above indicated that during the initial incubation with 600 nM StpA in 500 mM KCl, the DNA was bound with StpA but was not detected due to a lost of StpA DNA stiffening. Hence, when we exchanged the buffer to 50 mM KCl (buffer that favours StpA DNA stiffening) in the absence of StpA, the DNA stiffening effect was recovered. The DNA stiffening effect is also comparable to that observed in the presence of high StpA concentrations which indicated that StpA binding affinity was likely unaffected at high KCl and rather its filament organization (and thus rigidity) was affected.

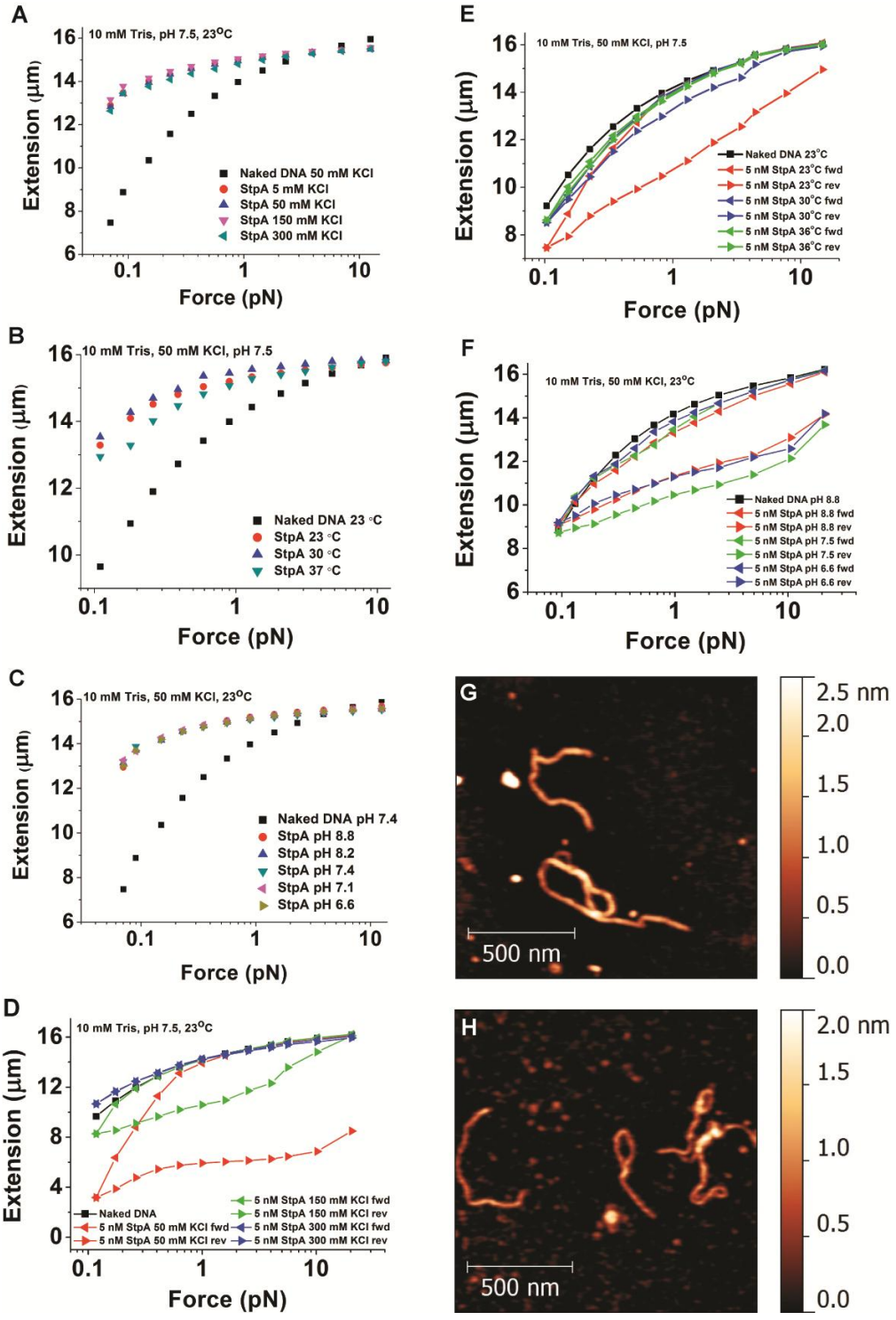

Figure 2.10 The StpA nucleoprotein filament and DNA bridging response against KCl, temperature and pH. (A) Force-extension curves (FECs) of λ-DNA in 600 nM StpA showed no significant change across 5-300 mM KCl buffer conditions. (B & C) Similar experiments done in 23-37 °C or 6.6-8.8 pH buffer conditions also showed no change to StpA nucleoprotein filament stability. (D-F) FECs in 5 nM StpA concentration (StpA DNA bridging mode) showed strong dependence on KCl concentration or buffer temperature but no on pH. The DNA extension hysteresis from forward and reverse force scans decreased with increasing KCl concentration and buffer temperature while it remained unchanged when pH was changed. (G & H) AFM images of StpA-DNA complexes at 1:1 StpA/DNA ratio incubated in 150 mM

and 300 mM KCl concentrations showed formation of rigid StpA nucleoprotein filaments and is consistent with the FEC measurements in panel A.

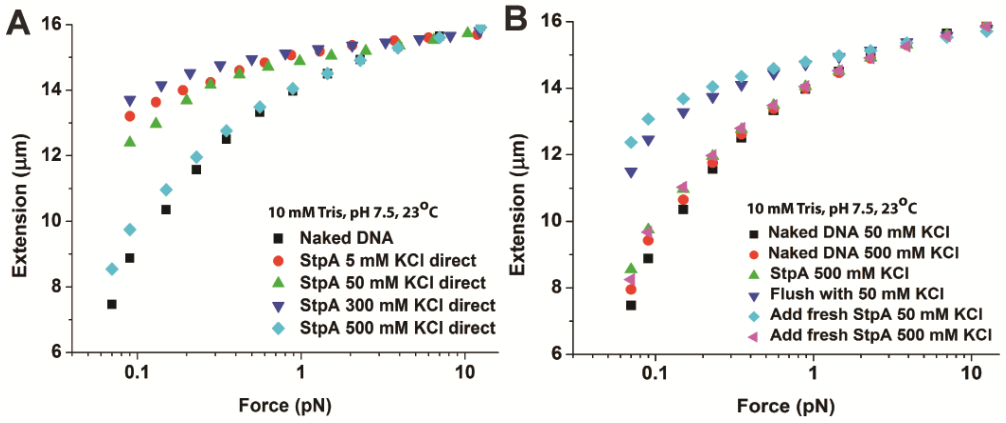

Figure 2.11 The StpA nucleoprotein filament was disrupted at high ionic strength buffer conditions. The reverse force scan curves are not plotted unless hysteresis was observed. (A) Force-extension curves (FECs) of λ-DNA with 600 nM StpA in buffer containing 5-500 mM KCl. Similar to figure 3.10, there were little change in StpA DNA stiffening effect between 5-300 mM KCl. However, in 500 mM KCl, no DNA stiffening was observed. (B) FECs of λ-DNA in 600 nM StpA during a series of buffer exchanges. After FEC measurement with 600 nM StpA in 500 mM KCl buffer condition, the unbound StpA proteins were washed away. The buffer was changed to 50 mM KCl condition without StpA, and saturated StpA DNA stiffening was observed. This implied at 500 mM KCl, StpA remain bound to DNA but do not cause DNA stiffening. When saturated level of StpA DNA stiffening was achieved in 50 mM KCl, the stiffening effect was eliminated upon changing the buffer back to 500 mM KCl condition.

The rigid StpA nucleoprotein filament prevented DNA access

Given that one of StpA functions is silencing genes in *E. coli* (125, 143). We hypothesized that the StpA nucleoprotein filament forms a physical barrier which blocks RNA polymerase DNA access thus inhibiting or suppressing transcription. To test our hypothesis that predicts StpA filament blocks DNA access, we studied StpA nucleoprotein filament digestion by DNase I. DNase I was used as it requires only 6 bp of DNA accessibility for cleavage, and thus provide a rigorous test to the prediction. To achieve a higher experimental throughput, we used a lower viewing objective to observe 8-10 StpA-coated DNA tethers simultaneously (held under 1-3

pN of force). The rate of tether digestion is defined as the time taken for complete digestion of all observed tethers upon the first tether digestion. The advantages of this method over traditional digestion assays are the tethers can be manipulated to prevent DNA condensation by the studied protein and the digestion kinetics can be observed in real-time.

In the absence of StpA, all the DNA tethers were cleaved within 30 seconds upon addition of 320 nM DNase I in 50 mM KCl buffer condition. In 500 mM KCl buffer condition, it took 3 minutes and higher concentration of DNase I (1,280 nM) to cleave all the DNA tethers (**Fig. 2.12A & B**, black and red line, respectively). This was expected since DNase I activity is known to be reduced in the presence of high salt buffer conditions. In 50 mM KCl buffer condition where StpA nucleoprotein filament formation is favoured, almost all the tethers were intact upon introducing 320 nM DNase I (**Fig. 2.12A** red line). However at 500 mM KCl buffer condition where StpA cannot form nucleoprotein filament but still bind to DNA, all the tethers were cleaved within ~ 5 minutes upon introducing 1,280 nM DNase I (**Fig. 2.12B**). The result confirms that the formation of StpA nucleoprotein filament block DNA access down to 6 bp. It also indicates that StpA binding alone is not enough for blocking DNase I, and filament formation is needed.

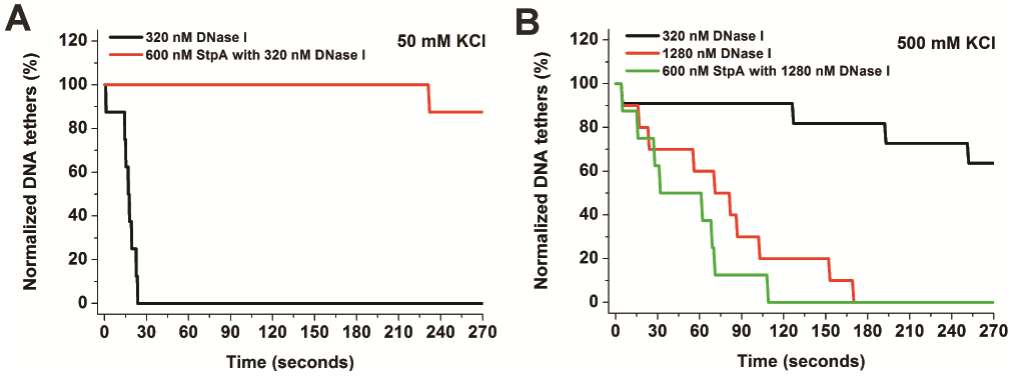

Figure 2.12 StpA nucleoprotein filament blocked DNase I access to DNA. (A) Normalized DNA tethers (sample population of 8-10 tethers) time course. The DNA tethers, in the absence of StpA, were all cleaved within 30 seconds upon addition of 320 nM DNase I (in 50 mM KCl buffer condition). In the presence of 600 nM StpA

in similar experimental condition, the DNA tethers were relatively well-protected with only 1 tether cleaved. (B) In the case of 500 mM KCl buffer condition, 320 nM DNase I showed reduced DNA cleavage activity (black line). To improve the DNA cleavage efficiency, the concentration of DNase I was increased to 1,280 nM, this resulted in cleavage of all the DNA tethers within 180 seconds (red line). In the presence of 600 nM StpA in similar experimental condition, all the DNA tethers were cleaved within 120 seconds (green line).

Magnesium promoted StpA DNA compaction via nucleoprotein filaments self-interactions

Magnesium (up to 4 mM in bacterial cell) is essential for numerous important biological processes in bacterial cells such as chromosomal DNA condensation and DNA damage repair (144, 145). Magnesium regulates and switches the distinctive DNA-binding modes of the *E. coli* H-NS (19), and this prompts us to ask if magnesium has the similar effect on StpA DNA-binding mode. Previous AFM studies showed that StpA in the presence of magnesium caused large DNA aggregation (132) and this was not observed in our AFM experiments in the absence of magnesium (**Fig. 2.4A & 2.6F**, where only DNA loops were observed). Hence we hypothesize that magnesium switches StpA from DNA bridging to higher-ordered DNA compaction. To test this hypothesis, AFM imaging experiments of StpA-DNA complexes were performed in the presence of 1-10 mM magnesium.

In 1 mM $MgCl_2$ buffer condition, the majority of StpA-DNA complex conformations were elongated with DNA loops (**Fig. 2.13A**), which is comparable with that in the absence of magnesium. When the magnesium concentration was increased to 10 mM $MgCl_2$, the DNA-StpA complexes were highly compacted (Fig. 3.13B & C). DNA compaction by StpA was also observed when shorter 576 bp DNA was used (**Fig. 2.13D)**. It should be noted that in the absence of magnesium, with similar experimental conditions, we observed StpA formed monomeric nucleoprotein filaments (**Fig. 2.6F)**. We found that DNA compaction by StpA started from 5 mM

$MgCl_2$ (**Fig. 2.14A-C**) buffer condition onwards which is similar to *in vivo* magnesium chloride concentration.

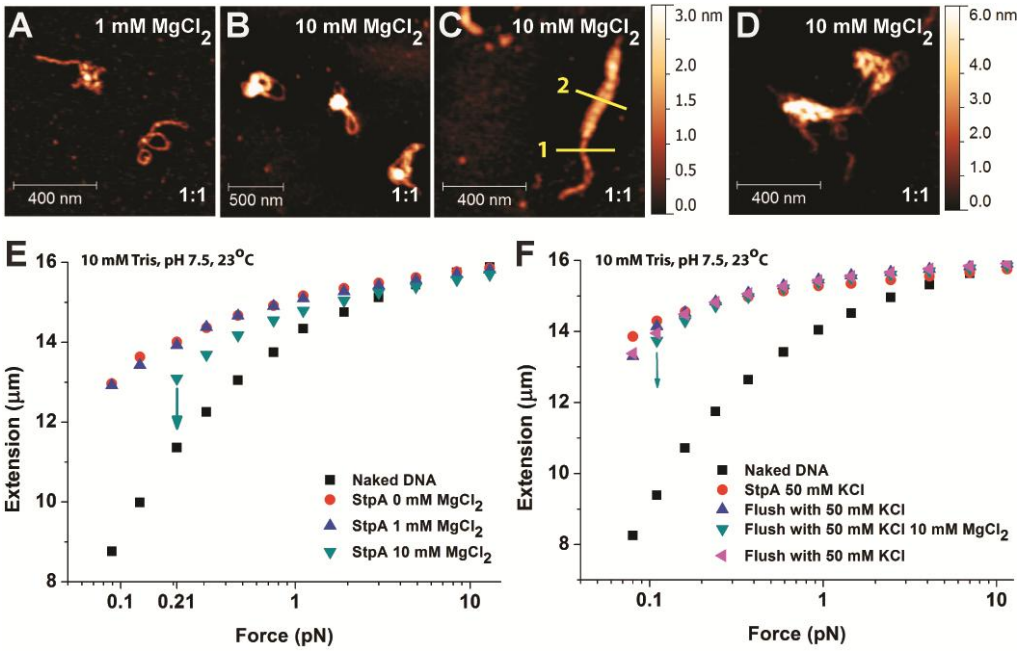

Figure 2.13 Magnesium chloride ($MgCl_2$) caused StpA to compact DNA via StpA nucleoprotein filaments self-interaction. (A) In 1 mM $MgCl_2$, AFM images of linearized φX174 DNA with 600 nM StpA showed similar conformation to Figure 3.4A. (B-C) At 10 mM MgCl2, the DNA was organized into higher order StpA-DNA complex aggregations. Analysis of the AFM image in panel C indicated the StpA coated DNA had an apparent width of 20.44 nm (yellow line 1), while the thicker region had an apparent width of 51.68 nm (yellow line 2). Subtracting the AFM tip widening effect (~ 12 nm), the thicker region is about 4 times thicker than the filament. (D) Linear 576 bp DNA with the same StpA:DNA ratio and in 10 mM $MgCl_2$ showed DNA aggregations. (E) Force-extension curves (FECs) of λ-DNA with 600 nM StpA in varying MgCl2 concentrations showed that StpA caused DNA stiffening at all tested magnesium concentrations while at 10 mM $MgCl_2$, StpA caused DNA folding at lower DNA pulling force (downward arrows). (F) FECs of StpA nucleoprotein filament, without the presence of StpA in the buffer, at different buffer conditions. DNA folding by StpA was only observed in the presence of 10 mM MgCl2 while no DNA folding was observed when $MgCl_2$ was removed from the buffer. This is further verified by another magnetic tweezers experiment which showed that in the absence of magnesium, the DNA was not folded by StpA even when held at a low DNA pulling force (~ 0.08 pN) for up to 20 minutes, which would otherwise promote DNA looping and thus any StpA DNA folding (Figure 3.15C).

To verify our AFM experiments data, we performed magnetic tweezers force-extension measurements of λ-DNA in the presence of magnesium. As expected, we observed DNA stiffening in experimental buffers containing 1-10 mM $MgCl_2$, and the level of DNA stiffening was not affected by magnesium (Figure 3.13E). No DNA

folding was observed in 1 mM $MgCl_2$ (blue up-triangles) but as the magnesium concentration was increased to 10 mM $MgCl_2$, (green down-triangles), the DNA started to fold when the DNA pulling force (tension) was lower than 0.2 pN. The DNA folding/unfolding time-course are shown in **Figure 2.15A**. We also showed that the effect of $MgCl_2$ on StpA DNA binding property is history independent (See **Fig. 2.15B**). Overall, the magnetic tweezers experiment data agree with the AFM imaging experiment data.

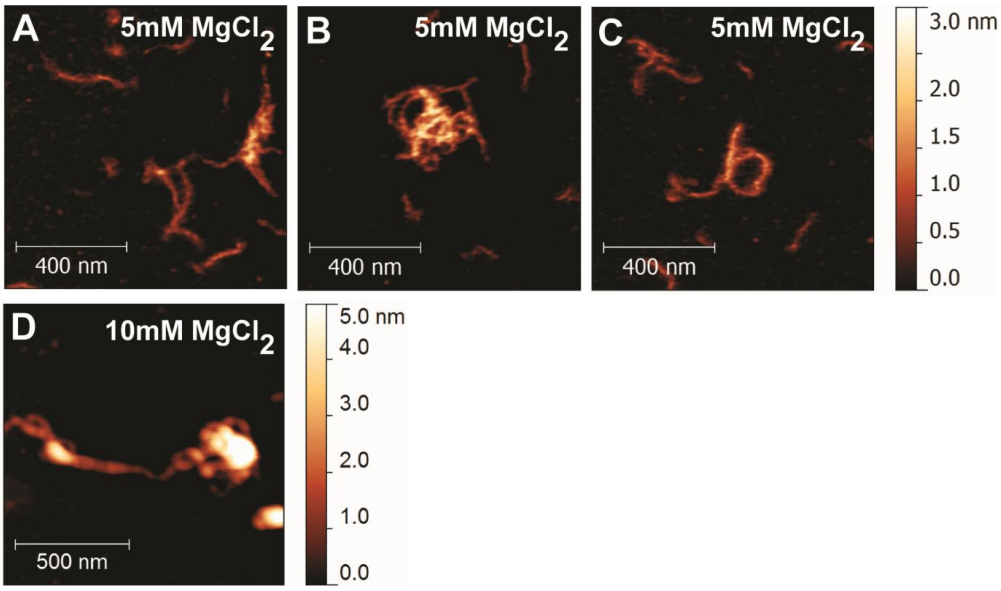

Figure 2.14 StpA compaction of short 576 bp DNA in 5 & 10 mM $MgCl_2$ buffer conditions. (A-C) AFM images of linear 576 bp DNA incubated with 1 StpA per 1 bp ratio in buffer containing 5 mM $MgCl_2$ showed the monomeric StpA nucleoprotein filaments were aggregated. (D) Increasing the magnesium concentration to 10 mM $MgCl_2$ resulted in a more severe aggregation of StpA nucleoprotein filaments.

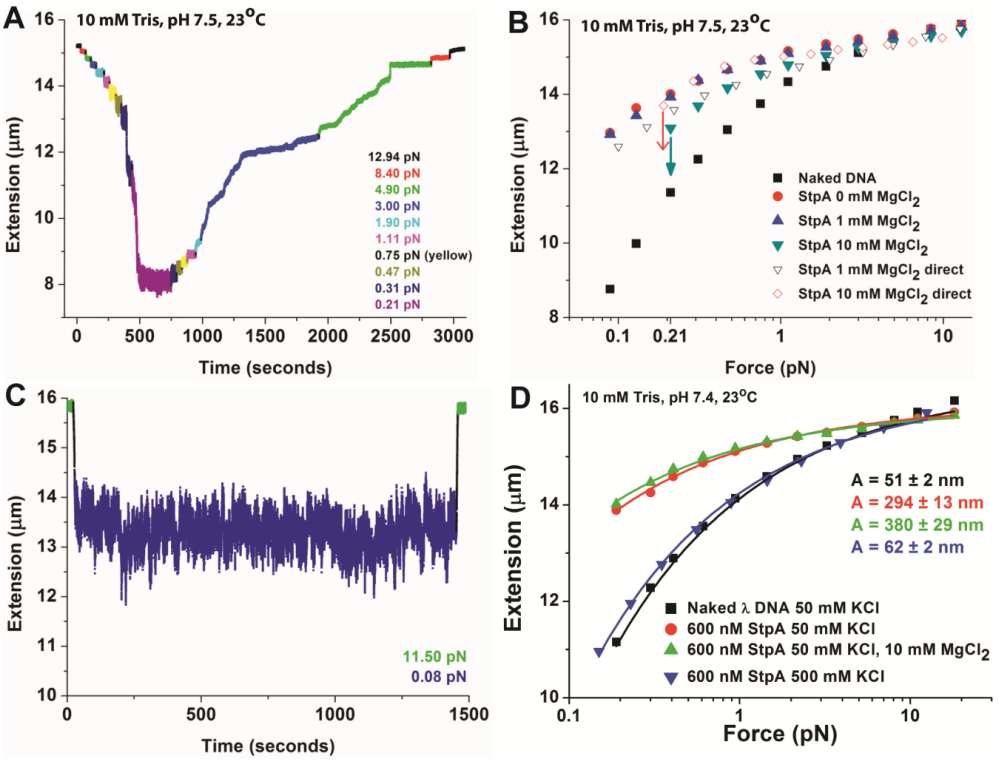

Figure 2.15 Magnetic tweezers studies on the StpA nucleoprotein filament compaction in the presence of magnesium chloride. (A) StpA nucleoprotein filament folding time-course showing the filament started folding at ~ 0.31 pN and by increasing the DNA pulling force to > ~ 4.90 pN, the filament original extension can be recovered. (B) Force-extension curves measurements of StpA nucleoprotein filament (λ-DNA) in buffer containing 1 mM or 10 mM $MgCl_2$, which was done on another λ-DNA, were similar to that measured on a single λ-DNA tether when $MgCl_2$ concentration was progressively increased from 0 to 1 to 10 mM. This indicated the magnesium effect is independent on the history of the nucleoprotein complex state. (C) In the absence of magnesium (buffer containing 0 mM $MgCl_2$), we showed that the StpA nucleoprotein filament did not fold when held at 0.1 pN pulling force for up to 20 minutes. This experiment was performed after it was shown that the same DNA used was folded when 10 mM $MgCl_2$ was included in the buffer (Fig. 3.13F). (D) The measurement of the intrinsic rigidity of StpA nucleoprotein filament, in the presence of DNA folding caused by magnesium, was performed by force-jump method. The measurement of the filament extension was done by rapidly changing the pulling force from a base line force that does not allow DNA to fold (i.e. ~ 10 pN) to the desired force, averaging the extension in a five seconds window, and then changing the pulling force back to the base line force. The short time window to measure the filament extension was to minimize the mixing of the DNA folding signals with the intrinsic DNA stiffening effects as the DNA folding had a slower kinetics. Using this method, we obtained the force-extension curves (FECs) in the absence of DNA folding, and fitted the FECs with the DNA WLC model to obtain the DNA or filament persistence length values (as indicated in panel D inset which were averaged values, N=9). All fittings have R^2 of >0.98.

The compaction of DNA in presence of high StpA DNA coverage and magnesium concentration cannot be explained by StpA DNA bridging (observed in

the absence of magnesium), which was due to the attraction between StpA nucleoprotein filament and DNA. One major reason is that the StpA DNA stiffening was saturated in presence of magnesium, and thus implies few or no naked DNA segments were left along the DNA tether. This was verified by a buffer exchange experiment between 0 and 10 mM $MgCl_2$, for a fully StpA-coated DNA tether in the absence of StpA in buffer (**Fig. 2.13F**) which showed reversible switching between StpA DNA stiffening in 0 mM $MgCl_2$ and simultaneous StpA DNA stiffening/folding at 10 mM $MgCl_2$. This indicated that the StpA compaction of DNA in the presence of magnesium is likely due to StpA nucleoprotein filaments self-interactions.

This model also predicts that, in the presence of magnesium, the StpA nucleoprotein filaments will aggregate to form higher-ordered StpA-DNA complexes, which is in agreement with previous studies (132) and our AFM imaging data (**Fig. 2.13A-D**). In addition, we showed that the StpA filament rigidity was preserved in the presence of magnesium (persistence length of 459.31 ± 93.76 nm (N = 6)) hence we predicted that the StpA nucleoprotein filaments formed in magnesium may also inhibit DNA access similar to that in the absence of magnesium (**Fig. 2.12**). This prediction was confirmed by the single-molecule DNase I digestion experiment (**Fig. 2.16**). Taking all of the above together, in the presence of magnesium, StpA formed a protective nucleoprotein filament with DNA and simultaneously compact the DNA into higher-ordered structures via StpA nucleoprotein filaments self-interaction.

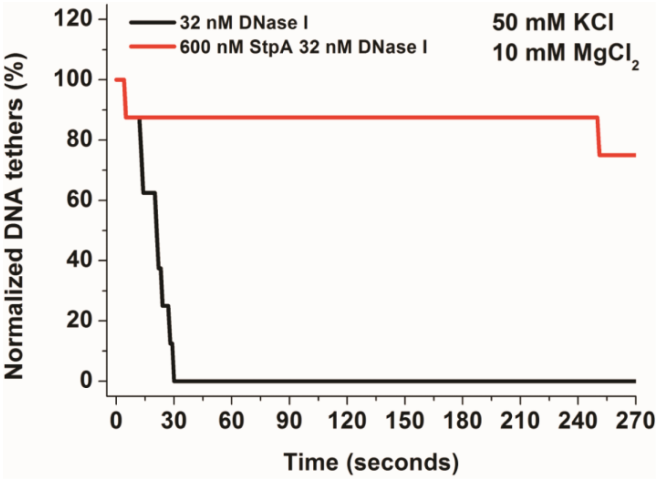

Figure 2.16 StpA nucleoprotein filament blocked DNA access in the presence of 10 mM $MgCl_2$. The activity of DNase I was strongly enhanced in 10 mM $MgCl_2$ buffer condition thus a lower DNase I concentration was used to achieve similar digestion rate as previous experiments in **Figure 2.12**. In 10 mM $MgCl_2$ buffer condition, the DNA tethers were protected from DNase I cleavage in the presence of 600 nM StpA. This is seen by comparing the red line (with 600 nM StpA, 8 DNA tethers) with the black line (without StpA, 8 DNA tethers).

2.4. Discussions & Conclusion

StpA forms a rigid protein filament along double-stranded DNA

From our AFM imaging and magnetic tweezers experiments, we showed that StpA formed a rigid nucleoprotein filament with DNA when StpA coverage along was sufficiently high. The StpA nucleoprotein filament was able to form (thus also stable) across a physiological-relevant range of salt, magnesium, temperature and pH, which suggests rigid nucleoprotein filament is a fundamental structure in StpA-DNA complexes. StpA organized DNA into three distinct types of StpA-DNA complex conformations; the linear rigid nucleoprotein filament, the DNA loops bridged by StpA nucleoprotein filament and DNA interactions ($\leq$ 1 mM $MgCl_2$), and the higher-ordered DNA compaction formed by StpA nucleoprotein filaments self-interactions (> 1 mM $MgCl_2$). The StpA nucleoprotein filament is a rigid structure with a bending persistence length of about 450 nm, which is around ten times as stiff as the DNA backbone.

The StpA nucleoprotein filament was not observed previously due to the type of AFM mica surface used and limited buffer conditions tested (132, 146). The above mentioned studies only reported StpA mediated DNA-bridging and aggregation and this might not be a complete representation of StpA multiple DNA-binding mode as the mica surface may accumulate large amount of divalent ions (i.e. magnesium) during rapid drying of the deposited sample. According to our results, the presence of high magnesium caused the StpA nucleoprotein filaments to form compacted higher-ordered structures, and this naturally makes it difficult to see the formation of rigid nucleoprotein filaments. In addition, single-molecule manipulation measurements which can directly measure the bending rigidity of DNA and protein-DNA complexes (i.e. **Fig. 2.8A-B**) were not employed in these studies. Our data also replicates the previous findings (132) by showing that at low StpA coverage along DNA (or low StpA concentration in solution), StpA caused DNA bridging (DNA loops) via StpA nucleoprotein filament interactions with DNA.

We do not exclude the possibility that the multitude DNA organizations by StpA is due to the concentration-dependent oligomerization states of StpA in solution (147, 148), For example, theoretical studies have shown that DNA bridging can be mediated by non-interacting H-NS dimers (149, 150). However, our data do not support this possibility as we showed that the coverage of StpA along DNA, and not StpA concentration (thus also oligomerization), is the major regulating factor in the kinetic competition between formation of StpA nucleoprotein filaments and DNA-bridging (**Fig. 2.17**). For example, at 1:1 StpA:bp ratio (300 nM StpA), we observed StpA DNA-bridging and not StpA DNA-stiffening. In contrast, with just StpA in solution, we observed StpA DNA-stiffening at similar StpA concentration (see **Fig. 2.9A**). Although we showed that the StpA multitude organization of DNA is based on StpA coverage along DNA, we do not yet know the oligomeric state of StpA that binds to DNA (i.e. if StpA works as monomers or dimers or even higher oligomers)

hence further studies are needed to elucidate the working oligomeric state of StpA, and even H-NS.

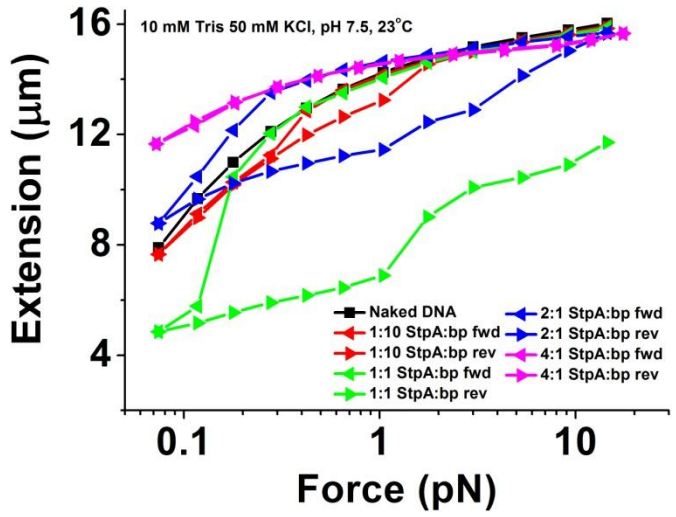

Figure 2.17 Magnetic tweezers experiments of λ-DNA in various ratios of StpA:bp. This was done by measuring the force-extension curves of λ-DNA in the presence of StpA and solution λ-DNA pre-incubated at the stated ratios. At 1:10 ratio (effective 30 nM StpA concentration), The DNA extension was slightly lower at 0.1 pN and a small amount of extension hysteresis was observed. Increasing to 1:1 ratio (300 nM StpA) resulted in DNA folding and thus larger hysteresis during the reverse force scan. Increasing the ratio to 2:1 (600 nM StpA), DNA stiffening was observed while the hysteresis was reduced. Finally, at 4:1 ratio (1,200 nM StpA), the DNA was very stiff and hysteresis had disappeared which indicated a fully-formed StpA nucleoprotein filament.

We wish to point out that in the bacterial cytoplasm, there are many nucleoid associated proteins (NAPs) that are able to compete with StpA for chromosomal DNA occupancy. The *in vivo* concentration of NAPs, if combined together, would modestly estimate to exceed 100 µM. Hence this would average to having one NAP binding to every 10 bp of chromosomal DNA which is of similar order to the ratios used in our AFM imaging experiments (i.e. 1:10 and 1:1 ratios). For the magnetic tweezers experiments, the StpA:bp ratio is not easily defined due to the nature of single-molecule manipulation experiments where the number of DNA tethers is not exactly known, and would vary across different flow cell. However, given the fact

that the density of DNA tethers in a flow cell was controlled to be low, we would estimate the StpA to DNA bp ratio to be a lot higher than that used in our AFM imaging experiments. Hence in magnetic tweezers experiments, only the concentration of StpA is meaningful. Of course, this may be circumvented if we add pre-incubated StpA-DNA complexes of a specified ratio, as in **Figure 2.17**, instead of just a specific concentration of StpA. This is because the added DNA molarity would be a lot more than the DNA tethers and thus the DNA tethers may be neglected in calculating the actual StpA:bp ratio. Also, since the *in vivo* StpA concentration is in the order of μM, our magnetic tweezers experiments using 0.6-2.4 μM of StpA are the most relevant to cellular conditions and is higher than the measured DNA-binding affinity of StpA (151). We do not observe any significant difference in StpA DNA-binding affinity when tested in all of our experimental buffer conditions using EMSA experiments.

Biological implications of StpA nucleoprotein filament

How StpA organizes DNA must be relevant for its role as a NAP in chromosomal DNA packaging and gene regulation. For its gene regulatory function, StpA mainly function as a negative regulator of gene transcription (29, 125). As revealed in this study, StpA nucleoprotein filament is the basis of how StpA organizes DNA into elongated filamentous structures, DNA loops or higher-ordered DNA condensates (**Fig. 2.8B & 2.13E**). We showed that the StpA nucleoprotein filament can protect the buried DNA from digestion or cleavage by DNA nuclease, DNase I. This is likely due to the StpA filament forming a physical barrier that can prevent DNase I from binding to the DNA to cleave it. Since the DNase I requires 6 bp of DNA for effective DNA cleavage (152), the *E.coli* RNA polymerase which requires 70-80 bp of DNA for transcription (153), would find it significantly harder to bind to the promoter site for transcription initiation. Hence we would like to propose that the

StpA nucleoprotein filament blocks the *E.coli* RNA polymerase from binding to its promoter site thus silencing the gene expression.

StpA has a copy number of 25,000 during its peak at *E.coli* late exponential growth phase, and considering the bacterial chromosome is 4.6 million bp in length (16), this would translates to an estimated 1 StpA per 200 bp of chromosomal DNA and an cellular StpA concentration of 10 μM. We argue that at such high StpA concentration, StpA nucleoprotein filament formation is likely the dominating StpA-DNA complex structure in *E.coli*. Similar to H-NS, StpA has preference DNA binding sites on the chromosomal DNA (154) which coupled with DNA occupancy competition with other NAPs, would likely resulted in StpA being localized to StpA high affinity sites. The highly localized StpA binding sites may then serve as nucleation sites to direct StpA cooperative binding which then lead to formation of the rigid StpA nucleoprotein filaments. This provides a plausible mode which explains how StpA nucleoprotein filaments selectively target genes for silencing

Our results that showed StpA can either bridge DNA or cause higher-ordered DNA compaction suggest StpA may also be involved in chromosomal DNA packaging. Specifically, we showed that, in the presence of $\geqslant$ 5 mM magnesium, StpA compacted DNA into higher-ordered condensed StpA-DNA complexes. As the estimated *E.coli* cellular magnesium concentration is about 4 mM (145), we propose that discrete StpA nucleoprotein filaments formed at high-affinity sites would interact with each other to aid chromosomal DNA packaging, in addition to their gene silencing functions.

Comparison between StpA and H-NS DNA organization properties

As StpA is the *E. coli* paralogue of the *E. coli* H-NS, and they both shared a common set genes silenced by them, it will be interesting to compare their similarities and

differences in DNA organization (**Fig. 2.18**). Although both H-NS and StpA are able to form rigid nucleoprotein filaments with DNA (19) (see **Fig. 2.8B** for StpA), they are distinct from each other in how they respond to environmental changes. The StpA nucleoprotein filament is stable against ionic strength changes within 50 – 300 mM KCl, temperature changes within 23–37^{o}C and pH changes within 6.6 – 8.8 (**Fig. 2.10A-C**). In contrast, the H-NS nucleoprotein filament was disrupted at 200 mM KCl or 37^{o}C buffer conditions (19).

The differential responses of the H-NS and StpA nucleoprotein filament to environmental stimuli suggest the StpA nucleoprotein filament is more stable than H-NS nucleoprotein filament, and may prove to be relevant to the cellular responses of H-NS and StpA during similar environmental changes. For example, when the cellular K^+ or temperature is elevated, StpA may be more resistive in maintaining its biological roles than H-NS since StpA nucleoprotein filament will be still able to maintain its structural integrity while H-NS nucleoprotein filament will be disrupted. Indeed, it has been shown that the H-NS suppressed StpA gene (125) was up-regulated when the growth medium osmolarity or temperature is increased (130), inferring the lost of H-NS silencing function during elevated osmolarity or temperature conditions. In addition, super-resolution microscopy has revealed that H-NS and StpA were localized differently in *E.coli* live cells (155). The above suggests further studies need to be conducted to determine the relationship between H-NS and StpA DNA organization properties to their *in vivo* functions and localizations.

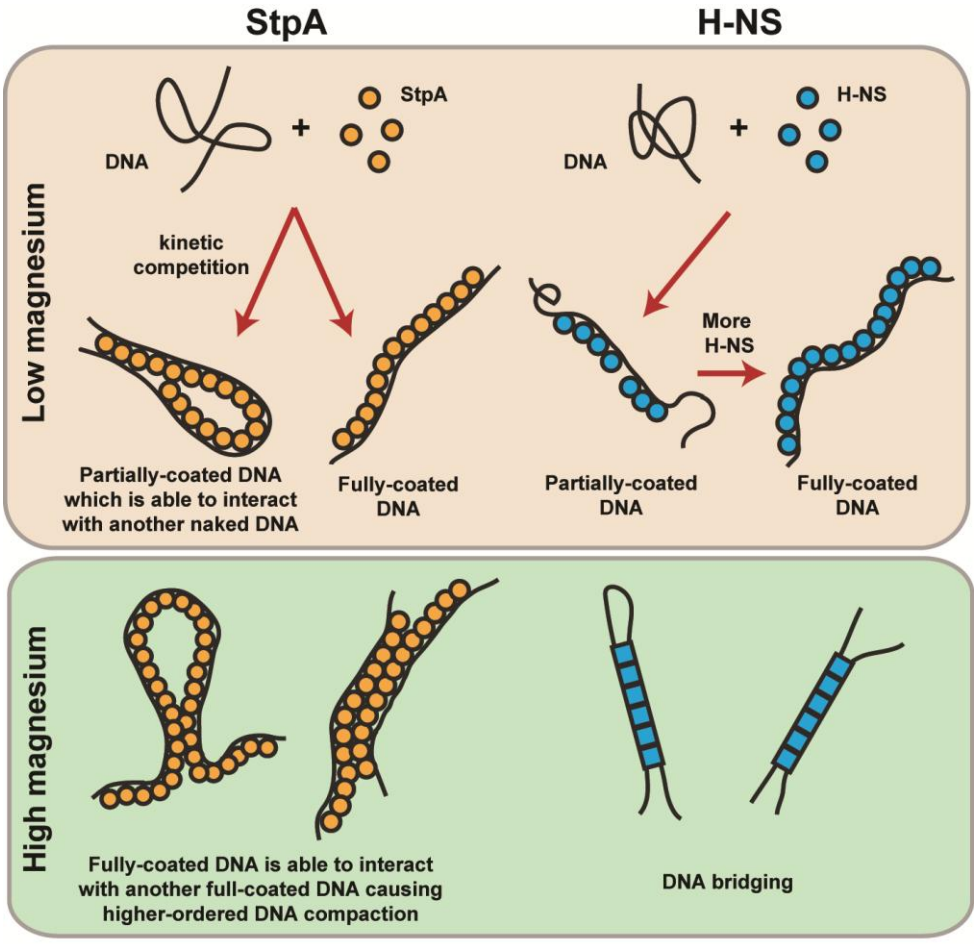

Figure 2.18 The comparison of H-NS and StpA DNA organization properties. In the presence of low magnesium ions concentration, the StpA (orange circles) forms rigid nucleoprotein filaments with DNA whereby the filament is able to interact with DNA to form StpA DNA bridges but would not be able to self-interact. In similar condition, the H-NS (blue circles) also forms rigid nucleoprotein filaments with DNA but it is relatively inert and does not interact with DNA or itself (19). In the presence of high magnesium ions concentration, the StpA still forms rigid nucleoprotein filaments, but it results in DNA compaction through the filaments self-interactions. In contrast, for similar conditions, H-NS does not forms rigid nucleoprotein filaments and instead, causes DNA bridging (19). The blue circles and squares depict different DNA-binding species of H-NS at low and high magnesium ions concentration respectively.

The StpA nucleoprotein filament ability to interact with DNA suggests the StpA filament is able to bind to two independent tracts of DNA. Interestingly, such DNA-protein-DNA filament scaffold model was proposed for H-NS (39), but is yet to be observed or verified in the case of H-NS. The H-NS filament is predominantly at low magnesium concentrations (< 2 mM) and once formed, it does not interact with DNA to form the proposed DNA-H-NS-DNA filament scaffold (19). At higher

magnesium concentration (> 5 mM), the H-NS predominantly forms DNA bridges and no filament is formed (19), which also does not support the DNA-H-NS-DNA filament scaffold model. Bearing all these, it seems now that the H-NS distinct DNA-binding modes are mutually exclusive and dependent on magnesium concentration, but we do not exclude that there may exists a range of magnesium concentration or any conditions whereby H-NS forms a DNA-H-NS-DNA filament scaffold. However, it would seem that the proposed DNA-protein-DNA filament scaffold model is more suitable for StpA at the present moment.

Since both H-NS and StpA function as NAP in *E.coli*, it will be interesting to compare their DNA compaction capability, in view of their roles in chromosomal DNA packaging. At low magnesium concentration conditions (e.g. < 2 mM), H-NS would not be able to compact DNA as it forms rigid nucleoprotein filaments which does not interact with DNA or itself to form compacted DNA (19). In contrast, at similar condition, StpA formed nucleoprotein filaments which can interact with DNA to fold DNA (provided free DNA are available). At high magnesium concentration conditions (> 5 mM), both H-NS and StpA are able to effectively compact DNA; H-NS forms DNA bridges which folds DNA while StpA forms nucleoprotein filaments which can self-interact to form highly compacted structures. It is difficult to pinpoint whether H-NS or StpA is more involved in chromosomal DNA packaging given the lack of *in vivo* relevant data, but the above direct comparison indicates StpA has a stronger DNA compaction capability than H-NS in both low and high magnesium concentrations conditions, and would suggests StpA potentially play a bigger role than H-NS in *E.coli* chromosomal DNA packaging.

Mechanically, the H-NS and StpA nucleoprotein filaments have distinct rigidity properties. The H-NS bending persistence length was reported to be about 130 nm which is around 2-3 times stiffer than the DNA value of 50 nm (41). In contrast, our work showed that the StpA nucleoprotein filament bending persistence

length is about 450 nm which is around 10 times stiffer than DNA. Hence the StpA filament formed along DNA is more rigid than H-NS's (at least 3-fold stiffer), and we attribute this difference to how the protein filaments are organized or formed along the DNA.

Nucleoprotein filament is a conserved structure important for H-NS-like proteins

In this work, the *E. coli* StpA has been shown to form rigid nucleoprotein filaments, similar to that of the *E. coli* H-NS. In parallel to this study, it was found that the rigid nucleoprotein filaments are also observed in other H-NS-like proteins (**Fig. 2.19**) such as the *Mycobacterium tuberculosis* Lsr2 (156) and *Pseudomonas aeruginosa* MvaT (157). Dan, a newly identified *E. coli* NAP expressed during oxidative stress condition, is also found to form rigid nucleoprotein filament (158). In all cases, the formation of nucleoprotein filament caused an increase in DNA-bending rigidity of the DNA-protein complexes. The DNA-stiffening effect of NAPs may then be interpreted as formation of rigid nucleoprotein filament. Henceforth, the DNA-stiffening effect of the archaeal alba protein (159) and eukaryotic high-mobility group B (HMGB) protein (160) suggests the formation of nucleoprotein filament by DNA-binding proteins in archaea and eukaryotic cells.

Evidently, there are an increasing number of studies showing the formation of nucleoprotein filament by chromosomal DNA-associated proteins. The formation of nucleoprotein filament implies an extensive stretch of protein coverage along dsDNA which potentially serve as a physical barrier to prevent access of other proteins to the dsDNA. This filamentous structure potentially serves as the bacteria analog to the eukaryotic transcription repressive structure; the nucleosome.

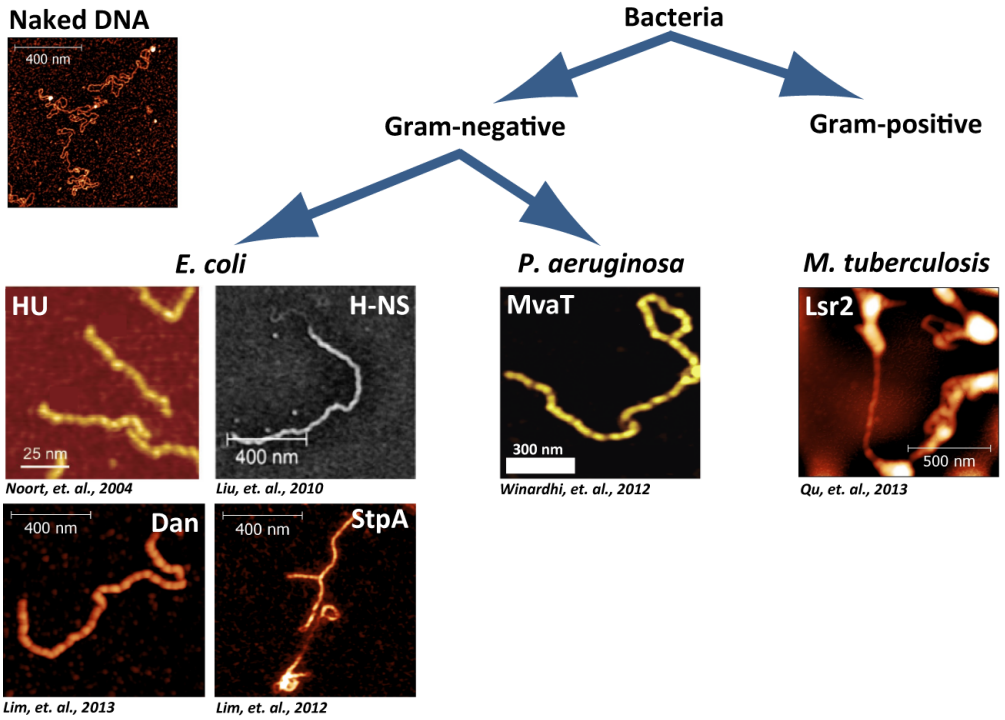

Figure 2.19 The bacteria NAPs and H-NS-like proteins that are found to form rigid nucleoprotein filaments. The accompanying AFM images are a compilation from various studies of NAPs that silence genes. Including this work, *E. coli* has four tested NAPs, that are known to be involved in gene silencing functions, that are able to form nucleoproteins filaments – HU (20), H-NS (19), StpA (23) and Dan (161). In addition, gene silencing NAPs from *P. aeruginosa*, MvaT (157) and *M. tuberculosis*, Lsr2 (156) are also shown to form such rigid nucleoprotein filaments.

Chapter 3

H-NS nucleoprotein filament is the structural basis for its gene silencing function

3.1. Introduction

The bacterial nucleoid-associated proteins (NAPs) are small abundant proteins that bind to chromosomal DNA and are heavily involved in gene regulation functions and chromosomal DNA packaging (16, 18, 162). The Histone-like Nucleoid Structuring (H-NS) protein is a major NAP in *Escherichia coli* (*E.coli*) that plays a key role in silencing numerous genes (62, 121). H-NS regulates approximately 5% of *E.coli* genes, and 80% of these are silenced by H-NS (26) including horizontally-acquired genes that are involved in pathogenesis (29). This point to the global gene silencer role H-NS play in *E.coli*. In addition to its gene regulatory function, H-NS has been proposed to be involved in chromosomal DNA organization through compacting DNA and interaction with DNA supercoiling (64, 163, 164).

H-NS has two distinct DNA-binding modes; rigid nucleoprotein filament formation and DNA bridging, which are regulated by divalent ions (19). This prompted us to ask a question on how these H-NS DNA-binding modes are used to mediate its *in vivo* functions of gene regulation and chromosomal DNA packaging (19, 40, 41, 165, 166). The recent emergence of rigid nucleoprotein filament formation by H-NS family proteins (e.g. *E.coli* StpA (23) and Dan (158),

M.tuberculosis Lsr2 (156), see chapter 2) provides an intuitive model to explain how these bacterial NAPs perform their gene silencing functions. In the previous chapter (Chapter 2), we showed that StpA nucleoprotein filament is able to prevent DNA-binding proteins from access the buried DNA, and we proposed that the filament may block the *E.coli* RNA polymerase from binding to its promoter site thus resulting in gene silencing. This model is supported by a study that showed the H-NS nucleoprotein filament was disrupted with environmental factors changes that are known to alleviate H-NS gene silencing functions *in vivo* (19, 28, 41, 167). In addition, the importance of NAP nucleoprotein filament was further proven when it was shown that the *Salmonella* anti-silencing protein SsrB could only displace H-NS from DNA when H-NS nucleoprotein filament was formed (44).

The above strongly suggests a strong relationship between the H-NS nucleoprotein filament and H-NS gene silencing functions. This led us to hypothesize that the structural basis of H-NS gene silencing functions is the formation of nucleoprotein filaments. We seek to test this hypothesis by determining whether the formation of H-NS nucleoprotein filament is disrupted in H-NS mutants that were previously shown to be defective in gene silencing. The obvious predictions are the H-NS mutant proteins that are unable to silence genes *in vivo* will not be able to form nucleoprotein filaments. While the H-NS mutants that are able to retain its gene silencing functions will be able to form the filaments. Since the formation of H-NS nucleoprotein filaments led to the stiffening of DNA, the elasticity of the DNA may be used to detect nucleoprotein filament formation by H-NS mutants. The AFM imaging and magnetic tweezers experiments provide a mean to measure the change in DNA elasticity upon addition of H-NS proteins (19, 168).

Here, we used AFM imaging and magnetic tweezers to examine four H-NS mutants (R15E, L26P, L30P and P115A) that defers from the native H-NS protein by a single amino-acid substitution, and were previously shown to be defective in gene

silencing *in vivo* (36, 38, 48, 169), Their DNA organization properties were probed by both AFM imaging and magnetic tweezers studies and then compared with the native H-NS data (hereafter termed as wtH-NS). As a positive control, similar experiments was also performed on a H-NS mutant (L30K) that was previously shown to still retain its gene silencing function after the single amino-acid substitution (169). We found that all four of the H-NS gene silencing defective mutants were unable to form rigid nucleoprotein filaments or that as rigid as the native nucleoprotein filament. Consistently, we showed that H-NS gene silencing mutant L30K retained its ability to form rigid nucleoprotein filaments. Collectively, our result showed that the formation of rigid H-NS nucleoprotein filament is required for the *in vivo* gene silencing functions of H-NS, and provide further ties between the *in vitro* studies of H-NS DNA organization properties and the *in vivo* studies of H-NS functions. This also shows that the rigid nucleoprotein filament is the structural basis for H-NS gene silencing functions.

3.2. Materials & Methods

H-NS protein mutation, expression and purification

We performed site-directed mutagenesis to *hns* gene that was inserted into the pET-28 plasmid. Individual single amino-acid substitution mutation was verified with DNA sequencing before subjecting to protein expression and purification protocols. All the proteins were induced by adding final 1 mM IPTG into the culture flasks when the cell growth reached OD_{600} of 0.5-0.6. The expressed proteins contain a C-terminal 6X HIS-tag which we used to purify the proteins using nickel column as described previously (19). The purified H-NS proteins were dialyzed against a buffer containing 10 mM Tris-HCl, 500 mM KCl, pH 7.5 to remove residual immidazole before concentrating to > 1 mg/ml and then storing in -20 °C with final 30 % (v/v)

glycerol. The purity of the proteins was verified by running SDS-PAGE while the concentration was quantified using UV-Vis absorbance spectroscopy at 280 nm with extinction coefficient of 9,999 $cm^{-1} M^{-1}$.

Mica preparation and atomic force microscopy imaging

Glutaraldehyde-modified mica (hereafter termed as glu-mica) was prepared as described previously (19, 142, 168). Briefly, 0.1 % (v/v) of freshly prepared (3-aminopropyl)-triethoxysilane (APTES) solution in deionised (DI) water was dropped onto the surface of a freshly cleaved mica and allowed to incubate for 10 minutes. The mica was then rigorously washed with DI water to remove unbound APTES or loosely bound from the APTES-coated mica surface before drying the surface with a stream of clean nitrogen gas. Next, a freshly prepared 1 % (v/v) glutaraldehyde solution in 1X PBS buffer (pH 7.5) was added onto the APTES-coated mica and allowed to incubate for at least 15-20 minutes. The mica was again rigorously washed with DI water to remove the unbound glutaraldehyde molecules and then dried with nitrogen gas. At this stage, the glutaraldehyde should be covalently bonded to the APTES-mica surface to form the glu-mica.

The H-NS-DNA complex samples were prepared by mixing 10 ng of linearized λ-DNA with an appropriate H-NS concentration (300 nM of protein and 10 ng of DNA in 50 µl sample volume equates to 1 protein per 1 DNA bp ratio) and is allowed to incubate for 20 minutes. The sample was then added to the glu-mica and allowed to incubate for 20 minutes. The density and incubation were chosen to achieve well-separated H-NS-DNA complexes (but sufficient sample population) on the glu-mica surface for single-molecule imaging. After incubation, the glu-mica was gently rinsed with 3 ml of 1X PBS buffer to remove any unbound H-NS-DNA complexes before dried gently with nitrogen gas and ready for AFM imaging experiments. The Agilent 5500 AFM (Agilent Technologies, U.S.A) was used to

perform the dried sample AFM imaging experiments with AC (tapping) mode. The AFM tip used had a specified resonance frequency of 300 Hz and a force constant of 40 N/nm. The scanning speed adopted during the experiments was set at 1 line per second. The AFM image resolution during the scanning was kept at 512 x 512 pixels unless otherwise stated. The AFM images were then processed with the freeware Gwyddion software (http://gwyddion.net).

Magnetic tweezers single λ-DNA force-response measurements

The transverse magnetic tweezers setup was used to stretch a single λ-DNA tether in the presence of proteins to measure the DNA force-response changes. The magnetic tweezers setup is similar to that described previously (19, 23, 139). The B-λ-B DNA used for tethering was prepared by incorporating multiple biotin-labelled dUTPs into both 5' overhangs of the λ-DNA using DNA polymerase. A flow cell was constructed as previously described in the materials & methods section in chapter 2 or in a previous study (19). To recap briefly, the 150-200 µl volume flow cell was made from a sandwich of glass slides and a coverslip whereby the coverslip long edge was polished and functionalized with streptavidin. The flow cell was blocked with 10 mg/ml of Bovine Serum Albumin (BSA) for at least 1 hour at room temperature before adding B-λ-B DNA (500 pg/µl). The DNA was allowed to incubate for 10 minutes to let one end of the B-λ-B tethered to the streptavidin-coated coverslip edge before washing away the untethered B-λ-B. Streptavidin-coated 2.8 µm magnetic beads was then added into the flow cell and allowed to incubate for 20 minutes to allow B-λ-B DNA tethers to form.

The λ-DNA tether extension was calculated by measuring the distance between the magnetic bead centroid position and the edge of the tethered surface with offset consideration of the magnetic bead size. This was done using a virtual instrument (VI) written using the LabVIEW program (National Instruments, U.S.A). The force

stretching the DNA tether was calibrated as described in chapter 2 materials & methods section. The force-extension curve (FEC) of the DNA tether was obtained by measuring the DNA tether extension (averaged value within 25 seconds) at different force points, starting with decreasing the force and then increasing the force again (hereafter termed as forward and reverse force scans respectively). The force-jump FECs measurements were performed as previously described in chapter 2 materials & methods. Briefly, the DNA was held at a baseline force of 10 pN to prevent DNA folding by H-NS, and the force was quickly changed to the desired measurement force for 1 second to measure the DNA extension before returning to the baseline force. This allowed us to measure the intrinsic DNA extension due to H-NS DNA stiffening before DNA folding starts to occur. By repeating this process over several force points, we can obtain a FEC that is not affected by any DNA folding and allow us to quantify the intrinsic bending rigidity of the H-NS nucleoprotein filament.

3.3. Results

H-NS gene silencing defective mutants failed to form wtH-NS-like nucleoprotein filaments

λ-DNA was incubated with wtH-NS at 5:1 protein/DNA bp ratio (1.5 μM protein) in imaging buffer (10 mM Tris, 50 mM KCl, 2 mM $MgCl_2$, pH 7.5) before depositing on the glu-mica surface for AFM imaging studies. 2 mM $MgCl_2$ was added into all experimental buffers to better relate the observations to *in vivo* situation. After incubation with wtH-NS, we observed the formation of rigid nucleoprotein filaments as can be seen from the evidently extended and thick protein-coated DNA complexes (**Fig. 3.1A & B**). This is in agreement with a previous study (19), and serves as a wild-type control for the following mutant AFM imaging studies. Although majority of the H-NS-DNA complexes were rigid nucleoprotein filaments, we saw that some

parts of the complexes are bridged which we attributed it to H-NS DNA bridging (**Fig. 3.1B, yellow arrows**). This is also consistent with the previous AFM imaging studies of H-NS-DNA complexes in buffer containing 1 mM $MgCl_2$ (19).

We performed similar AFM imaging experiments with the four H-NS mutants (R15E, L26P, L30P and P115A) that were defective in their gene silencing functions. We consistently found that the H-NS-DNA complexes formed by these H-NS mutants had dramatic differences in conformation as compared to the wtH-NS (**Fig. 3.1C-J**). We found that the R15E-DNA complexes had highly heterogeneous conformation (**Fig. 3.1C & D**) with localized DNA bundles and aggregates (**Fig. 3.1D, yellow arrow**). In the case of H-NS mutants L26P and L30P, we observed large-scale globular DNA aggregations (**Fig. 3.1E & F for H-NS L26P and 3.1G & H for H-NS L30P**). In the case of the H-NS C-terminal mutant P115A, we also observed similar globular DNA aggregation (**Fig. 3.1I & J**). In general, all the H-NS gene silencing defective mutants exhibited dramatically different H-NS-DNA complex conformations from the elongated nucleoprotein filaments formed by wtH-NS. When we performed AFM imaging experiments using the H-NS gene silencing mutant L30K, we observed rigid nucleoprotein filament formation (**Fig. 3.1K & L**) and occasional H-NS DNA bridging (**Fig. 3.1L, yellow arrow**) that is similar to the wtH-NS control (**Fig. 3.1A & B**).

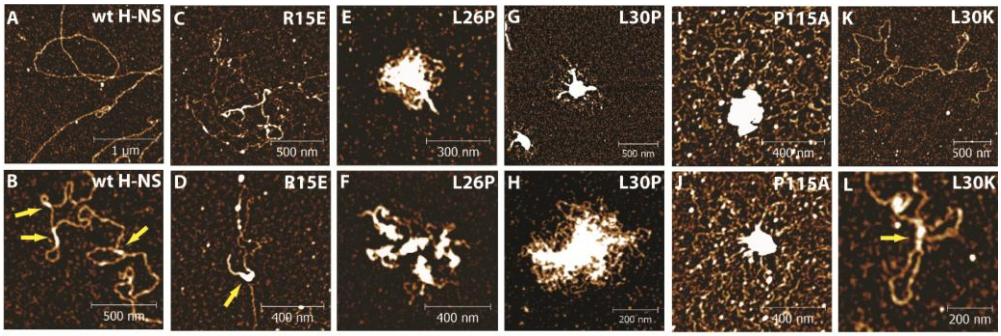

Figure 3.1 AFM images of H-NS-DNA complexes formed by wtH-NS and H-NS mutants. (A & B) λ-DNA (10 ng) incubated with wtH-NS (1.5 µM) showed rigid nucleoprotein filament formation with occasional H-NS-mediated DNA hairpin formations as indicated by yellow arrows in panel B. (C-J) All the gene silencing

defective H-NS mutants had a distinct difference in H-NS-DNA complex conformations as compared to wtH-NS. (C-D) The R15E-DNA complexes were highly heterogeneous DNA-protein complex with occasional small-scale DNA condensation as pointed out by the yellow arrow in panel D. (E & F, G & H) The H-NS mutants L26P and L30P-DNA complexes were large globular DNA aggregates. (I & J) The H-NS mutants P115A also showed similar results as H-NS mutants L26P and L30P. (K & L) In contrast, the H-NS mutant L30K, which retains its gene silencing capability, exhibited elongated H-NS-DNA complex conformations with occasional DNA hairpin formations (indicated by the yellow arrow in panel L) that are similar to wtH-NS. The AFM images Z-axis were renormalized with a scale of 0-1.5 nm.

H-NS gene silencing defective mutants were unable to stiffen DNA like wtH-NS

Using AFM imaging, we showed that the H-NS gene silencing defective mutants were unable to form extend H-NS-DNA complex conformations that are atypical of the wtH-NS rigid nucleoprotein filament, which suggests these H-NS mutants may be unable to form rigid nucleoprotein filament. However, AFM imaging conformational analysis of protein-DNA complexes are limited, and do not reveal nucleoprotein filament formation if strong DNA condensation follows the formation of filament. In other words, actual rigid nucleoprotein filament formed by the H-NS mutants may be buried in condensed H-NS-DNA structures such as those seen with H-NS mutants L26P and L30P (**Fig. 3.1E & F for H-NS L26P and 3.1G & H for H-NS L30P**). To resolve this, we used the transverse magnetic tweezers to investigate a single DNA tether force-response in the presence of these H-NS proteins, and quantified their changes to the DNA bending rigidity (87). The transverse magnetic tweezers was setup as previously described (19, 139, 168) (**Fig. 3.2A**).

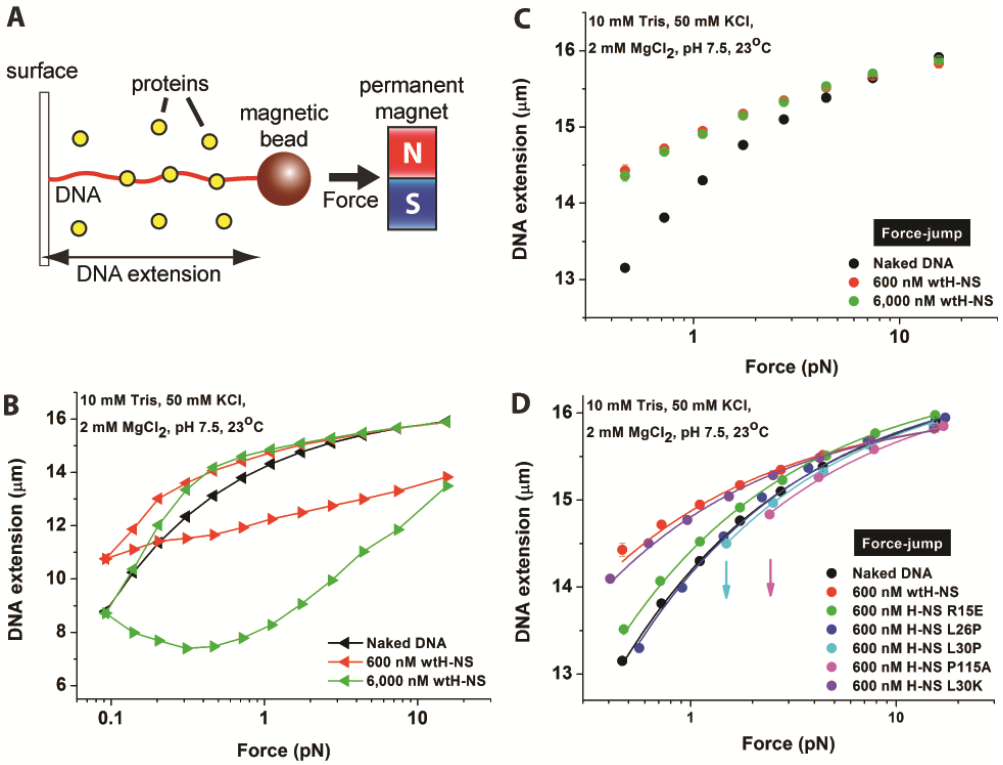

Figure 3.2 Magnetic tweezers studies of λ-DNA tether in the presence of wtH-NS or H-NS mutants. (A) The cartoon drawing of the transverse magnetic tweezers setup whereby a λ-DNA tether is stretched by a magnetic force imposed on the magnetic bead. (B) The force-extension curves (FECs) of the λ-DNA in the presence of saturating binding H-NS concentrations (600 and 6,000 nM H-NS). The forward and reverse force scan curves are represented by left-triangle and right-triangle respectively. Both concentrations of wtH-NS showed co-existence of DNA stiffening and folding. (C) FECs of λ-DNA measured in the same condition as panel B but with the force-jump method. The H-NS induced DNA folding was eliminated from both 600 and 6,000 nM wtH-NS force-jump FECs and revealed H-NS DNA stiffening was saturated at 600 nM H-NS concentration. (D) Force-jump FECs of wtH-NS and gene silencing defective H-NS mutants at saturated DNA-binding 600 nM concentration. Significant DNA stiffening was observed for both the wtH-NS and the gene silencing retentive H-NS mutant L30K mutant. Weaker DNA stiffening was observed for the gene silencing defective H-NS mutant R15E. No or negligible DNA stiffening were observed for the rest of the gene silencing defective H-NS mutants (H-NS L26P, L30P and P115A).

Figure 3.2B shows the force-extension curves of a λ-DNA tether incubated with 600 and 6,000 nM wtH-NS, and in the same experimental buffer as the AFM imaging experiments. In the presence of 600 nM wtH-NS, during the forward force scan (**Fig. 3.2B, red-left triangles**), the λ-DNA extension was significantly longer as the DNA pulling force was reduced which indicated the DNA was stiffened by H-NS. When the force was increased back gradually (reverse force scan process) (**Fig. 3.2B,**

red-right triangles), we observed that the DNA extension could not immediately return to its original extension thus it resulted in a large hysteresis between the forward and reverse force scan curves. This implies that other than H-NS DNA stiffening, H-NS also caused DNA folding. However, the DNA extension returned to its original extension when held at a high force of ~ 15 pN for sufficiently long enough time (~ 2-5 minutes). Once the DNA extension returned to its original extension, the H-NS concentration was increased to 6,000 nM and force-extension curve measurements were performed. We found that co-existence of DNA stiffening and folding were also observed at 6,000 nM wtH-NS (**Fig. 3.2B, green triangles**) and the hysteresis (between forward and reverse force scans) became larger, which is likely due to the effect of more free H-NS proteins in solution. The above results suggest that at the physiologically relevant magnesium concentration of 2 mM, wtH-NS simultaneously cause DNA stiffening and DNA folding. This is consistent with what we saw in our AFM imaging data (**Fig. 3.1A & B**).

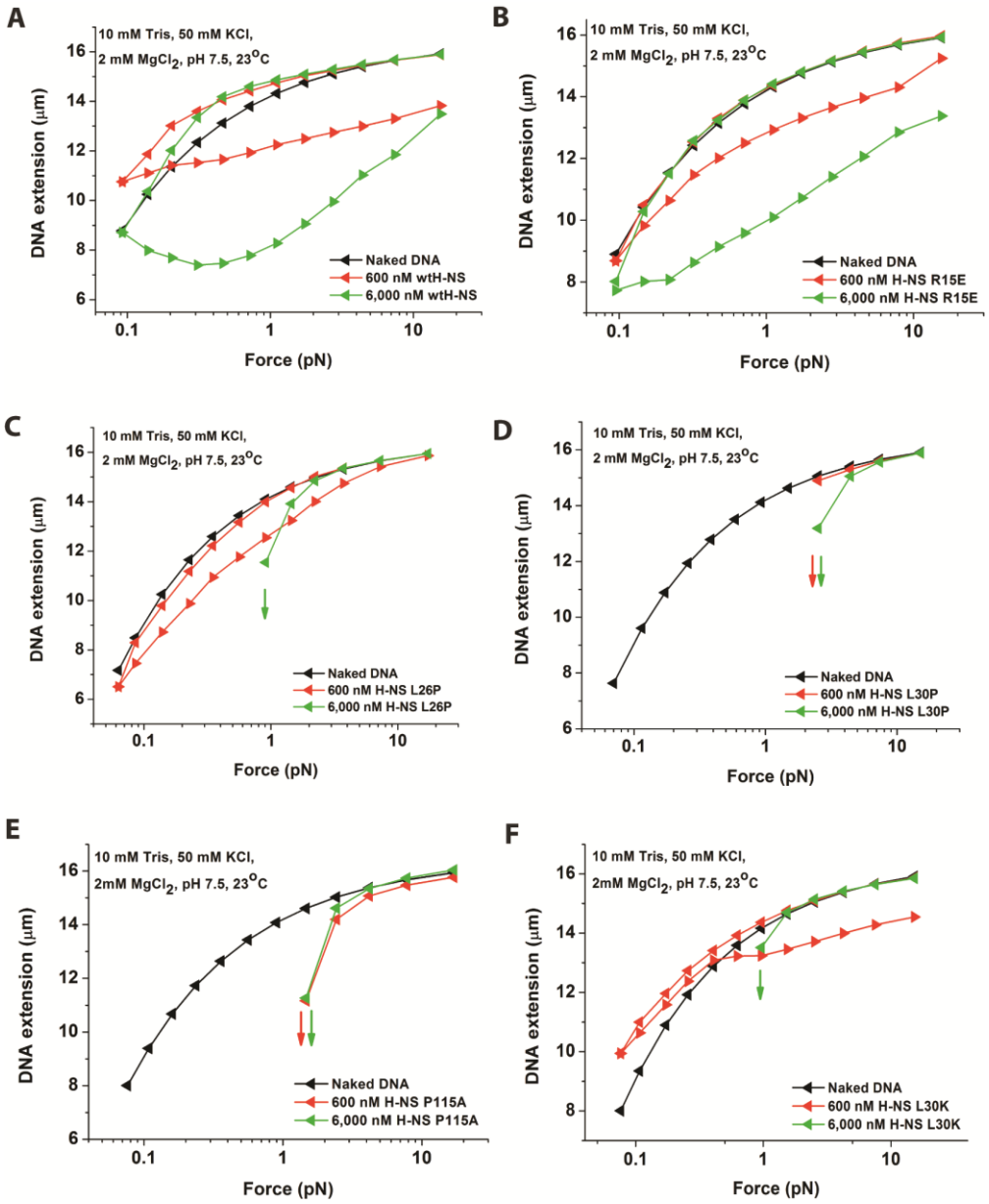

Figure 3.3 Magnetic tweezers force-extension curve measurements of λ-DNA in the presence of wtH-NS or H-NS mutants. (A Taken from Figure 4.2B for ease of comparison. In the presence of 600 and 6,000 nM wtH-NS, co-existence of DNA stiffening and folding was observed. (B-E) For all H-NS gene silencing defective mutants, only DNA folding and DNA extension hysteresis were observed as indicated by DNA extension hysteresis (e.g. H-NS R15E mutant, panel B) or by downwards arrows indicating DNA folding (e.g. H-NS L30P mutant, panel D). (F) In the case of H-NS gene silencing mutant L30K, we observed similar co-existence of DNA stiffening and folding as wtH-NS (panel A). However when H-NS L30K concentration was increased to 6,000 nM, we observed strong folding of DNA folding as pointed out by the downwards arrow.

In the case of H-NS mutants, R15E, L26P, L30P & P115A, we only observed DNA folding or large DNA extension hysteresis (**Fig. 3.3B-E**) while no DNA

stiffening was observed. In contrast, for the H-NS gene silencing mutant L30K, we observed co-existence of DNA stiffening and folding (**Fig. 3.3F**) that is similar to that of wtH-NS (**Fig. 3.3A**). Although the force-extension curve data is in full agreement with the AFM data, we do not exclude the possibility that DNA folding by H-NS mutants may obscure the DNA stiffening effect of the mutants and thus affects the measurement of the DNA bending rigidity.

To circumvent the effect of DNA folding, we adopted the force-jump method (see Materials & Methods). This method minimizes the effect of DNA folding on the DNA extension measurements. To determine that the force-jump method does not have a bias effect to DNA force-response measurement, we compared the FECs obtained from the standard and force-jump method and showed that there was no difference between the two methods (**Fig. 3.4**). This means both methods allow us to probe the steady-state value of DNA extension upon reaching the desired DNA force. This is expected since DNA longitudinal (direction of force) relaxation is significantly faster than that in the transverse direction (170). The force-jump FECs of λ-DNA in 600 nM and 6,000 nM wtH-NS revealed DNA stiffening that was saturated by 600 nM wtH-NS as evident from the overlapping curves (**Fig. 3.2C**).

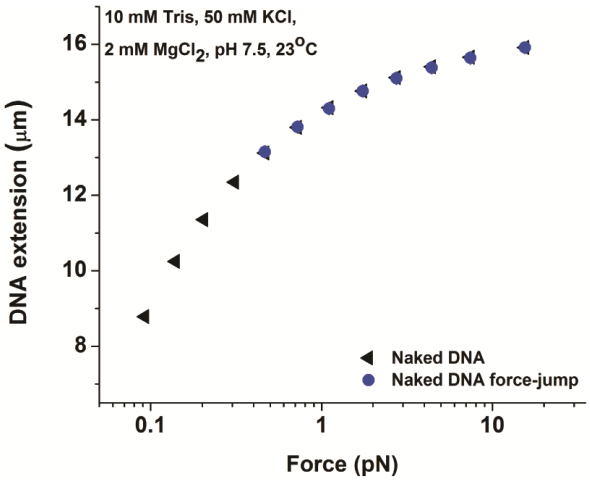

Figure 3.4 Comparison of λ-DNA force-extension curves that were obtained from standard method or the force-jump method. The FECs overlaps entirely which

suggests the force-jump method does not cause an biased in the DNA elasticity measurement.

The force-extension curves of the λ-DNA in the presence of H-NS mutants were repeated with the force-jump method (**Fig. 3.5B-E**). We found that all the H-NS gene silencing defective mutants (R15E, L26P, L30P and P115A) did not exhibit DNA stiffening which is similar and confirmed the FEC data obtained from the standard method (**Fig. 3.3B-E**). In addition, we also saw that increasing the protein concentration 10-fold (to 6,000 nM) did not result in DNA stiffening and instead resulted in aggressive DNA folding. In contrast, the H-NS gene silencing mutant L30K data revealed strong DNA stiffening which is of similar level as wtH-NS's (**Fig. 3.5A**). However, we also saw that increasing the H-NS mutant L30K concentration to 6,000 nM caused strong DNA folding, similar to **Figure 3.3F**. Comparing the wtH-NS and H-NS mutants force-jump FECs (**Fig. 3.2D**), we can see that the force-response data can be clearly classified into two distinct groups; rigid protein-DNA complex (wtH-NS and H-NS mutant L30K) and DNA-like protein-DNA complex (DNA, H-NS mutant R15E, L26P, L30K and P115A). To quantify the bending rigidity of each H-NS-DNA complex, we fitted the force-jump FECs with Marko-Siggia Worm-Like Chain (WLC) model (86) (**Fig. 3.2D solid lines**) which yielded the H-NS-DNA complex contour length and persistence length (also the bending rigidity). The results are summarized in **Table 1**.

	Naked DNA	Wt H-NS	H-NS R15E	H-NS L26P	H-NS L30P	H-NS P115A	H-NS L30K
Apparent contour length (nm)	16491.02 ± 9.99	16118.40 ± 20.30	16510.85 ± 9.04	16527.77 ± 20.41	16534.54 ± 25.51	16461.38 ± 11.94	16141.99 ± 18.65
Apparent persistence length (nm)	53.10 ± 0.92	173.85 ± 10.87	64.18 ± 1.20	50.29 ± 2.18	45.95 ± 1.65	44.46 ± 1.54	151.39 ± 7.62

Table 3.1 The H-NS-DNA complex contour length and persistence length obtained from the Marko-Siggia WLC model fitting to the H-NS-DNA complexes FEC. All the fittings have a R2 of > 0.99. All computed fits were obtained from the N=5 independent experiments.

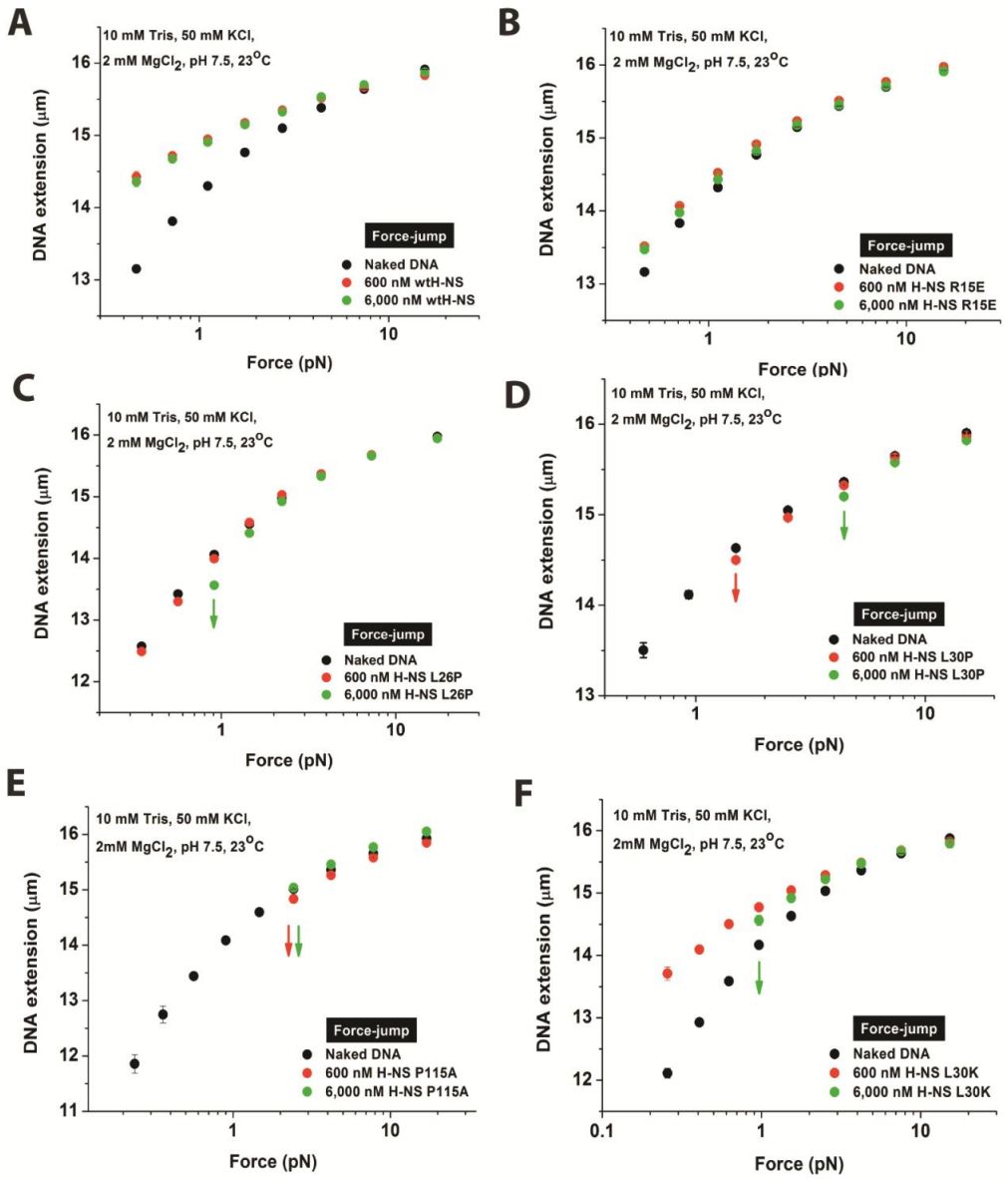

Figure 3.5 The force-extension curves of H-NS-DNA complexes obtained with the force-jump method. (A) H-NS DNA stiffening was observed, and the stiffening effect achieved saturation at 600 nM wtH-NS concentration. (B-E) All the H-NS gene silencing defective mutants did not cause DNA stiffening as evident from the overlapping FECs with the naked DNA's. Consistent with the standard FECs data, we observed DNA folding in these mutants. (F) The H-NS gene silencing mutant L30K caused strong DNA stiffening which is similar to that observed in wtH-NS. In addition, we also observed co-existence of DNA stiffening and folding when the concentration was increased to 6,000 nM, which is consistent with the standard FEC data (**Fig. 3.3 F**).

The WLC model fittings revealed the DNA contour length did not significantly change (< 2.5%) in all cases, even in the case where DNA stiffening was saturated. However, the apparent DNA persistence length showed great variation

across the tested H-NS mutants. The measured values confirmed what was already visually suspected, that the wtH-NS and H-NS gene silencing mutant L30K caused similar stiffening of DNA; the wtH-NS persistence length is 173.85 ± 10.87 nm while the H-NS mutant L30K is 151.39 ± 7.62 nm. Also as expected, all the H-NS gene silencing defective mutants have almost similar persistence length value to the naked DNA. We also like to point out that the force-jump FEC measurements of H-NS mutants L30P and P115A were pre-maturely terminated due to strong DNA folding (**Fig. 3.2D**, see downward arrows), although it is unlikely any DNA stiffening effect by these mutants were obscured by the folding.

The above clearly shows that all the tested H-NS gene silencing defective mutants lost their ability to form rigid nucleoprotein filament with DNA, while the H-NS mutant retains the ability to form rigid nucleoprotein filament.

3.4. Discussions & Conclusion

H-NS rigid nucleoprotein filament formation is lost in gene silencing defective point mutations

From our single-molecule studies on the H-NS mutants' ability to form nucleoprotein filaments, we collectively showed that the rigid nucleoprotein filament formation directly correlates with the H-NS ability in mediating gene silencing. The four H-NS mutants (R15E, L26P, L30P and P115A) that lost their gene silencing functions *in vivo* (36, 38, 48, 169) also lost their ability to form rigid nucleoprotein filaments. This was proven by visualizing the H-NS-DNA complexes conformation and measuring the complexes force-response. We also showed that single amino-acid substitution mutation is not responsible for the lost of nucleoprotein filament formation but rather the lost of its gene silencing function. This is supported by the observation that the H-NS mutant L30K, which retains its gene silencing function, is able to form rigid

nucleoprotein filament. Hence, we conclude that the formation of H-NS nucleoprotein filament is critical and provides a structural basis to H-NS gene silencing mechanism.

Co-existence of H-NS nucleoprotein filament and DNA bridging in physiological Mg2+ conditions

Before the discovery of H-NS nucleoprotein filament,(19), it was believed that H-NS only causes DNA bridging which leads to DNA hairpin conformations (40). The two DNA-binding modes of H-NS are reconciled by a study which showed magnesium can regulate the two DNA-binding modes; at 2 mM or lower magnesium concentrations, H-NS prefers to form rigid nucleoprotein filaments while at higher magnesium concentrations, H-NS causes DNA hairpins formation through bridging DNA segments (19). Although it has been suggested that H-NS DNA bridging mode is mediated by H-NS dimers (166, 171), the mediating H-NS oligomeric state involved in rigid nucleoprotein filament is not known. It is reasonable to postulate that the oligomeric state may be higher than dimer since H-NS form higher oligomers at higher concentrations (37, 148). However, we also do not exclude the possibility that both DNA-binding modes are mediated by the same H-NS oligomeric state, which in other words, suggests that the H-NS DNA hairpin structures are formed through H-NS nucleoprotein filament bridging with a DNA segment. This model is supported by a structural analysis study that predicted H-NS filaments can bridge two DNA segments to form a DNA-H-NS-DNA nucleoprotein filament (39). Our study which was performed at 2 mM magnesium concentration, though is physiological relevant, was also done in a grey area where both H-NS nucleoprotein filament and DNA bridging co-exists, thus suggesting a possibility of a H-NS nucleoprotein filament that may be able to interact with another DNA to form DNA-H-NS-DNA complexes.

Possible H-NS gene silencing mechanisms based on nucleoprotein filament formation

Before the emergence of H-NS nucleoprotein filament, models on how H-NS mediates its gene silencing function are mostly based on H-NS DNA bridging properties. For example, a current existing model is that H-NS traps the *E.coli* RNA polymerase inside a DNA hairpin loop that is stabilized by H-NS DNA bridging and prevents the RNA polymerase from promoter clearance (33, 43, 172). However, our work here strongly suggests that H-NS nucleoprotein filament should be considered in models that describe how H-NS mediate gene silencing. Hence we propose three alternative H-NS gene silencing mechanisms based on the H-NS nucleoprotein filament (**Fig. 3.6**). All the three models require H-NS to be specifically recruited to the RNA polymerase binding site(s) and allow H-NS to spread along the DNA to form a nucleoprotein filament. This scenario was previously proposed and supported by the cooperative DNA binding nature of H-NS (33, 43).

After H-NS forms the nucleoprotein filament at the RNA polymerase promoter site, the first possible mechanism which by H-NS can use to silence genes is that the filament directly serves as an extensive barrier to block the RNA polymerase from accessing the promoter site (**Fig. 3.6A**). This model is consistent with studies showing H-NS protection of DNA from nuclease digestion (34, 41). The model also provides a direct mechanism to explain how H-NS can restrict RNA polymerase accessibility to DNA as shown in a study (29). The second model is that the H-NS nucleoprotein filament impedes RNA polymerase during the elongation process (**Fig. 3.6B**). The third model is the trapping of RNA polymerase in a DNA hairpin loop formed by H-NS nucleoprotein filament bridging with DNA thus preventing promoter clearance of RNA polymerase (**Fig. 3.6C**). Although this trapping model is

similar to what was proposed (42), the difference is that the DNA bridging is mediated by a nucleoprotein filament.

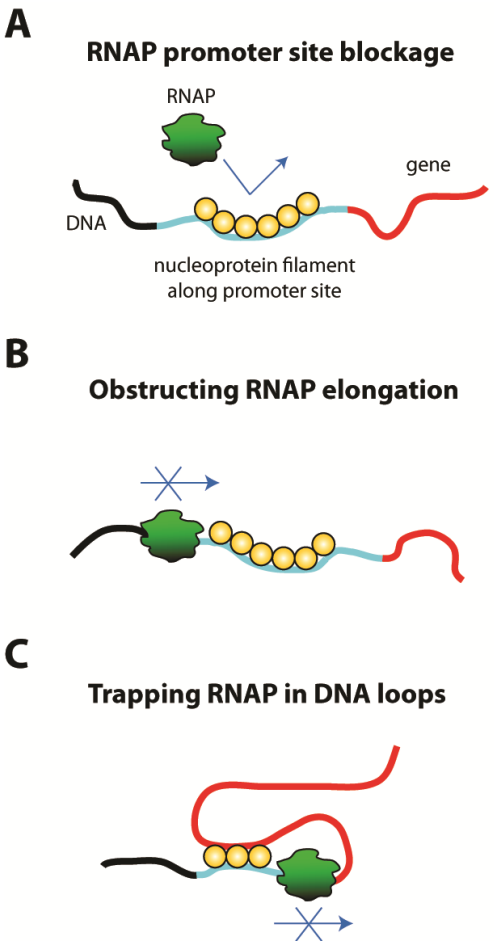

Figure 3.6 The proposed mechanisms of how H-NS performs its gene silencing function based on the nucleoprotein filament. (A) A H-NS nucleoprotein filament formed at the promoter site blocks RNA polymerase from binding. (B) The filament is able to impede the bound RNA polymerase from elongating. (C) The filament bridges with a distal DNA segment to form a DNA hairpin which traps the RNA polymerase and prevents promoter clearance.

Nucleoprotein filament: a conserved structure for transcription silencing in the prokaryotes?

We argued in the previous chapter that nucleoprotein filament formation in bacteria NAPs may be a conserved nucleoprotein structure, as evident from the emergence of many studies reporting the formation of such filaments by NAPs. Here, we showed

that the nucleoprotein filament is important for H-NS gene silencing, and this prompts us to wonder if the bacterial NAP nucleoprotein filament is a conserved canonical nucleoprotein structure utilized by the bacteria in repressing transcription, akin to the eukaryotic nucleosome (**Fig. 3.7**). The nucleosome is a globular nucleoprotein structure formed by DNA molecule wrapping approximately twice around the histone octamer protein core. The structure prevents transcription factors from accessing the wrapped DNA (173, 174), and the nucleosome unwrapping dynamics regulate transcription dynamics (175, 176). The bacterial NAP nucleoprotein filament provides similar observations and this warrants future experiments entailing bioinformatics, genetics, and biochemical studies to investigate the role(s) of nucleoprotein filament in bacterial transcription regulation.

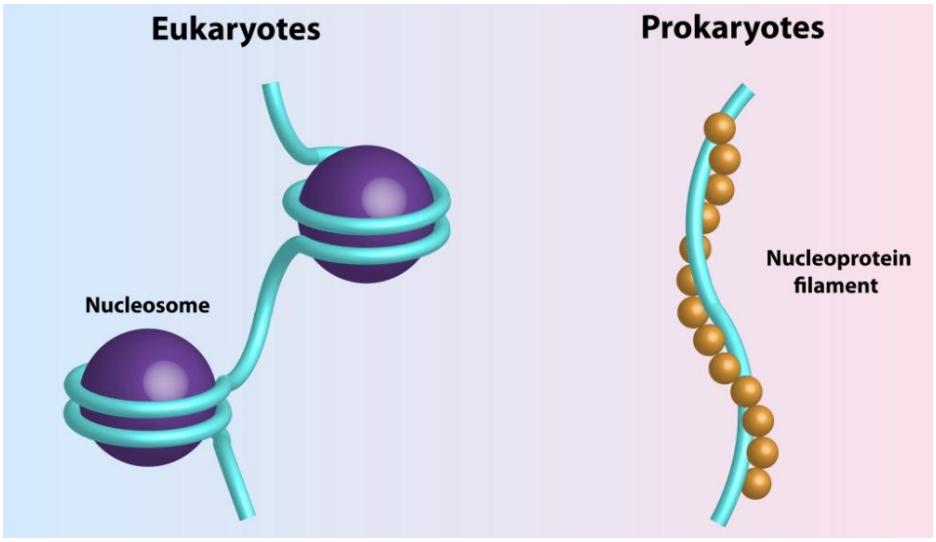

Figure 3.7 Analog comparison of transcription silencing nucleoprotein complexes in eukaryotes and prokaryotes.

Chapter 4

Two distinct DNA-binding modes of H-NS differentially regulate DNA supercoiling

4.1. Introduction

The right-handed DNA double-helix has a helical pitch of h = 3.6 nm, containing 10.5 DNA base pairs (bp). Its two strands wind over each other once per helical turn. The number of the times the two strands wind each other is the linking number. A torsion-unconstrained DNA with N base pairs and a contour length L, has a relaxed linking number, Lk_0, calculated by N/10.5 or by L/h. For torsion-constrained DNA, winding or unwinding of DNA can cause a change in the linking number: $\Delta Lk = Lk\text{-}Lk_0$. The superhelical density, $\sigma = \Delta Lk/Lk_0$, is a common parameter used to define the DNA supercoiling state. Negative/positive σ values refer to negatively or positively supercoiled DNA respectively.

Escherichia coli (E. coli) has a large circular genomic DNA that is negatively supercoiled (177). The tightly-regulated bacterial chromosomal DNA supercoiling state is important for numerous important biological processes such as DNA replication (178, 179), gene expression (6, 180, 181) and chromosomal DNA organization (1, 182). The *in vivo* level of bacterial DNA supercoiling is regulated by ATP-dependent topoisomerases and structural maintenance of chromosomes (SMC) proteins, as well as a set of abundant DNA binding architectural proteins referred to

as the nucleoid-associated proteins (NAPs) (4). Approximately a dozen different NAPs are present in *E. coli*, and are widely studied for their chromosomal DNA packaging and global gene regulation roles (14, 18). However, how NAPs affect DNA supercoiling (and vice versa) has not been well characterized.

In this study, we focused on an important *E. coli* NAP, the histone-like nucleoid structuring protein (H-NS). H-NS is highly expressed during the exponential growth phase of *E. coli* and plays a critical role in chromosomal DNA organization (62, 64, 164). It also serves as a global gene silencer (62, 164, 165, 167), especially for laterally-acquired genes (29). The negatively supercoiled *E. coli* nucleoid implies that H-NS likely associate with a supercoiled DNA template to mediate some or all of its biological functions. Indeed, previous studies have demonstrated that H-NS can constrain DNA supercoiling *in vivo* and *in vitro* (64, 164) but the mechanism is not well understood.

H-NS is capable of two DNA-binding modes; a DNA-stiffening mode caused by rigid H-NS nucleoprotein filament formation (41) and a DNA bridging-mode presumably resulting from H-NS dimers (40) or mediated by the H-NS filament (39). The switch between the two modes is regulated by divalent ions (19). Both DNA-binding modes have been proposed to be important in mediating H-NS gene silencing and DNA packaging functions (42, 43, 183). To address how H-NS affects DNA supercoiling, the effects of H-NS in its two distinct DNA-binding modes on DNA supercoiling need to be considered. Magnetic tweezers provide such a means to study DNA-protein interactions at a single-molecule DNA level whereby the DNA supercoiling level and tension can be precisely controlled.

In the present work, we showed that H-NS DNA-stiffening mode suppresses formation of DNA plectonemes and after DNA plectonemes are formed, H-NS DNA-stiffening mode weakly stabilizes the DNA in plectoneme form. The suppression of DNA plectoneme formation by H-NS DNA-stiffening mode led to DNA melting

during DNA unwinding. The H-NS DNA-bridging mode showed opposite effects by promoting DNA plectoneme formation and blocking twists diffusion to form constrained supercoiled DNA domains. Overall, these findings provide mechanistic insights to how H-NS performs chromosomal DNA organization through an intricate interplay with DNA supercoiling.

4.2. Materials & Methods

Protein expression and purification

The *hns* gene was cloned into pET-28 expression vector for expression in *E.coli* BL21 cells. The expressed H-NS protein has a C-terminal 6X-HIS-tag for performing affinity-tag purification. The expression and purification protocol is essentially the same as previously described (19, 183). Briefly, transformed BL21 cells were induced with IPTG and lysed by sonication. Over-expressed His-tagged H-NS was purified using nickel-column chromatography and then further concentrated by gel filtration. The proteins were dialyzed against 25 mM Tris, 500 mM KCl, pH 7.5 to remove any residual imidazole. H-NS protein was stored in -20°C in 50% glycerol. H-NS protein purity was verified by SDS-PAGE and the concentration quantified using optical absorbance at 280 nm and converted to molarity using the calculated H-NS extinction coefficient.

Magnetic tweezers experimental Setup

A simple micro flow-channel was constructed using two #1.5 coverslips held by melted parafilm. Typical channel volume was about 40-50 µl. Channel buffer exchange was done by adding the desired buffer at one end of the channel using Kimwipes (Kimberly-Clark) to draw from the other end. The bottom coverslip was coated with PEG-NHS (Silane-PEG-NHS, Nanocs) as previously described (184). Anti-digoxigenin fragments (Roche) were then added to form covalent bonds with the

NHS group on the PEG. Nick-free DNA with multiple biotin and digoxigenin at each end was constructed for the supercoiling experiments. Briefly, plasmid pRL574 (7,474 bp) was digested using XhoI and BamHI restriction enzymes and then ligated with multiple digoxigenin- and biotin-labeled 500 bp DNA handles.

The digoxigenin-labeled handles were XhoI-digested while the biotin-labeled handles were BamHI-digested. For the ssDNA stretching experiment, a 4,410 bp DNA with biotin at one end was obtained through PCR using the pRL574 plasmid as a template. The PCR product was then digested with BstXI to yield a 3,291 bp DNA with biotin at one end and 3' overhang at the other. Terminal deoxynucleotidyl transferase (New England Biolabs) was used to add 50-100 copies of dUTP-DIG to the 3' overhang end to obtain a 3,291 bp DNA with biotin and DIG labeled on the same DNA backbone strand. 1 ng/µl of DNA was added to the flow channel and incubated for 10 min. 50 µg/ml of 1 µm sized streptavidin-coated magnetic beads (Dynabeads MyOne Streptavidin, Invitrogen) was then added and incubated for another 10 min to form DNA tethers.

The unbound magnetic beads and DNA were washed away before performing experiments. The magnetic tweezers setup is similar to that previously described (100). Briefly, a pair of Neodymium magnets were mounted onto a micromanipulator (MP-285, Sutter Instruments) and a rotation stage (M660, Physik Instruments) for three-dimensional control and rotation, respectively. The tethered beads positions were tracked with 5 nm spatial resolution at 80 Hz. The buffers used in the experiments were either stiffening buffer (10 mM Tris, 50 mM KCl, pH 7.5) or bridging buffer (10 mM Tris, 50 mM KCl, 10 mM $MgCl_2$, pH 7.5). All experiments were conducted at 23°C. Force-extension curve measurements were performed by measuring DNA extension averaged for 10 sec at different DNA-stretching forces. Twist-extension curve measurements were similarly performed but at constant force

and at different DNA turns. For obtaining single-ssDNA, the 3,291 bp DNA was force-melted at overstretching forces (~ 65 pN) in TE buffer.

4.3. Results

Winding or unwinding of a torsion-constrained DNA tether by magnetic tweezers can cause DNA twist and hence an increase in DNA twisting energy (**Fig. 4.1a**). The accumulated twist energy can be relaxed through chiral DNA bending or DNA structural transitions. At sufficiently low DNA tension, DNA supercoiling is a chiral DNA bending process to relax the level of DNA twist. This leads to formation of positive (left-handed) plectonemes during winding or negative (right-handed) plectonemes during unwinding (100, 185). The onset of DNA plectoneme formation upon twist accumulation is indicated by the DNA buckling transition. After the DNA buckling transition, subsequent twists are rapidly converted to writhes in DNA to form DNA plectonemes. In this region, DNA extension is linearly dependent on the number of twists introduced and shows symmetric behavior on either side of turns (186, 187). At higher DNA tension, the symmetry between positive and negative twists is broken due to DNA melting during DNA unwinding (negative twist). However, during DNA winding, formation of plectonemes still occurs up to ~ 5 pN (188). These previous observations were reproduced on a torsion-constrained DNA in our experimental setup as shown in **Fig. 4.1b**.

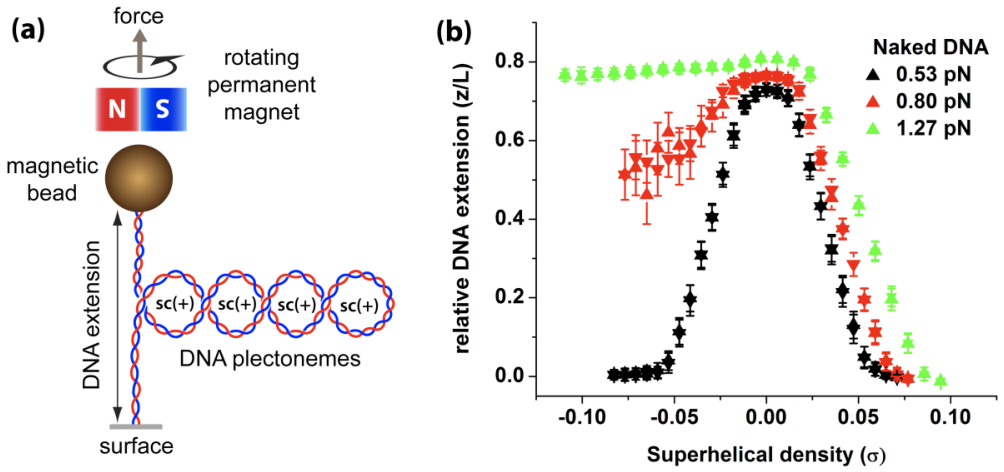

Figure 4.1 Single-DNA stretching and winding/unwinding using magnetic tweezers setup. a) A micron-sized paramagnetic bead is tethered to a functionalized glass surface via a single DNA molecule which is multiply-anchored to form a torsion-constrained DNA tether. Translating or rotating the magnet allows us to regulate the imposed DNA tension and twists. b) Twist-extension curves of a 7,474 bp DNA used in this study held at various DNA tensions. Up-triangles represent increasing DNA winding (+ σ)/unwinding (-σ) data while down-triangles represent decreasing DNA winding/unwinding data.

The H-NS DNA-stiffening mode suppresses DNA supercoiling by delaying the DNA buckling transition

At low magnesium conditions (⩽ 2 mM), H-NS forms a rigid filament along DNA, causing DNA-stiffening to predominate, while at higher magnesium conditions (> 5 mM), DNA-bridging is the predominant form of DNA-binding (19, 40, 41). In previous single-DNA stretching experiments using torsion-unconstrained DNA, the H-NS DNA-stiffening mode results in longer DNA extension at low DNA tension (< 1 pN), while the H-NS DNA-bridging mode causes progressive reduction of DNA extension at low tension (< 1 pN) (19).

Here, on a torsion-constrained DNA (7,474 bp) at σ = 0, we re-examined the effects of H-NS on the force-extension curves of the DNA. In stiffening buffer (10 mM Tris, 50 mM KCl, pH 7.5), addition of 6μM H-NS (**Fig. 4.2a, red symbols**) caused the DNA bending persistence length to increase to > 100 nm from the naked DNA value of ~ 50 nm (**Fig. 4.2a, black symbols**). In bridging buffer (10 mM Tris, 50 mM KCl, 10 mM $MgCl_2$, pH 7.5), 6 μM H-NS caused DNA-folding, with no

apparent DNA stiffening (**Fig. 4.2a, blue symbols**). These observations are in general agreement with previous results obtained on torsion-unconstrained DNA (19, 41), indicating torsion-constrained DNA does not affect H-NS DNA-binding modes.

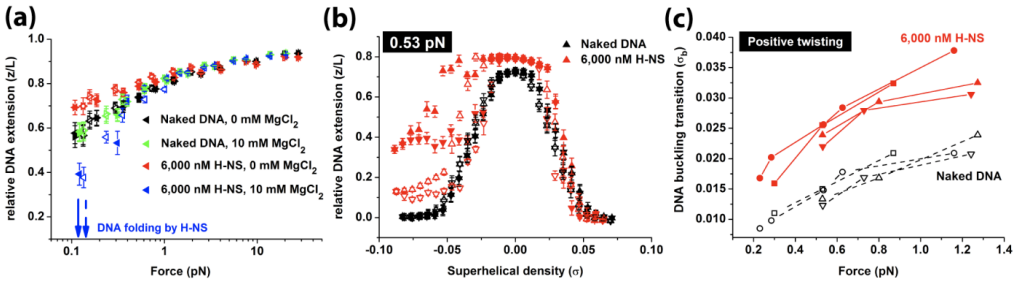

Figure 4.2 H-NS DNA-stiffening mode delays DNA buckling transition. a) DNA force-extension curves in the H-NS DNA-stiffening mode (0 mM MgCl2) or H-NS DNA-bridging mode (10 mM MgCl2) b) DNA twist-extension curve in the presence of H-NS DNA-stiffening mode shows H-NS delayed DNA buckling transition during DNA winding or unwinding. Two independent data sets – solid and hollow symbols are plotted. c) The delay in DNA buckling transition was also observed across DNA tension of 0.2 – 1.2 pN. The plot represents 4 independent sets of data.

In the absence of magnesium, H-NS binding to DNA delayed the DNA buckling transition (**Fig. 4.2b**). For naked DNA, the measured DNA buckling transition (**Figures 4.3**) at 0.53 pN is a smooth process and is estimated to occur at $\sigma = \pm$ 0.010-0.015 (**Fig. 4.2b, black triangles**). At 6 µM H-NS (**Fig. 4.2b, red triangles**), the DNA buckling transition upon positive twisting (DNA winding) was abrupt and delayed to σ = 0.018-0.024. For negative twisting (DNA unwinding), H-NS also caused a delay in the buckling transition to σ = -0.022-0.028. Similar measurements of the DNA buckling transition during DNA winding in the presence of H-NS at DNA tension range of 0.2-1.2 pN (**Fig. 4.2c**) were performed, and consistently showed that H-NS binding to DNA caused a delay in the DNA buckling transition over the DNA tension range of ~0.5-1.5 pN (**Fig. 4.2c**). DNA buckling studies higher than 0.53 pN for DNA unwinding were not performed due to the complication from DNA torsion-melting at higher DNA tension (i.e. > 0.7 pN).

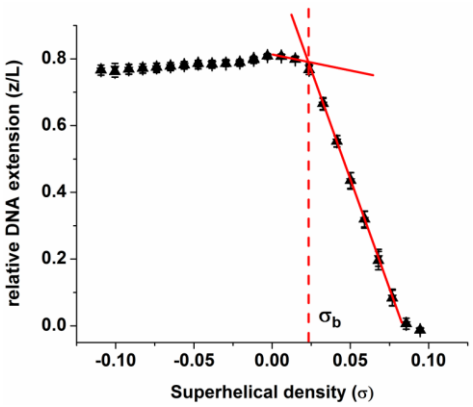

Figure 4.3 The DNA buckling transition measurement from the DNA twist-extension curve. There are two regions of DNA extension vs. turns (σ) that are approximately linear which can be defined before and after DNA buckling transition. The linear region before DNA buckling is often approximately linear in a short window of twists. The linear region after DNA buckling is often more well-defined. A linear curve is fitted to individual regions and the number of data points used is optimized to obtain R2 of > 0.99. The two linear fits intersection's projection on the x-axis (Superhelical density, σ) is defined here as the DNA buckling transition point, σb.

At a tension of 0.53 pN, the plectoneme formation of naked DNA between DNA winding and unwinding is symmetric, (**Fig. 4.1b and 4.2b**). However, in the presence of 6 μM H-NS in DNA-stiffening mode, the symmetric behaviour is lost (**Fig. 4.2b, red filled triangles**). This asymmetric behaviour is reminiscent of naked DNA superhelical density-extension curves at higher DNA tension (0.73 pN) where DNA unwinding led to partial DNA melting (100). This suggests that DNA stiffening has a similar effect to increasing DNA tension in promoting DNA melting during unwinding. Overall, these results show that H-NS DNA-stiffening delays the DNA buckling transition and hence suppresses DNA supercoiling.

The H-NS DNA-stiffening mode restricts DNA conformation changes during DNA winding

Winding of DNA bound with H-NS in the absence of magnesium at 0.53 pN and 1.27 pN showed a delayed buckling transition (**Fig. 4.4a**, see black and blue arrows). This was then followed by the formation of plectonemes with a larger DNA extension reduction against twist as compared to naked DNA (see the slope of curve in **Fig.**

4.4a after DNA buckling). Consequently, the DNA extension reached that of naked DNA or even lower than the naked DNA extension at sufficiently high superhelical density (**Fig. 4.4a**, black (σ = 0.06) and blue (σ = 0.09) up-triangles). The shortened DNA extension after DNA winding could be recovered by unwinding at similar DNA tension although hysteresis was observed. The hysteresis is defined by the extension difference between the DNA winding (**Fig. 4.4a**, up-triangles) and unwinding curves (**Fig. 4.4a**, down-triangles).

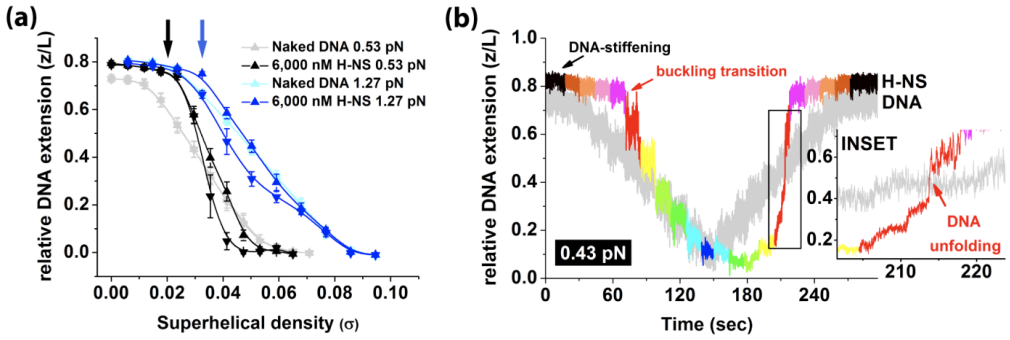

Figure 4.4 H-NS DNA-stiffening mode restricts DNA conformational changes upon DNA twisting. a) DNA extension hysteresis was observed between DNA winding (up-triangles) and DNA unwinding (down-triangles) in the presence of H-NS DNA-stiffening mode. b) Time-kinetics of DNA extension during showed DNA extension cannot be recovered immediately upon DNA unwinding. Inset showed a DNA unfolding event which indicates H-NS DNA-stiffening mode transiently traps DNA in plectoneme conformation.

Closer examination of the kinetics revealed that during DNA winding, at each constant σ value, no progressive reduction in DNA extension was observed (**Fig. 4.4b**). This was confirmed by an independent experiment on a longer time scale holding DNA at high σ values for up to 5 minutes (**Fig. 4.5**). These results suggest that the larger reduction in DNA extension during DNA winding is not the result of H-NS-mediated DNA-bridging (as observed in 10 mM $MgCl_2$ (19)). Further, the time trace during DNA unwinding to recover the original DNA extension occasionally revealed DNA unfolding signals that were mixed with gradual and step-wise DNA extension increases (**Fig. 4.4b**, inset from an additional experiment).

In summary, H-NS in the stiffening-binding mode tends to maintain the current supercoiling state of the DNA; H-NS bound extended DNA at low superhelical density delays formation of plectoneme while after formation of the plectonemes, H-NS weakly stabilizes it against twist relaxation (see Discussion for the implications of these observations).

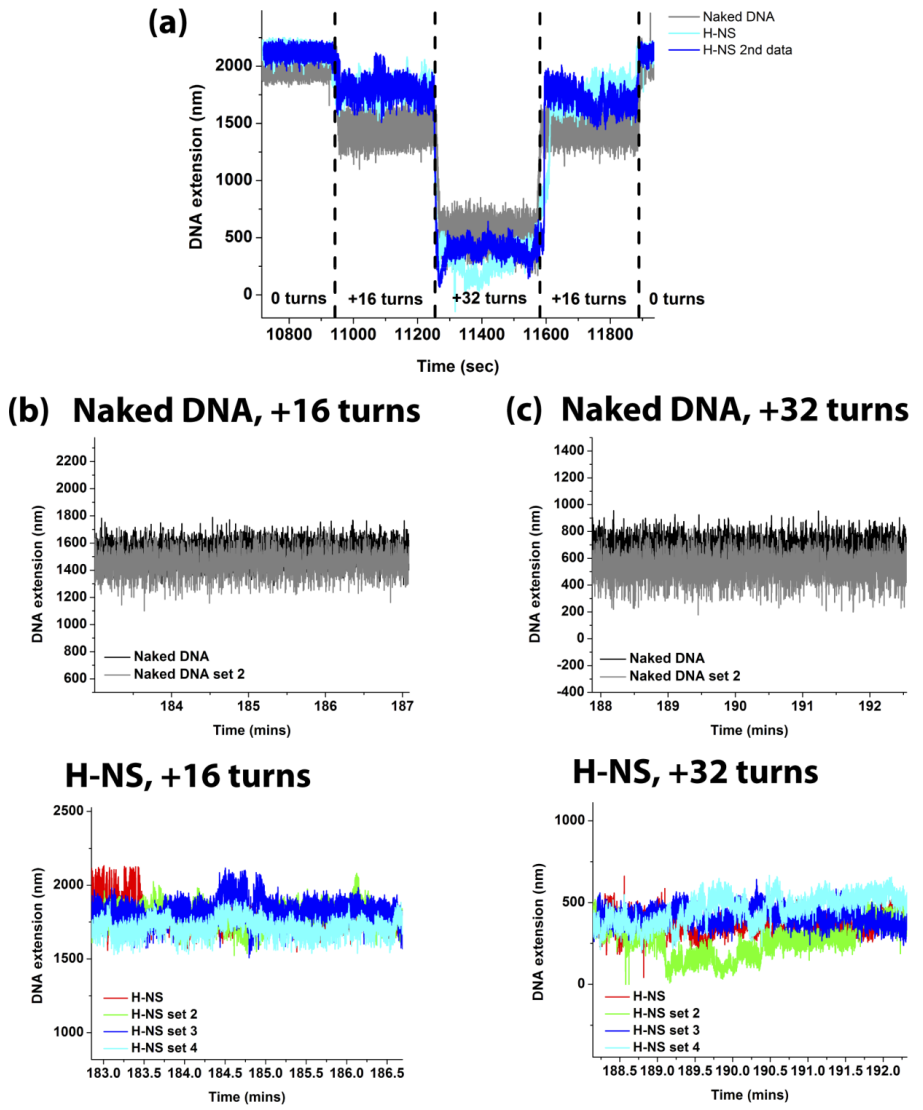

Figure 4.5 DNA extension stability in the presence of H-NS in DNA-stiffening mode at high superhelical density during DNA winding. a) Time-trace of single DNA extension in the presence of H-NS DNA-stiffening mode during sequential DNA winding and unwinding. Two independent data sets are presented in the figure panel. Black and grey lines refer to two independent naked DNA data while the blue and cyan lines refer to two independent data in the presence of H-NS DNA-stiffening mode. b) A close-up of naked DNA (top) and H-NS (bottom) after adding +16 turns (σ = 0.023) showed the DNA extension for both conditions are stable across 5

minutes. However, in the presence of H-NS DNA stiffening mode, the DNA extension fluctuations is larger. c) The results are similar when DNA is further twisted to +32 turns (σ = 0.045). This implies that H-NS DNA-stiffening mode does not compacts/folds DNA at reasonably high σ values.

The H-NS DNA-stiffening mode promotes DNA melting during DNA unwinding

We next performed twist-extension measurements of the DNA bound with H-NS in DNA-stiffening mode at different DNA tension in increasing order (**Fig. 4.6**). The H-NS DNA-stiffening mode promoted DNA melting during DNA unwinding at DNA tension which otherwise would result in DNA plectoneme formation with naked DNA. This can be seen by the asymmetric shape of the twist-extension curve of H-NS bound DNA at low DNA tension (0.53 pN) (**Fig. 4.6a** red symbols), which otherwise, would result in a symmetric shape for naked DNA (**Fig. 4.6a** black symbols). In addition, the shape of the curve is similar to that of a partially melted naked DNA held at higher DNA tension (0.8 pN) (**Fig. 4.6b** black symbols). The trend continued when we compared the data at 0.80 pN of H-NS-bound DNA (**Fig. 4.6b** red symbols) with the naked DNA twist-extension curve at 1.27 pN (**Fig. 4.6c** black symbols). This result indicates that H-NS DNA-stiffening has a similar effect to DNA tension in promoting DNA melting by preventing plectoneme formation.

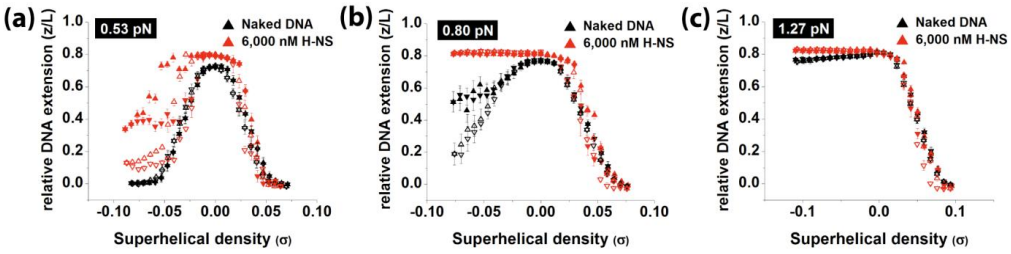

Figure 4.6 H-NS DNA-stiffening mode promotes DNA melting during DNA unwinding. a) At 0.53 pN, H-NS DNA-stiffening effect caused partial DNA melting while naked DNA formed DNA plectonemes. b) At 0.80 pN, in the presence of H-NS DNA-stiffening effect, the DNA was completely melted while the naked DNA was partially melted. c) At 1.27 pN, both naked DNA and DNA in the presence of H-NS DNA-stiffening mode were completely DNA melted during DNA unwinding.

At a DNA tension of 1.27 pN, whereby both the naked DNA and the H-NS-bound DNA undergo complete melting during unwinding, the melted DNA extension in the presence of H-NS was higher than naked DNA (**Fig. 4.6c**). We also observed that whenever there was partial DNA melting during DNA unwinding in the presence of H-NS (i.e., at low DNA tension ~ 0.5 pN), a large hysteresis in DNA extension occurred as compared to naked DNA (**Compare Fig. 4.6a,** red symbols with **Fig. 4.6b**, black symbols). The cause of both observations is unclear, but the presence of ssDNA suggests they may be mediated by H-NS-ssDNA (single-stranded DNA) interactions since H-NS is known to bind ssDNA but at a lower affinity than double-stranded DNA (189).

To elucidate how H-NS binding affects the mechanical property of ssDNA, we generated an ssDNA tether *in situ* based on a previously published method (190) (**Fig. 4.7**) and performed ssDNA stretching experiments in the presence of H-NS in stiffening buffer. We found that H-NS has no drastic effect on ssDNA mechanical properties even up to 2.4 and 6.0 μM H-NS and only weak folding of ssDNA by H-NS was observed (**Fig. 4.8**). This indicates that H-NS organizes ssDNA in a totally different manner from double-stranded DNA. It also provides a reasonable explanation to why the melted DNA extension in the presence of H-NS is higher (**Fig. 4.6c**); which can be due to the formation of a stiffer ssDNA-H-NS-ssDNA bundle complex, and also why there is a larger hysteresis during DNA unwinding recovery at low DNA tension (**Fig. 4.6a**, red symbols); which can be due to H-NS induced ssDNA segments interactions.

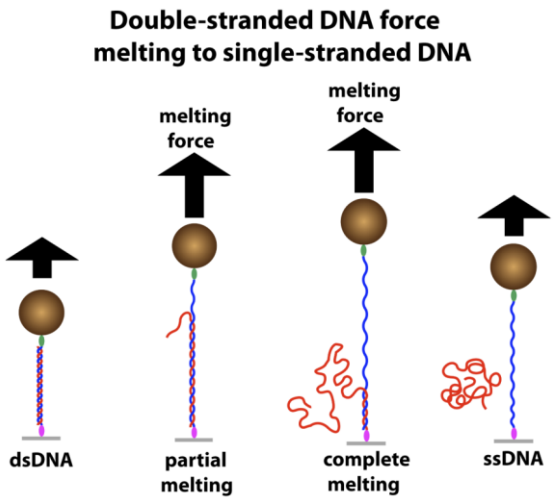

Figure 4.7 Force-induced melting of dsDNA to ssDNA strategy. The DNA is tethered to the paramagnetic bead and surface via the same strand from the double-stranded DNA helix. Upon increasing the DNA tension to $\geqslant$ 65 pN in the presence of low salt buffer condition, the DNA helix undergoes a peeling-transition where the un-tethered DNA strand is melted from the tethered strand. Holding the DNA at this tension for sufficient long time ($\approx$ 10-15 seconds) allows the un-tethered DNA to completely melt from the tethered strand which eventually leads to a remaining tethered ssDNA. The un-tethered strand may be washed away by flushing the reaction buffer with the experimental buffer.

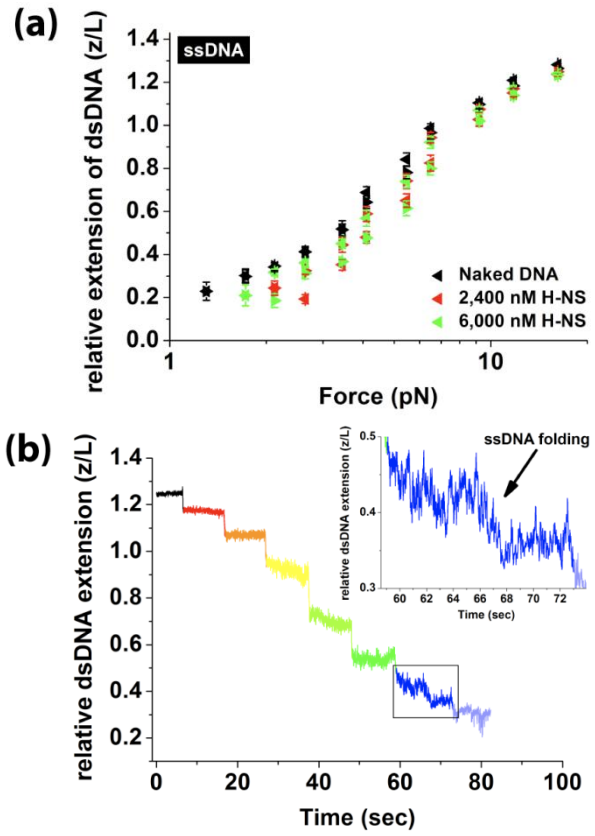

Figure 4.8 H-NS effects on ssDNA mechanical properties. a) The force-extension curve of ssDNA in the presence of H-NS in stiffening buffer showed a slight reduction in ssDNA extension (red and green symbols) as compared to naked DNA (black symbols), indicating H-NS weakly fold/compact ssDNA. b) Time-trace of ssDNA as DNA tension is reduced. Difference colour presents different DNA tension – black (15.8 pN), red (13.2 pN), orange (12.6 pN), yellow (11.3 pN), lime (9.0 pN), green (7.2 pN), blue (6.3 pN) and lavender (5.5 pN). Inset shows that the ssDNA extension drops suddenly when held at (6.3 pN) which is consistent with H-NS folding of ssDNA.

The H-NS DNA-bridging mode promotes DNA supercoiling and blocks twist diffusion

In the presence of high magnesium concentrations (~ 10 mM $MgCl_2$), the H-NS DNA-stiffening effect is abolished and H-NS DNA-bridging predominates (19). Under this condition, the effect of H-NS on DNA supercoiling is a sharp contrast to H-NS DNA-stiffening mode at low $MgCl_2$. The DNA twist-extension curve in the presence of H-NS in bridging buffer (10 mM Tris, 50 mM KCl, 10 mM $MgCl_2$, pH 7.5) at 1.50 pN resulted in plectonemes formation during DNA winding or unwinding,

exhibiting a considerably symmetric curve (**Fig. 4.9a**, green symbols). This is in contrast to naked DNA case (**Fig. 4.9a**, black symbols), which undergoes complete melting during unwinding at similar DNA tension.

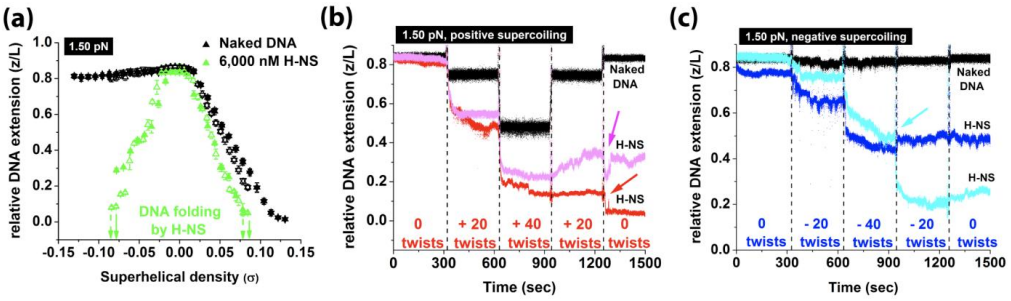

Figure 4.9 H-NS DNA-bridging mode promotes DNA plectoneme formation and also blocks twist diffusion. a) DNA twist-extension curves in the presence of H-NS DNA-bridging mode showed DNA plectonemes were more rapidly formed in the presence of H-NS. b) Time-kinetics of DNA extension in the presence of H-NS DNA-bridging mode through a controlled DNA winding and unwinding cycle. DNA extension was not fully recovered upon untwisting and instead resulted in further DNA extension drops (see arrows). c) Similar experiment done with first DNA unwinding and then DNA winding showed similar observations.

In addition, the naked DNA extension is constant at constant σ values, but with H-NS, a progressive drop in the DNA extension was observed in during constant σ values and tension (**Fig. 4.10**). We only plotted the DNA twisting curves for both DNA winding/unwinding (**Fig. 4.9a**, green symbols) as the original DNA extension could not be recovered through DNA untwisting once H-NS completely folded the DNA. This is in contrast to the case of the H-NS DNA-stiffening mode, where the DNA extension can be fully recovered through DNA untwisting, although hysteresis was apparent (**Fig. 4.4a**). All of these results can be simply explained by H-NS-mediated DNA bridging. The H-NS DNA bridging mode naturally promotes DNA plectoneme formation through DNA-H-NS-DNA bridging which reduces DNA bending energy (see discussion below). The promotion of DNA plectoneme formation during DNA unwinding at high DNA tension thus also help prevented DNA from melting (**Fig. 4.9a**, $\sigma < 0$).

H-NS is proposed to play a role in forming topologically distinct domains (65), likely through blocking twist diffusion across domains. To test whether H-NS blocks twist diffusion, we first introduced twists to DNA in the presence of H-NS in bridging buffer, allowed H-NS DNA-bridging to stabilize the resulting DNA plectonemes, and then removed the introduced DNA twists through untwisting. If H-NS can block twist diffusion, DNA untwisting would not affect the H-NS stabilized DNA plectonemes and instead cause new opposite chirality DNA plectonemes to form. This would be detected with a further sharp drop in DNA extension.

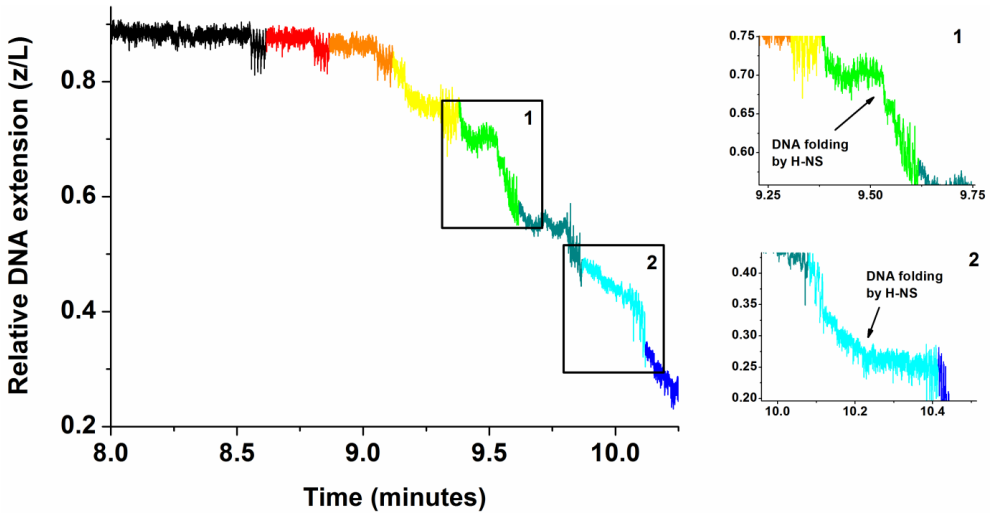

Figure 4.10 H-NS DNA-bridging mode causes DNA folding at constant DNA superhelical density values. The DNA was held at ~ 1 pN throughout the experiment. The data colours represent superhelical density values, σ – black (0), red (0.007), orange (0.014), yellow (0.021), green (0.028), olive (0.035), cyan (0.042) and blue (0.049). Inset 1 and 2 shows the close up of the DNA extension kinetics at σ = 0.028 (inset 1) and σ = 0.042 (inset 2). The DNA extension decreased in the presence of 6 μM H-NS DNA-bridging while the DNA was held at a constant σ value.

Indeed, this prediction was observed in our experiments. **Figure 4.9b** (DNA winding) shows the DNA extension time-trace as +20 DNA twists were introduced at a time interval of 5 minutes up to +40 twists before reversing the DNA twisting process. We observed that the DNA extension remained nearly constant when DNA was untwisted from +40 twists to +20 twists, suggesting that the supercoiled domain

cannot be relaxed by untwisting. In addition, the DNA extension decreased sharply with a large step-size when the DNA was further untwisted from +20 twists to 0 twists (**Fig. 4.9b**, see the red or pink arrow). Similar results were obtained with DNA unwinding case when we untwisted the DNA from -40 twists to -20 twists (**Fig. 4.9c**, see the cyan arrow).

These sharp and large DNA extension drops occurred during the process of DNA untwisting. This extension decrease is unlikely due to spontaneous H-NS DNA bridging but rather due to the formation of new DNA plectonemes of opposite chirality. This was what we observed, when the DNA extension did not reduce sharply with large step-sizes when held at similar tension for up to 5 minutes at constant σ values (**Fig. 4.9b & c**, note DNA extension time-trace at constant σ, twists). Overall, our results suggest that the H-NS DNA-bridging mode is able to block DNA twist diffusion and thus isolates H-NS stabilized DNA plectonemes from external topological changes.

4.4. Discussions & Conclusion

Our work shows for the first time how the DNA supercoiling state is differentially regulated by H-NS based on its two distinct DNA-binding modes - DNA-stiffening and DNA-bridging (**Fig. 4.11**). The DNA-stiffening mode is a result from the structural impact on DNA caused by H-NS nucleoprotein filament formation which leads to an increase in the DNA-bending rigidity (19, 41, 183). The higher rigidity naturally results in a higher energy cost in forming the highly-curved DNA plectonemes. It helps explain why H-NS DNA-stiffening mode can suppress DNA plectoneme formations during DNA winding and why it promotes DNA melting during DNA unwinding. One peculiar finding is that once DNA plectoneme forms, H-NS DNA-stiffening mode is able to passively trap DNA in its supercoiled conformation. Although the cause is unclear, its passive nature is different from the

magnesium ($MgCl_2$) induced H-NS DNA-bridging which is progressive in nature (19, 171). Overall, these findings suggest that H-NS stiffening binding mode tends to maintain the current topological state of the DNA.

In the presence of 10 mM $MgCl_2$, whereby H-NS DNA–bridging mode predominates (19), H-NS promoted DNA plectoneme formation. This is expected as the close-proximity DNA strands at the loop apex and base would allow H-NS-DNA-H-NS bridges to nucleate and progressively zip up the DNA loop, which leads to DNA plectonemes stabilization. In other words, H-NS DNA-bridging reduces the energy cost in DNA plectonemes formation and stabilization during DNA winding/unwinding. This also explains why DNA melting was suppressed during DNA unwinding at high DNA tension.

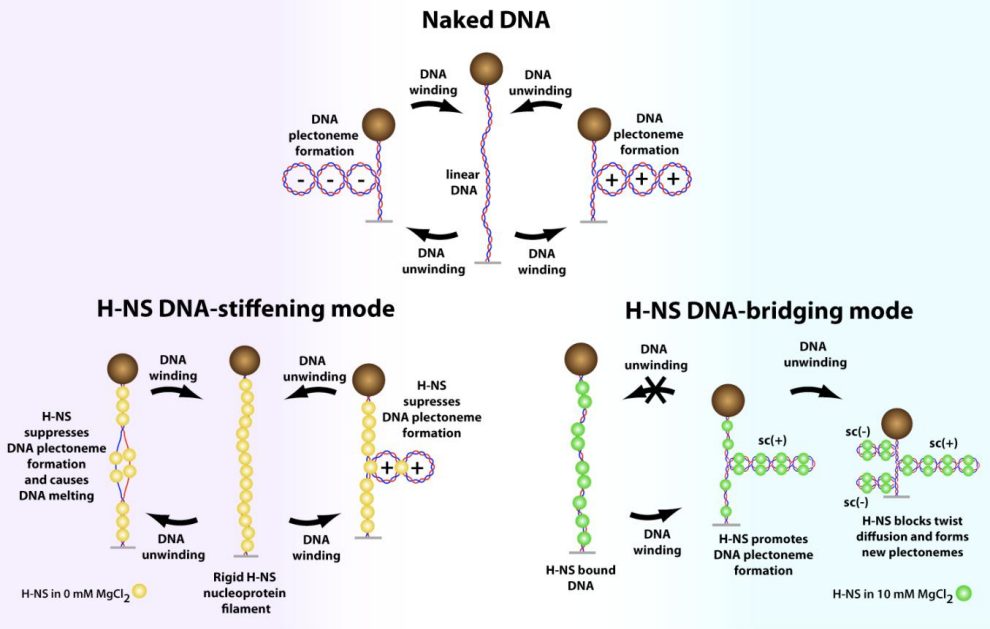

Figure 4.11 A summary of H-NS DNA-binding modes effects on DNA supercoiling. DNA unwinding or winding results in DNA plectoneme formation at illustrated DNA tension. With H-NS DNA-stiffening mode, the increase in DNA bending rigidity causes DNA melting instead of DNA plectoneme formation during DNA unwinding, while it suppresses DNA plectoneme formation during DNA winding. For H-NS DNA-bridging mode, H-NS promotes DNA plectoneme formation through stabilizing DNA plectoneme formation with DNA bridging. H-NS DNA-bridging also isolates the stabilized DNA plectonemes from external twist changes. This is demonstrated by the formation of new DNA plectonemes of opposite supercoiling chirality when the twisted DNA is untwisted.

One interesting finding in this work is that accumulated twists in H-NS DNA-bridging stabilized DNA plectonemes cannot be removed externally, i.e. twists cannot diffuse in or out of these H-NS stabilized plectonemes. It implies that when H-NS bound to DNA in its DNA-bridging mode, it forms a barrier to twist diffusion and leads to formation of topologically isolated supercoiled DNA domains. Henceforth, this work represents the first direct mechanical evidence that H-NS behave as a domainin as proposed in a previous *in vivo* study (65).

At the *in vivo* concentration of magnesium (1-4 mM $MgCl_2$) (145), both DNA binding modes of H-NS likely co-exist (19). This suggests that at low superhelical density, the rigid H-NS nucleoprotein filaments will constrain the DNA in the extended conformation, causing suppression of DNA plectoneme formation. On the other hand, on existing DNA plectonemes (or supercoiled regions), H-NS DNA-bridging mode will be preferred which locks DNA in plectonemes and topologically isolates it. Past studies have shown that the *in vivo* level of H-NS affects the DNA supercoiling state of plasmid DNA and chromosomal DNA (63-65). The general idea from these studies is that H-NS is able to constrain DNA in its current supercoiling state. Henceforth our work here provides a mechanical platform to understanding these *in vivo* findings. Other than this work, there is only one other single molecule study of how the NAP *B. stearothermophilus* (*Bst*) HU protein can affect DNA supercoiling (191). Since most studies on the DNA-binding properties of NAPs were performed using torsion-unconstrained DNA (non-supercoiling DNA) (41, 141, 158, 159), future single-molecule studies of NAPs using supercoiled DNA will provide a more physiologically relevant understanding to how NAPs perform their *in vivo* functions.

In addition, our findings provides a long-reaching prediction that DNA-stiffening proteins should suppress DNA plectoneme formation and promote DNA melting during unwinding due to an increase in DNA-bending rigidity; while DNA-

bridging proteins have opposite effects by promoting DNA plectonemes and suppresses melting during DNA unwinding. Given that DNA-stiffening, DNA-bridging/looping and DNA-bending/wrapping have been reported for numerous bacterial NAPs (20, 21, 23, 54, 156, 192), our findings obtained from the two distinct DNA-binding modes of H-NS and the previous *Bst* HU study (191) suggest that DNA architectural proteins, i.e. bacterial NAPs, may employ their distinct DNA-binding modes to passively regulate the supercoiling state of the bacterial nucleoid.

Chapter 5

Passive regulation of DNA supercoiling by distinct DNA-binding modes of nucleoid-associated proteins

5.1. Introduction

The bacterial chromosomal DNA supercoiling state regulates many major biological events such as gene transcription (6, 180, 181) and chromosomal DNA organization (1, 182). The topoisomerases, Structural Maintenance of Chromosomes (SMC) proteins and Nucleoid-Associated Proteins (NAPs) play crucial roles in dictating the DNA supercoiling state *in vivo (4)*. Gyrase, a specific type II topoisomerases, drives negative supercoiling of DNA that requires ATP-hydrolysis (193, 194). The supercoiled DNA can be equilibrium relaxed by type I topoisomerases in an ATP-independent manner or non-equilibrium relaxed by other type II topoisomerases in an ATP-dependent manner (195-197). The competition between these topoisomerases is important in maintaining *in vivo* supercoiling state of the bacterial chromosomal DNA (198, 199). Bacteria SMC protein complex are also responsible for chromosome segregation (10, 200) through DNA-bridging and DNA-loop constrain (201, 202).

Other than the ATP-dependent topoisomerases and SMC proteins, the ATP-independent NAPs also contribute to maintaining the overall topology of bacterial nucleoid (1, 14, 18, 194). The Escherichia coli (*E. coli*) histone-like nucleoid

structuring (H-NS) protein is one of the major NAPs that is involved in chromosomal DNA organization (62, 64, 164) and is shown to constraint DNA supercoiling both *in vivo* and *in vitro* (64, 164). H-NS paralogue in *E. coli*, StpA, can also constrains DNA supercoiling (125). Other major *E. coli* NAPs, heat unstable (HU) and integration host factor (IHF) proteins are also known to mediate their functions through interplays with DNA supercoiling state; HU is able to regulate DNA supercoiling (203) while IHF was proposed to be a sensory transducer of chromosomal DNA supercoiling state (204).

The above suggests NAPs DNA organization properties (hereafter termed as DNA-binding modes) play a role in regulating DNA supercoiling. It is thus important to understand the mechanical consequences of these DNA-binding modes to DNA supercoiling. The main NAPs DNA-binding modes can be classified by 1) DNA-stiffening (protein binding increases apparent DNA stiffness), 2) DNA-bending and 3) DNA-bridging. Therefore, now it becomes a matter of classifying the effects of individual DNA-binding modes to DNA supercoiling. In the previous chapter (chapter 4), we showed that the *E.coli* H-NS differentially regulates DNA supercoiling through its two distinct DNA-binding modes. The H-NS rigid nucleoprotein filament suppresses DNA plectoneme formation while its DNA-bridging mode promotes DNA plectoneme formation and also traps DNA in the plectoneme form. In this work, two more major *E. coli* NAPs; HU and IHF are used to extend the range of NAPs DNA-binding modes tested. The *E.coli* HU has two distinct DNA-binding modes; DNA-bending at low concentration of HU, while DNA-stiffening at high concentration of HU and low concentration of monovalent salt (20, 141). IHF, the "master bender", is primarily a DNA-bending protein (59) although it has the capability to form DNA networks at high protein concentration in the presence of magnesium (22).

The magnetic tweezers allow one to study and manipulate DNA supercoiling state through mechanical twists introduction/reduction at single-molecular level (99, 100). In this work, we used magnetic tweezers to investigate the effects of HU and IHF on DNA supercoiling. We found that *E.coli* HU DNA-stiffening mode delayed the DNA buckling transition during mechanical DNA winding and this is consistent with what was observed in H-NS DNA stiffening mode (see chapter 4). We then showed that both HU and IHF DNA-bending modes had an antagonistic behaviour to DNA-stiffening mode whereby they promoted DNA plectoneme formation and stabilized B-DNA structure from torsion-melting upon unwinding stress. To provide a mechanistic explanation to our observations, we proposed that the preference of NAPs DNA-binding modes to different DNA supercoiling states is due to the preference of DNA-binding modes to extended (linear DNA) or curved DNA (supercoiled DNA) local topology. This was proved when we showed that curved DNA drives off bound DNA-stiffening proteins while it stabilizes bound DNA-bending proteins. All of these provide many novel structural insights to how NAPs play their roles in bacterial chromosomal DNA organization and segregation.

5.2. Materials & Methods

E.coli HU and IHF proteins

Both the *E.coli* HU and IHF proteins were directly obtained from other labs. The *E.coli* HU protein is a kind gift from Dr. Sankar Adhya's lab (NIH) while the *E.coli* IHF protein is a kind gift from Dr. Peter Droge's lab (NTU). The proteins purity was confirmed by SDS-PAGE while the concentrations for HU and IHF were quantified by Bradford assay and UV-Vis spectroscopy.

Magnetic tweezers setup and experiments

The magnetic tweezers setup is exactly the same as what was described in chapter 4 materials and methods section. Briefly, a pair of permanent neodymium borate magnets was mounted on a rotating piezo stage (M660, Physik Instrumente) which was in turn, mounted on a X-Y-Z translator (Sutter MP-285). This allowed us to manipulate the X-Y-Z and θ coordinates of the magnets. The setup was constructed on a commercial inverted microscope (IX-71, Olympus Inc.) to allow integration of magnetic force manipulation and high-magnification biological sample visualization. The observation flow cell was constructed using an anti-DIG-functionalized no. 1 coverslip and no.1.5 coverslip sandwiched with parafilm in-between.

A 7,474 bp DNA with multiple DIG and biotin molecules labeled at either ends were used for the supercoiling experiments (see chapter 4 for DNA construct preparation). A torsion-constrained DNA tether may be quickly identified by first twisting the tether by 30-40 turns and then reducing the DNA pulling force to < 1 pN. If the diffraction pattern of the magnetic bead changes drastically, it means the extension of the tether changes a lot which indicates the formation of DNA plectonemes and thus indicates the DNA tether is torsion-constrained. For the protein DNA dissociation experiments, the transverse magnetic tweezers setup was used instead. The setup is described in chapter 2 materials & methods section. The λ-DNA (~50 kbp) was used for tethering. The construction of the biotin-labeled λ-DNA is also described in chapter 2 materials & methods section.

5.3. Results

HU differentially regulates DNA plectoneme formation depending on its DNA-binding modes

The *E.coli* HU exhibits two distinct DNA-binding modes which are dependent on the HU concentration; DNA-bending mode at low HU concentrations and DNA-

stiffening mode at high HU concentrations (20, 141). To determine if torsion-constrained DNA has any effect on HU DNA-binding modes, we performed force-extension curves (FEC) measurements (**Fig. 5.1**) on a torsion-constrained 7,474 bp DNA tether in the presence of 50, 600 and 2,400 nM (buffer = 10 mM Tris, 50 mM KCl, pH 7.5). At 50 nM HU concentration, HU exhibited DNA-bending effect as shown by the reduction in DNA extension at lower DNA pulling forces. Where else at 2,400 nM HU concentration, HU exhibited DNA-stiffening effect as indicated by the increment in DNA extension at lower DNA pulling forces. At 600 nM HU concentration, the FEC measurement represents a mixture or composition of both the DNA-stiffening and –bending mode by HU. Overall, these observations suggest *E.coli* HU concentration-dependent DNA-binding modes are not affected by the DNA torsional constraint.

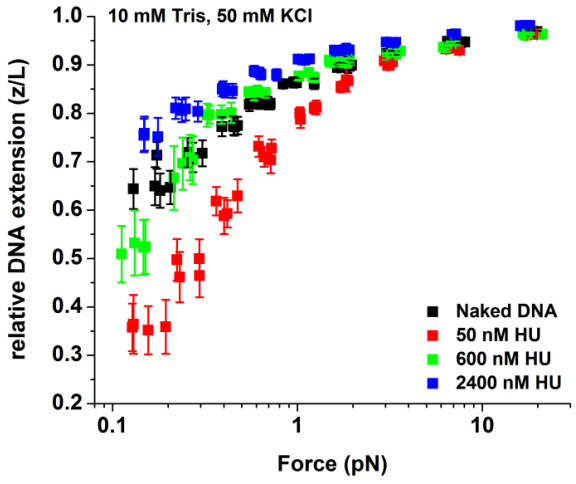

Figure 5.1 *E.coli* HU exhibits concentration-dependent DNA-binding modes with torsion-constraint DNA. At 50 nM HU concentration, HU caused DNA-bending while at 2,400 nM HU concentration, it caused DNA-stiffening. A mixture of both DNA-bending and DNA-stiffening was observed at intermediate HU concentration of 600 nM.

Next, we measured the twist-extension curves (TECs) (**Fig. 5.2**) of the same DNA in the presence of *E.coli* HU DNA-bending mode (50 nM HU) and DNA-stiffening mode (2,400 nM HU) at a low DNA pulling force (0.28 pN) which allows DNA plectonemes formation with either DNA winding or unwinding, and at a

comparative higher DNA pulling force (1.05 pN) which allows DNA melting with DNA unwinding. Two independent data sets were plotted to demonstrate the result repeatability. At the lower DNA pulling force and 50 nM HU (**Fig. 5.2A**, red symbols), we observed an approximate 20 turns shift of the TEC curve to the left as compared to the naked DNA TEC. We also saw that the DNA extension at the peak of the TEC curve is shorter than the peak of the naked DNA TEC. In addition, the linear region (where linear DNA is converted to DNA plectoneme during DNA twisting) in the presence of HU DNA-bending showed a gentler slope than the naked DNA's.

In contrast, at similar DNA pulling force, when we increased the HU concentration to 2,400 nM to induce DNA-stiffening (**Fig. 5.2A**, green symbols), we saw a dramatic change in the shape of the TEC as compared to both that of 50 nM HU and naked DNA. There was also a left-shift in the TEC but with a smaller magnitude of approximately 10 turns. The corresponding DNA extension at the peak of the TEC was higher than the naked DNA's, indicating DNA-stiffening by HU. The hat of the TEC also became broader as compared to naked DNA's which indicate more DNA turns are needed to start DNA buckling transition during both DNA winding and unwinding. In addition, the linear region is steeper than both the naked DNA and that in the presence of 50 nM HU.

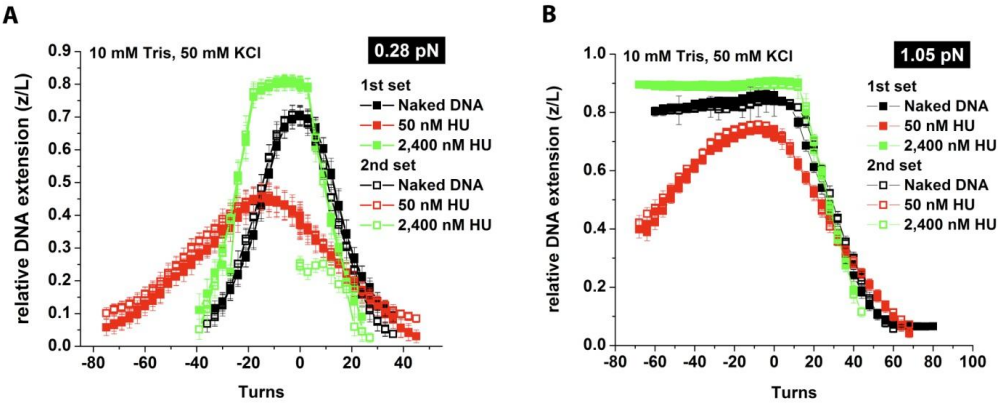

Figure 5.2 Twist-extension curves (TEC) of HU-DNA complexes in HU DNA-bending and DNA-stiffening modes. A) At low DNA pulling force of 0.28 pN, where DNA plectonemes are formed with either DNA winding or unwinding in the absence of HU, 50 nM HU caused a 20 turn left-shift of the TEC with DNA-bending. The linear region slope was also significantly reduced. B) In the case of 2,400 HU, the left-shift was reduced and DNA-stiffening was observed. The cap of the TEC was also broader than naked DNA, indicating a delay in DNA buckling transition with both DNA winding and unwinding. In addition, the linear region slope was also steeper in the presence of HU DNA-stiffening. When the DNA pulling force was increased to 1.05 pN, where the naked DNA is melting with DNA unwinding, addition of 50 nM HU prevented DNA melting during DNA unwinding. DNA-bending was also observed with a 10 turn left-shift of the TEC. Similar to panel A, the linear region slope was lower than the naked DNA's. When 2,400 nM HU was added, DNA melting was instead promoted with also DNA stiffening. The linear slope was also steeper as compared to naked DNA's.

At the DNA pulling force of 1.05 pN, DNA unwinding and winding caused DNA melting and DNA plectoneme formation respectively (**Fig. 5.2B**, black symbols). In the presence of 50 nM HU (**Fig. 5.2B**, red symbols), the TEC was shifted 10 turns to the left as indicated by the peak of the curve when compared with naked DNA. Comparison of the DNA extensions at the corresponding peaks suggest DNA-bending by low concentration HU is unaffected at higher DNA pulling force. An interesting observation is that DNA melting during DNA unwinding was abolished and instead DNA plectonemes were formed. When HU concentration was increased to 2,400 nM (**Fig. 5.2B**, green symbols), the DNA extension was almost constant as DNA was constantly unwound, while when DNA was wound, there was an abrupt DNA buckling transition which started later than naked DNA's. The higher

DNA extension suggests that DNA stiffening by HU was also not affected by a higher DNA pulling force.

We also observed that the DNA twist was affected by HU binding. HU DNA-binding caused a negative shift in the DNA twist center as the HU concentration was increased. The twist shift reached maximum value at 300 nM HU concentration before starting to reduce as the HU concentration was further increased to 2,400 nM HU where HU DNA-stiffening is saturated (**Fig. 5.3A**). A negative shift in the DNA twist center implies that the DNA was wound by HU upon HU binding. As HU exhibits two distinct DNA-binding modes (DNA-bending and DNA-stiffening) depending on HU concentration, it is interesting to compare the amount of DNA winding by HU at the two DNA-binding modes. **Figure 5.3B** compares the change in twist center with the change in z/L (relative DNA extension). It is obvious both the change in twist center and z/L shares the same trend with increasing HU concentration. The amount of DNA winding increased with the amount of DNA-bending by HU, and the HU induced DNA winding started to reduce when HU starts to cause DNA-stiffening. This suggests that HU adopts a different DNA-binding configuration in DNA-stiffening mode as compared to its DNA-bending mode.

Taken together, we showed that the *E.coli* HU exhibited two distinct regulation of DNA plectoneme formation depending on HU concentration. At low HU concentration (e.g. 50 nM HU), HU DNA-bending mode promoted DNA plectonemes formation and this prevented DNA melting during DNA unwinding. At higher HU concentration (e.g. 2,400 nM HU), HU DNA-stiffening suppressed DNA plectoneme formations through a delay in DNA buckling transition which was also observed with H-NS DNA-stiffening mode in the previous chapter (Chapter 4). Our studies also revealed that the *E.coli* HU binding caused DNA winding as evident from the left-shift of the HU-DNA complex TECs.

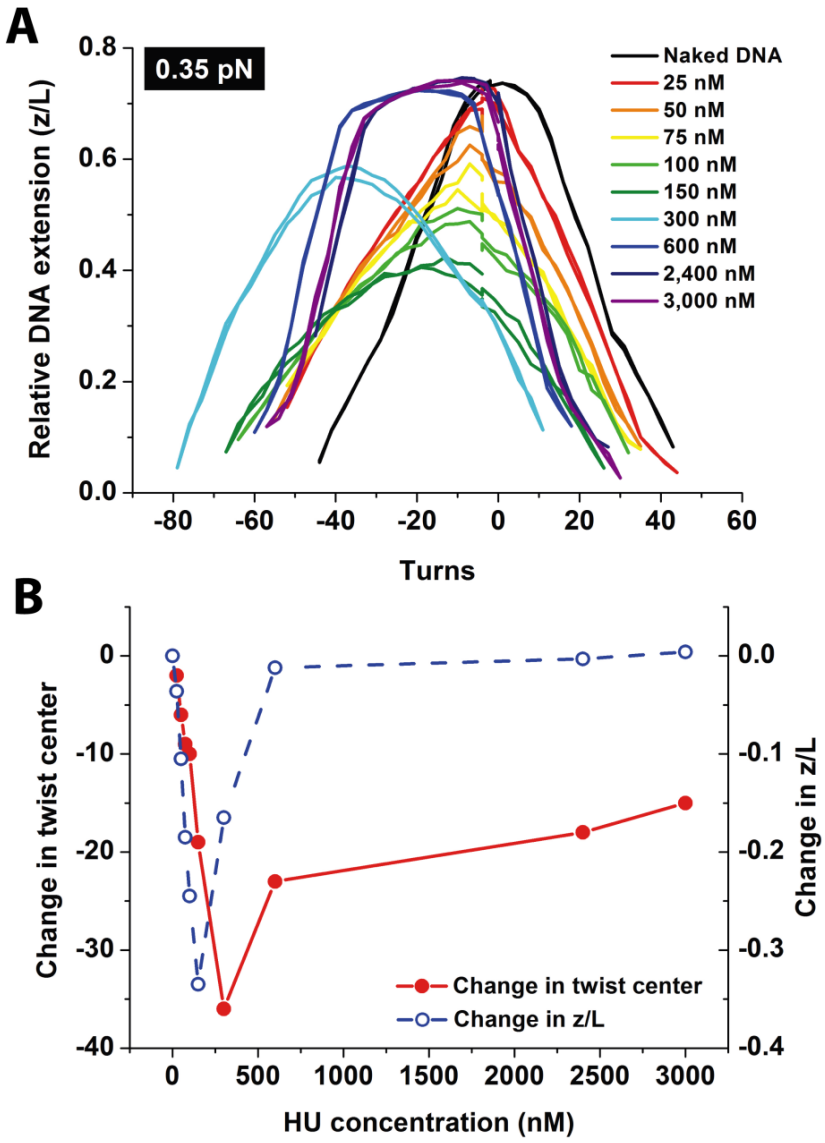

Figure 5.3 *E.coli* HU DNA-binding caused a change in DNA twist property and the change is dependent on HU concentration, and hence HU DNA-binding modes. A) Twist-extension curves of HU at various protein concentrations. The twist center of the peak shifted to the left with increasing HU concentrations, until it reached a peak at 300 nM HU before reducing again. This shift "turn-over" coincides with the HU DNA bending transition to DNA stiffening. B) A quantitative plot of the change in twist center and relative DNA extension (z/L) showed the negative shift of twist center follows closely with the HU DNA-bending transition to DNA-stiffening.

IHF DNA-bending mode promotes DNA plectoneme formation

In previous section, we showed that the HU DNA-bending mode promoted DNA plectoneme formation and we expected this observation to also be extended to the

"master-bender" protein, the *E.coli* IHF. We performed force-extension curve measurements of a 7,474 bp torsion-constrained DNA in the presence of 100 nM IHF (**Fig. 5.4A**). We saw that the DNA extension was drastically reduced as the DNA pulling force was reduced which indicates DNA bending by the IHF proteins. This was similar to what was observed when torsion-unconstrained DNA was used in similar magnetic tweezers experiments (21, 22). This means that the *E.coli* IHF DNA-bending mode is not affected by DNA torsion.

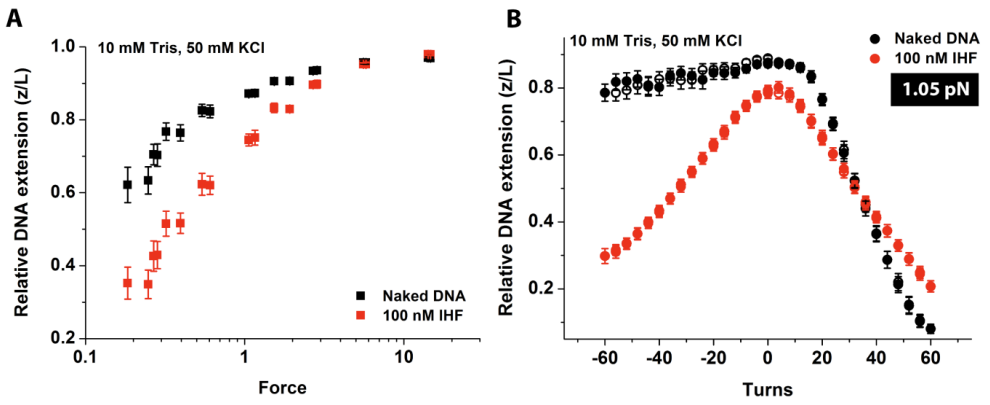

Figure 5.4 Magnetic tweezers force-extension and twist-extension curves measurements of a torsion-constrained DNA in the presence of 100 nM *E.coli* IHF. A) IHF caused DNA bending upon binding to a torsion-constrained DNA similar to that observed with a torsion-unconstrained DNA. B) Twist-extension curve of the same DNA done at 1.05 pN DNA pulling force typically resulted in DNA melting when DNA was progressively unwound (black symbols, negative turns portion). However, in the presence of 100 nM IHF, the curve adopted a significantly more symmetric shape which also means the DNA was not melting during DNA unwinding in the presence of IHF. Comparing the DNA extensions at the peaks of the naked DNA and IHF curves indicates IHF DNA-bending.

Twist-extension curve (TEC) measurements (**Fig. 5.4B**) of the same torsion-constrained DNA in the presence of 100 nM IHF (red symbols) at 1.05 pN DNA pulling force showed a significant contrast in the TEC shape as compared to naked DNA TEC (black symbols). The IHF TEC was significantly more symmetric than the naked DNA TEC. The asymmetric shape of the naked DNA TEC was due to DNA melting when DNA was unwound (negative turns). This means IHF DNA-bending

mode prevents DNA melting during DNA unwinding similar to what was observed in the *E.coli* HU DNA-bending mode at low HU concentration (e.g. 50 nM HU, see chapter 4 results). The IHF DNA-bending effect can also be seen by comparing the peak DNA extension of the respective TECs between IHF and naked DNA. In addition, we also observed another similarity to the *E.coli* HU DNA-bending mode, which is DNA bending by IHF caused the slope at the linear region of the TEC to be shallower than that of the naked DNA.

However, unlike the *E.coli* HU, the *E.coli* IHF did not cause any shift in the TEC (**Fig. 5.4B**) which indicates that IHF do not cause DNA winding upon binding like the HU. Another distinction from HU is that IHF does not stiffen DNA at high concentrations. These distinctions suggest that IHF and HU bind to DNA based on different mechanisms. Overall, we showed that the *IHF* DNA-bending mode exhibited similar effect on DNA supercoiling as the *E.coli* HU DNA-bending mode which is the prevention of DNA melting during DNA unwinding, but did not cause a change in DNA twist like the *E.coli* HU.

Preference of NAP DNA-binding modes to extended or bent DNA conformations

It is clear from our results that different NAP DNA-binding mode had contrasting effects on DNA supercoiling; DNA-stiffening mode prevents DNA plectoneme formation while DNA-bending mode favours it. We believe this can be explained by the energetic preference of DNA-stiffening mode to extended DNA conformation and DNA-bending mode preference to curved/bent DNA conformation. To test this, we used magnetic tweezers to observe the dissociation rate of pre-bound H-NS (DNA-stiffening mode) and IHF (DNA-bending mode) at different DNA pulling force (DNA tension) in the absence of protein. The DNA conformation is regulated by the imposed pulling force; the DNA conformation is extended (or stretched) at high force while it is more curved (or randomly coiled) at low force (<< 1 pN).

For the H-NS DNA-stiffening mode, we first pre-incubated a single λ-DNA tether with 150 nM of H-NS (10 mM Tris, 50 mM KCl, pH 7.5) to achieve partial DNA stiffening (an increase in DNA extension at low force), after which we removed the remaining unbound H-NS by excessively flushing the flow cell with buffer containing no H-NS and then recorded the DNA extension at a particular DNA pulling force until the DNA extension reached its original naked DNA extension. We did not use higher H-NS concentration to achieve DNA-stiffening saturation as the time taken for the H-NS to dissociate completely took at least > 10 hours. We performed the dissociation experiment (**Fig. 5.5A**) at three DNA pulling forces (0.2, 0.5 and 4.4 pN) to determine the dependence of H-NS DNA dissociation based on DNA tension and thus DNA local conformation. We observed that as the DNA pulling force is higher, H-NS took a longer time to completely dissociate. A simple comparison between the time taken for the DNA extension to return to its original extension between 4.4 pN (**Fig. 5.5A** black line, ~ 180 minutes) and 0.2 pN (**Fig. 5.5A** green line, ~ 70 minutes) demonstrates the case.

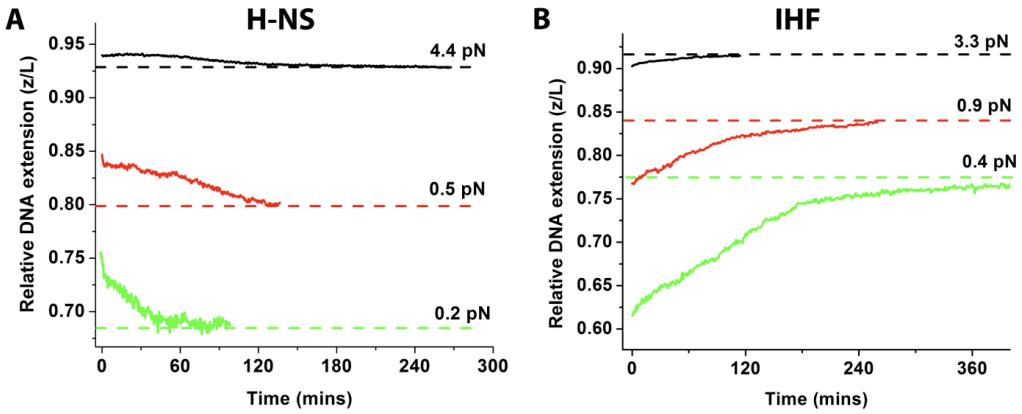

Figure 5.5 Dissociation kinetics of H-NS and IHF at different DNA pulling force. A) Experiments done with 150 nM H-NS in DNA-stiffening mode in 10 mM Tris, 50 mM KCl & pH 7.5 buffer showed that H-NS DNA dissociation rate increased with decreasing DNA tension. B) For 6nM IHF in similar buffer, we saw that IHF dissociation rate instead decreased with decreasing DNA tension.

For the IHF DNA-bending mode, we performed similar experiments (**Fig. 5.5B**) with 6 nM IHF at three DNA pulling forces (0.4, 0.9 and 3.3 pN). Similar to H-NS's case, we used 6 nM IHF to obtain data in a feasible experimental time frame. From our data, we found that in contrast to the case of H-NS, the IHF instead had an opposite dependence on the DNA pulling force. We saw that IHF completely dissociate faster with a higher DNA tension, and this can be clearly seen by comparing the complete dissociation time taken at 3.3 pN (**Fig. 5.5B** black line, ~ 90 minutes) and 0.4 pN (**Fig. 5.5B** green line, ~ 360 minutes). This opposing behaviour of dissociation rate dependence on DNA tension by DNA-stiffening protein (H-NS) and DNA-bending protein (IHF) is in agreement with our prediction and thus demonstrates the selective preference of distinct NAP DNA-binding modes to extended or curved/bent DNA conformations.

5.4. Discussions & Conclusion

NAPs distinct DNA-binding modes differentially regulate DNA supercoiling

Our work here describes a novel concept regarding how distinct nucleoid-associated proteins DNA-binding modes affect DNA supercoiling. This concept was originated from our finding that *E.coli* H-NS distinct DNA-binding modes differentially regulate DNA supercoiling property (see chapter 4). This work provides a comprehensive study using other two major *E.coli* NAPs, the HU and IHF proteins. We showed that the HU protein, which has two distinct DNA-binding modes that are dependent on HU solution concentration, differentially regulate DNA supercoiling. The HU DNA-bending mode promoted DNA plectoneme formation (the conformation consequence of supercoiled DNA) at low HU concentration, and the HU DNA-stiffening mode suppressed DNA plectoneme formation at higher HU concentrations. For the case of the IHF protein, we found that its DNA-bending mode promoted DNA plectoneme

formation similar to HU DNA-bending mode. This effect allows HU and IHF DNA-bending mode to prevent DNA melting during DNA unwinding under high DNA tension. This also indicates that both proteins may share similar mechanism to bending DNA upon binding.

From this work and our H-NS studies (chapter 4), we have consistently seen that DNA-stiffening by H-NS or HU caused a delay in DNA buckling transition. Consequently, this caused suppression in DNA plectoneme formation. We also saw consistency in the promotion of DNA plectoneme formation when HU or IHF bends the DNA. An important consequence is that this can prevent DNA from melting during excessive DNA unwinding. The H-NS DNA-bridging mode also promotes DNA plectoneme formation and in addition, stabilizes the plectonemes and prevents twists relaxation (chapter 4). In summary, we showed we can classify the NAPs effect on DNA supercoiling into three groups depending on their DNA-binding modes; suppressing DNA supercoiling (DNA-stiffening), promoting reversible DNA supercoiling (DNA-bending), and promoting irreversible DNA supercoiling (DNA-bridging).

A topology-based mechanism of NAPs regulation of DNA supercoiling

It was predicted that the NAPs DNA-stiffening and DNA-bending effect can be described by local distortion of DNA elasticity, and the effect is scaled by the protein occupancy fraction (87). This was experimentally proven when the force-response measurements of DNA in the presence DNA-stiffening (23, 156-158, 183) or DNA-bending (21, 22) NAPs were fitted well with the predicted model. This means that the NAP DNA-binding modes may be described as various local alterations of the DNA topology; DNA-stiffening caused a localized increase in DNA bending rigidity (persistence length) while DNA-bending caused a localized effective decrease in DNA bending rigidity. Taking this into consideration, we proposed that the

differential regulation of DNA supercoiling by distinct NAPs DNA-binding mode can be explained by the preference for distinctive local DNA topology by individual DNA-binding mode.

We proved this concept experimentally (**Fig. 5.4**) by showing that the DNA-stiffening proteins (e.g. H-NS) prefer extended DNA conformation (a.k.a. stretched DNA) while DNA-bending proteins (e.g. IHF) prefer curved/bent DNA conformation (a.k.a. coiled DNA). In terms of thermodynamics principles, this observation can be easily explained. Since DNA-stiffening proteins rigidify the local DNA elasticity, an extended DNA conformation provides a lower energy cost to achieve such state. Similarly for DNA-bending proteins, a bent or curved DNA conformation also provides a lower energy cost for IHF to bend the local DNA.

The same principle may be used to explain how DNA-stiffening and -bending proteins suppress or promote DNA plectoneme formation respectively. DNA plectoneme formation is basically a conversion of twist energy to DNA conformation changes, where the DNA is converted from a less curved/bent conformation (e.g. linear DNA) to a more curved/bent conformation (e.g. DNA loops). In the case of DNA-stiffening protein, it caused an increase in DNA bending rigidity that led to an increase in the energy required to form the curved plectonemes. Hence in order to form the plectonemes, more twist energy is needed and thus resulted in a delay in DNA buckling transition. In contrast, the DNA-bending effect caused an effective decrease in DNA bending rigidity and also caused the DNA to adopt a bent conformation. This resulted in a decrease in the energy required to form the curved DNA plectonemes and thus promoted plectonemes formation. In the case of the DNA-bridging effect, it stabilizes DNA loop formation by bridging the loop stem thus reducing the energy required to form DNA plectonemes and leads to promotion of plectonemes formation. However, the DNA-bridging induced formation of plectonemes is irreversible as compared to that of DNA-bending induction.

Biological implications of NAPs regulation of DNA supercoiling

The bacterial RNA polymerase (RNAP) generates positive supercoiling ahead of it and the amount of supercoiling accumulated can regulate RNAP activity (76, 205). This suggests DNA stiffening NAPs such as H-NS or HU that bind downstream of the promoter site may constrain DNA positive supercoiling by RNAP and thus leads to gene silencing. Another possible gene silencing mechanism is that DNA-bending NAPs such as the IHF or HU at low concentration may reduce the probability of DNA melting caused by RNAP during transition from closed complex to opened complex thus preventing RNAP from maturing to elongation complex. Alternatively, NAPs DNA-bridging such as H-NS DNA-bridging mode may trap DNA in plectonemes which prevent twist diffusion and cause accumulation of DNA twist tension in front of RNAP which leads to RNAP activity inhibition. We also do not exclude the possibility that NAPs may indirectly regulate RNAP activity by interacting with other transcription factors via constraining DNA supercoiling.

DNA supercoiling is an important component in bacterial chromosomal DNA organization (7, 206). The fact that NAPs regulate DNA supercoiling suggests they play a role in controlling the distribution of supercoiled chromosomal domains in addition to their direct role in condensing DNA. In summary, we showed that the bacterial NAPs distinct DNA-binding modes differentially regulate DNA supercoiling. This provides a novel concept that NAPs passively regulate DNA supercoiling as compared to the ATP-dependent enzymes such as topoisomerases and SMCs proteins, and may play important roles in gene regulation and chromosomal DNA organization.

Chapter 6

Conclusion

This thesis describes the effort to characterize the bacterial nucleoid-associated proteins (NAPs) DNA-binding modes, and how the DNA-binding modes mediate the two primary functions of NAPs, gene regulation and chromosomal DNA packaging. In chapter 2, we showed that the H-NS *E.coli* paralogue StpA protein is able to form rigid nucleoprotein filament with DNA, similar to H-NS. Subsequently, rigid nucleoprotein filament formation was also observed in numerous NAPs across the bacterial kingdom, i.e. the *P.aeruginosa* MvaT and the *M.tuberculosis* Lsr2 proteins. This supported our hypothesis that the NAP nucleoprotein filament may be a conserved nucleoprotein structure. The relation between NAP nucleoprotein filament and NAP gene silencing function was established using the H-NS protein mutation in chapter 3. We showed that all the H-NS mutants that failed to silence genes *in vivo* were unable to form rigid nucleoprotein filament thus indicating that the nucleoprotein filament is an important nucleoprotein structure involved in bacterial gene silencing mechanism. This provides an important linkage between *in vivo* observation and *in vitro* mechanistic findings.

We also investigated how the individual DNA-binding modes of bacterial NAPs affect the supercoiling properties of DNA. In chapter 4, we showed that the *E.coli* H-NS, which has two distinct DNA-binding modes, differentially regulates DNA supercoiling. H-NS DNA-stiffening mode suppresses DNA plectoneme formation from DNA supercoiling. In contrast, the H-NS DNA-bridging mode

promotes DNA plectoneme formation and also traps the DNA in plectonemes. In chapter 5, we extended this observation with the help of two other major *E.coli* NAPs – HU and IHF. We showed that the suppression of DNA plectoneme formation is a general effect of DNA-stiffening NAPs, as seen by the plectoneme suppression effect of HU DNA-stiffening mode. We showed that DNA-bending NAPs generally promote DNA plectoneme formation and are also able to prevent DNA melting during DNA unwinding. Overall, we showed that the bacterial NAP DNA-binding modes provide an ATP-free way for the bacteria to regulate its chromosomal DNA supercoiling, in addition to the ATP-consuming topoisomerases and SMCs proteins.

The conserved property of nucleoprotein filament formation by gene silencing bacterial NAPs is intriguing and its relevancy to silencing genes suggests they may play a structural role in inhibiting transcription similar to the eukaryotic nucleosomes. The NAPs effect on DNA supercoiling is far reaching and would almost certainly be involved in regulating the bacterial RNA polymerase transcription activity, a process that induced DNA supercoiling near the transcription sites. In summary, the thesis showed that the bacterial NAPs DNA-binding modes provide a mechanism in how the NAPs perform their roles in chromosomal DNA packaging and gene regulation. This shows that DNA occupancy alone might not be sufficient for the NAPs to perform their functions and further requires their DNA architectural roles. This warrants future studies to further elucidate the mechanisms on how the bacterial NAPs perform specific functions through their DNA-binding modes.

Future work

H-NS gene silencing mechanism – involvement of RNA polymerase and specific sequences

Although we have showed that the H-NS nucleoprotein filament is required for a gene silencing functional H-NS, its gene silencing mechanism is still unclear. One of the bacterial operons that is controlled by H-NS is the proU operon (207). The proU operon is also regulated by the cellular osmolarity, likely through DNA supercoiling changes (208, 209). Our work (chapter 4) that showed H-NS is able to regulate DNA supercoiling suggests H-NS, DNA supercoiling and osmolarity may play an intricate intertwined roles in regulating the proU operon which otherwise was believed to be independent of each other (210). Henceforth, in the future, we wish to extend our work on H-NS DNA supercoiling with specific DNA sequence containing proU operon and its interaction with *E.coli* holoenzyme (RNA polymerase core enzyme with sigma 70, hereafter termed as RNAP). Specifically, we hope to develop a single-molecule transcription assay that provide kinetic information on RNAP binding, formation of RNAP open complex, initial transcribing complex and maturation to elongation complex in the presence of gene silencing NAPs such as the H-NS. The experimental setup will be similar to that previously described (211, 212). This approach may be used to study other bacterial operons that are regulated by NAPs.

We will also study the RNAP elongation process at a single-molecule level. Classic single-molecule studies on *E.coli* RNAP elongation rate had yield numerous insights to its elongation kinetics, such as homogenous elongation rates (75) and pauses (74). We will use the magnetic tweezers to study the effects of H-NS binding (in DNA-stiffening or bridging mode) on RNAP elongation kinetics. This will provide direct evidence to our hypothesis that H-NS filament can block RNAP elongation. A recent study showed that the *E.coli* RNAP elongation can be inhibited by imposing a certain amount of torque on the DNA template (76). Our study on H-NS regulation on DNA supercoiling provides a means to link H-NS regulation of RNAP elongation via DNA supercoiling transduction. Hence DNA supercoiling will be implemented into the single-molecule RNAP elongation studies and see how they

interplay with H-NS DNA-binding modes. This future work may also extend to other bacterial NAPs that may block RNAP elongation.

List of publications

Publications (Chronological order)

Y Qu, **CJ Lim**, YR Whang, J Liu, J Yan, Mechanism of DNA organization by Mycobacterium tuberculosis protein Lsr2, *Nucleic acids research* 41 (10), 5263-5272, (2013)

CJ Lim, SY Lee, J Teramoto, A Ishihama, J Yan, The nucleoid-associated protein Dan organizes chromosomal DNA through rigid nucleoprotein filament formation in E. coli during anoxia, *Nucleic acids research* 41 (2), 746-753, (2013)

CJ Lim, SY Lee, LJ Kenney, J Yan, Nucleoprotein filament formation is the structural basis for bacterial protein H-NS gene silencing, *Scientific reports* 2 (2012)

CJ Lim, YR Whang, LJ Kenney, J Yan, Gene silencing H-NS paralogue StpA forms a rigid protein filament along DNA that blocks DNA accessibility, *Nucleic acids research* 40 (8), 3316-3328, (2012)

Bibliography

1. Sinden RR & Pettijohn DE (1981) Chromosomes in Living Escherichia-Coli-Cells Are Segregated into Domains of Supercoiling. *P Natl Acad Sci-Biol* 78(1):224-228.
2. Delius H & Worcel A (1974) Electron microscopic studies on the folded chromosome of Escherichia coli. *Cold Spring Harb Symp Quant Biol* 38:53-58.
3. Robinow C & Kellenberger E (1994) The bacterial nucleoid revisited. *Microbiol Rev* 58(2):211-232.
4. Wang XD, *et al.* (2013) Organization and segregation of bacterial chromosomes. *Nat Rev Genet* 14(3):191-203.
5. Dorman CJ (1991) DNA supercoiling and environmental regulation of gene expression in pathogenic bacteria. *Infect Immun* 59(3):745-749.
6. Higgins CF, *et al.* (1988) A physiological role for DNA supercoiling in the osmotic regulation of gene expression in S. typhimurium and E. coli. *Cell* 52(4):569-584.
7. Postow L, *et al.* (2004) Topological domain structure of the Escherichia coli chromosome. *Genes Dev* 18(14):1766-1779.
8. Drlica K (1992) Control of bacterial DNA supercoiling. *Mol Microbiol* 6(4):425-433.
9. Luttinger A (1995) The twisted 'life' of DNA in the cell: bacterial topoisomerases. *Mol Microbiol* 15(4):601-606.
10. Britton RA, *et al.* (1998) Characterization of a prokaryotic SMC protein involved in chromosome partitioning. *Gene Dev* 12(9):1254-1259.
11. Hiraga S, *et al.* (1989) Chromosome partitioning in Escherichia coli: novel mutants producing anucleate cells. *J Bacteriol* 171(3):1496-1505.
12. Hirano T (2006) At the heart of the chromosome: SMC proteins in action. *Nat Rev Mol Cell Biol* 7(5):311-322.
13. Hirano M & Hirano T (2006) Opening closed arms: long-distance activation of SMC ATPase by hinge-DNA interactions. *Mol Cell* 21(2):175-186.
14. Dillon SC & Dorman CJ (2010) Bacterial nucleoid-associated proteins, nucleoid structure and gene expression. *Nat Rev Microbiol* 8(3):185-195.
15. Azam TA & Ishihama A (1999) Twelve species of the nucleoid-associated protein from Escherichia coli - Sequence recognition specificity and DNA binding affinity. *J Biol Chem* 274(46):33105-33113.
16. Azam TA, *et al.* (1999) Growth phase-dependent variation in protein composition of the Escherichia coli nucleoid. *J Bacteriol* 181(20):6361-6370.
17. Ali Azam T, *et al.* (1999) Growth phase-dependent variation in protein composition of the Escherichia coli nucleoid. *J Bacteriol* 181(20):6361-6370.
18. Browning DF, *et al.* (2010) Effects of nucleoid-associated proteins on bacterial chromosome structure and gene expression. *Curr Opin Microbiol* 13(6):773-780.

19. Liu Y, *et al.* (2010) A divalent switch drives H-NS/DNA-binding conformations between stiffening and bridging modes. *Genes Dev* 24(4):339-344.
20. van Noort J, *et al.* (2004) Dual architectural roles of HU: formation of flexible hinges and rigid filaments. *Proc Natl Acad Sci U S A* 101(18):6969-6974.
21. Ali BMJ, *et al.* (2001) Compaction of single DNA molecules induced by binding of integration host factor (IHF). *P Natl Acad Sci USA* 98(19):10658-10663.
22. Lin J, *et al.* (2012) Physical Organization of DNA by Multiple Non-Specific DNA-Binding Modes of Integration Host Factor (IHF). *Plos One* 7(11):e49885.
23. Lim CJ, *et al.* (2012) Gene silencing H-NS paralogue StpA forms a rigid protein filament along DNA that blocks DNA accessibility. *Nucleic Acids Res* 40(8):3316-3328.
24. Ceci P, *et al.* (2004) DNA condensation and self-aggregation of Escherichia coli Dps are coupled phenomena related to the properties of the N-terminus. *Nucleic Acids Res* 32(19):5935-5944.
25. Skoko D, *et al.* (2006) Mechanism of chromosome compaction and looping by the Escherichia coli nucleoid protein Fis. *J Mol Biol* 364(4):777-798.
26. Hommais F, *et al.* (2001) Large-scale monitoring of pleiotropic regulation of gene expression by the prokaryotic nucleoid-associated protein, H-NS. *Mol Microbiol* 40(1):20-36.
27. Tendeng C & Bertin PN (2003) H-NS in Gram-negative bacteria: a family of multifaceted proteins. *Trends Microbiol* 11(11):511-518.
28. Ono S, *et al.* (2005) H-NS is a part of a thermally controlled mechanism for bacterial gene regulation. *Biochem J* 391(Pt 2):203-213.
29. Lucchini S, *et al.* (2006) H-NS mediates the silencing of laterally acquired genes in bacteria. *PLoS Pathog* 2(8):e81.
30. Lawrence JG & Ochman H (1997) Amelioration of bacterial genomes: rates of change and exchange. *J Mol Evol* 44(4):383-397.
31. Fang FC & Rimsky S (2008) New insights into transcriptional regulation by H-NS. *Curr Opin Microbiol* 11(2):113-120.
32. Jordi BJ, *et al.* (1997) DNA binding is not sufficient for H-NS-mediated repression of proU expression. *J Biol Chem* 272(18):12083-12090.
33. Bouffartigues E, *et al.* (2007) H-NS cooperative binding to high-affinity sites in a regulatory element results in transcriptional silencing. *Nat Struct Mol Biol* 14(5):441-448.
34. Chen CC, *et al.* (2005) A cis-spreading nucleoprotein filament is responsible for the gene silencing activity found in the promoter relay mechanism. *J Biol Chem* 280(6):5101-5112.
35. Dorman CJ, *et al.* (1999) Domain organization and oligomerization among H-NS-like nucleoid-associated proteins in bacteria. *Trends Microbiol* 7(3):124-128.
36. Ueguchi C, *et al.* (1996) Systematic mutational analysis revealing the functional domain organization of Escherichia coli nucleoid protein H-NS. *J Mol Biol* 263(2):149-162.
37. Smyth CP, *et al.* (2000) Oligomerization of the chromatin-structuring protein H-NS. *Mol Microbiol* 36(4):962-972.
38. Spurio R, *et al.* (1997) The oligomeric structure of nucleoid protein H-NS is necessary for recognition of intrinsically curved DNA and for DNA bending. *Embo J* 16(7):1795-1805.

39. Arold ST, *et al.* (2010) H-NS forms a superhelical protein scaffold for DNA condensation. *Proc Natl Acad Sci U S A* 107(36):15728-15732.
40. Dame RT, *et al.* (2000) H-NS mediated compaction of DNA visualised by atomic force microscopy. *Nucleic Acids Res* 28(18):3504-3510.
41. Amit R, *et al.* (2003) Increased bending rigidity of single DNA molecules by H-NS, a temperature and osmolarity sensor. *Biophys J* 84(4):2467-2473.
42. Dame RT, *et al.* (2002) Structural basis for H-NS-mediated trapping of RNA polymerase in the open initiation complex at the rrnB P1. *J Biol Chem* 277(3):2146-2150.
43. Lang B, *et al.* (2007) High-affinity DNA binding sites for H-NS provide a molecular basis for selective silencing within proteobacterial genomes. *Nucleic Acids Res* 35(18):6330-6337.
44. Walthers D, *et al.* (2011) Salmonella enterica Response Regulator SsrB Relieves H-NS Silencing by Displacing H-NS Bound in Polymerization Mode and Directly Activates Transcription. *J Biol Chem* 286(3):1895-1902.
45. Bertin P, *et al.* (1999) The structural and functional organization of H-NS-like proteins is evolutionarily conserved in Gram-negative bacteria. *Mol Microbiol* 31(1):319-329.
46. Tauschek M, *et al.* (2010) Transcriptional Analysis of the grlRA Virulence Operon from Citrobacter rodentium. *J Bacteriol* 192(14):3722-3734.
47. Zhang A, *et al.* (1996) Escherichia coli protein analogs StpA and H-NS: regulatory loops, similar and disparate effects on nucleic acid dynamics. *Embo J* 15(6):1340-1349.
48. Williams RM, *et al.* (1996) Probing the structure, function, and interactions of the Escherichia coli H-NS and StpA proteins by using dominant negative derivatives. *J Bacteriol* 178(15):4335-4343.
49. Sonnenfield JM, *et al.* (2001) The nucleoid-associated protein StpA binds curved DNA, has a greater DNA-binding affinity than H-NS and is present in significant levels in hns mutants. *Biochimie* 83(2):243-249.
50. Free A, *et al.* (1998) The StpA protein functions as a molecular adapter to mediate repression of the bgl operon by truncated H-NS in Escherichia coli. *J Bacteriol* 180(4):994-997.
51. Dame RT, *et al.* (2005) DNA bridging: a property shared among H-NS-like proteins. *J Bacteriol* 187(5):1845-1848.
52. Castang S, *et al.* (2008) H-NS family members function coordinately in an opportunistic pathogen. *Proc Natl Acad Sci U S A* 105(48):18947-18952.
53. Chen JM, *et al.* (2006) Roles of Lsr2 in colony morphology and biofilm formation of Mycobacterium smegmatis. *J Bacteriol* 188(2):633-641.
54. Chen JM, *et al.* (2008) Lsr2 of Mycobacterium tuberculosis is a DNA-bridging protein. *Nucleic Acids Res* 36(7):2123-2135.
55. Dame RT (2005) The role of nucleoid-associated proteins in the organization and compaction of bacterial chromatin. *Mol Microbiol* 56(4):858-870.
56. Rouviere-Yaniv J, *et al.* (1979) E. coli DNA binding protein HU forms nucleosomelike structure with circular double-stranded DNA. *Cell* 17(2):265-274.
57. Kar S, *et al.* (2005) Nucleoid remodeling by an altered HU protein: Reorganization of the transcription program. *P Natl Acad Sci USA* 102(45):16397-16402.
58. Shindo H, *et al.* (1992) Preferential binding of E.coli histone-like protein HU alpha to negatively supercoiled DNA. *Nucleic Acids Res* 20(7):1553-1558.
59. Travers A (1997) DNA-protein interactions: IHF--the master bender. *Curr Biol* 7(4):R252-254.

60. Ohniwa RL, *et al.* (2013) Atomic Force Microscopy Analysis of the Role of Major DNA-Binding Proteins in Organization of the Nucleoid in Escherichia coli. *Plos One* 8(8):e72954.
61. Spurio R, *et al.* (1992) Lethal overproduction of the Escherichia coli nucleoid protein H-NS: ultramicroscopic and molecular autopsy. *Mol Gen Genet* 231(2):201-211.
62. McGovern V, *et al.* (1994) H-NS over-expression induces an artificial stationary phase by silencing global transcription. *Biochimie* 76(10-11):1019-1029.
63. Mojica FJ & Higgins CF (1997) In vivo supercoiling of plasmid and chromosomal DNA in an Escherichia coli hns mutant. *J Bacteriol* 179(11):3528-3533.
64. Tupper AE, *et al.* (1994) The chromatin-associated protein H-NS alters DNA topology in vitro. *Embo J* 13(1):258-268.
65. Hardy CD & Cozzarelli NR (2005) A genetic selection for supercoiling mutants of Escherichia coli reveals proteins implicated in chromosome structure. *Mol Microbiol* 57(6):1636-1652.
66. Grant RA, *et al.* (1998) The crystal structure of Dps, a ferritin homolog that binds and protects DNA. *Nat Struct Biol* 5(4):294-303.
67. Kim J, *et al.* (2004) Fundamental structural units of the Escherichia coli nucleoid revealed by atomic force microscopy. *Nucleic Acids Res* 32(6):1982-1992.
68. Vale RD, *et al.* (1985) Identification of a novel force-generating protein, kinesin, involved in microtubule-based motility. *Cell* 42(1):39-50.
69. Svoboda K, *et al.* (1993) Direct observation of kinesin stepping by optical trapping interferometry. *Nature* 365(6448):721-727.
70. Lang MJ, *et al.* (2002) An automated two-dimensional optical force clamp for single molecule studies. *Biophys J* 83(1):491-501.
71. Schnitzer MJ & Block SM (1997) Kinesin hydrolyses one ATP per 8-nm step. *Nature* 388(6640):386-390.
72. Visscher K, *et al.* (1999) Single kinesin molecules studied with a molecular force clamp. *Nature* 400(6740):184-189.
73. Schnitzer MJ, *et al.* (2000) Force production by single kinesin motors. *Nat Cell Biol* 2(10):718-723.
74. Davenport RJ, *et al.* (2000) Single-molecule study of transcriptional pausing and arrest by E. coli RNA polymerase. *Science* 287(5462):2497-2500.
75. Adelman K, *et al.* (2002) Single molecule analysis of RNA polymerase elongation reveals uniform kinetic behavior. *Proc Natl Acad Sci U S A* 99(21):13538-13543.
76. Ma J, *et al.* (2013) Transcription under torsion. *Science* 340(6140):1580-1583.
77. Woodside MT, *et al.* (2006) Nanomechanical measurements of the sequence-dependent folding landscapes of single nucleic acid hairpins. *Proc Natl Acad Sci U S A* 103(16):6190-6195.
78. Grandbois M, *et al.* (1999) How strong is a covalent bond? *Science* 283(5408):1727-1730.
79. Abbondanzieri EA, *et al.* (2005) Direct observation of base-pair stepping by RNA polymerase. *Nature* 438(7067):460-465.
80. Gosse C & Croquette V (2002) Magnetic tweezers: micromanipulation and force measurement at the molecular level. *Biophys J* 82(6):3314-3329.
81. Bustamante C, *et al.* (1994) Entropic Elasticity of Lambda-Phage DNA. *Science* 265(5178):1599-1600.
82. Rief M, *et al.* (1999) Sequence-dependent mechanics of single DNA molecules. *Nat Struct Biol* 6(4):346-349.

83. Greenleaf WJ, *et al.* (2005) Passive all-optical force clamp for high-resolution laser trapping. *Phys Rev Lett* 95(20):208102.
84. Fernandez JM & Li H (2004) Force-clamp spectroscopy monitors the folding trajectory of a single protein. *Science* 303(5664):1674-1678.
85. Oberhauser AF, *et al.* (2001) Stepwise unfolding of titin under force-clamp atomic force microscopy. *Proc Natl Acad Sci U S A* 98(2):468-472.
86. Marko JF & Siggia ED (1995) Stretching DNA. *Macromolecules* 28(26):8759-8770.
87. Yan J & Marko JF (2003) Effects of DNA-distorting proteins on DNA elastic response. *Phys Rev E Stat Nonlin Soft Matter Phys* 68(1 Pt 1):011905.
88. Liphardt J, *et al.* (2001) Reversible unfolding of single RNA molecules by mechanical force. *Science* 292(5517):733-737.
89. Woodside MT, *et al.* (2006) Direct measurement of the full, sequence-dependent folding landscape of a nucleic acid. *Science* 314(5801):1001-1004.
90. Cecconi C, *et al.* (2005) Direct observation of the three-state folding of a single protein molecule. *Science* 309(5743):2057-2060.
91. Shank EA, *et al.* (2010) The folding cooperativity of a protein is controlled by its chain topology. *Nature* 465(7298):637-640.
92. Shaevitz JW, *et al.* (2003) Backtracking by single RNA polymerase molecules observed at near-base-pair resolution. *Nature* 426(6967):684-687.
93. Abbondanzieri EA, *et al.* (2005) Picocalorimetry of transcription by RNA polymerase. *Biophys J* 89(6):L61-63.
94. Larson MH, *et al.* (2012) Trigger loop dynamics mediate the balance between the transcriptional fidelity and speed of RNA polymerase II. *Proc Natl Acad Sci U S A* 109(17):6555-6560.
95. Palangat M, *et al.* (2012) Efficient reconstitution of transcription elongation complexes for single-molecule studies of eukaryotic RNA polymerase II. *Transcription* 3(3):146-153.
96. Sun B, *et al.* (2011) ATP-induced helicase slippage reveals highly coordinated subunits. *Nature* 478(7367):132-135.
97. Cheng W, *et al.* (2011) Single-base pair unwinding and asynchronous RNA release by the hepatitis C virus NS3 helicase. *Science* 333(6050):1746-1749.
98. Yu J, *et al.* (2010) Coupling translocation with nucleic acid unwinding by NS3 helicase. *J Mol Biol* 404(3):439-455.
99. Strick TR, *et al.* (1998) Behavior of supercoiled DNA. *Biophys J* 74(4):2016-2028.
100. Strick TR, *et al.* (1996) The elasticity of a single supercoiled DNA molecule. *Science* 271(5257):1835-1837.
101. Lyubchenko YL, *et al.* (1992) Atomic force microscopy imaging of double stranded DNA and RNA. *J Biomol Struct Dyn* 10(3):589-606.
102. Lyubchenko Y, *et al.* (1993) Atomic force microscopy of long DNA: imaging in air and under water. *Proc Natl Acad Sci U S A* 90(6):2137-2140.
103. Bao Q, *et al.* (2007) A divalent metal-mediated switch controlling protein-induced DNA bending. *J Mol Biol* 367(3):731-740.
104. Ando T, *et al.* (2007) High-speed atomic force microscopy for observing dynamic biomolecular processes. *J Mol Recognit* 20(6):448-458.
105. Kodera N, *et al.* (2010) Video imaging of walking myosin V by high-speed atomic force microscopy. *Nature* 468(7320):72-76.
106. Uchihashi T, *et al.* (2011) High-speed atomic force microscopy reveals rotary catalysis of rotorless F(1)-ATPase. *Science* 333(6043):755-758.
107. Medina MA & Schwille P (2002) Fluorescence correlation spectroscopy for the detection and study of single molecules in biology. *Bioessays* 24(8):758-764.

108. Segers-Nolten GMJ, *et al.* (2002) Scanning confocal fluorescence microscopy for single molecule analysis of nucleotide excision repair complexes. *Nucleic Acids Res* 30(21):4720-4727.
109. Kues T, *et al.* (2001) Visualization and tracking of single protein molecules in the cell nucleus. *Biophys J* 80(6):2954-2967.
110. Mullineaux CW (2007) Localization and mobility of bacterial proteins by confocal microscopy and fluorescence recovery after photobleaching. *Methods Mol Biol* 390:3-15.
111. Heinisch JJ, *et al.* (2010) Single-molecule atomic force microscopy reveals clustering of the yeast plasma-membrane sensor Wsc1. *Plos One* 5(6):e11104.
112. Douglass AD & Vale RD (2005) Single-molecule microscopy reveals plasma membrane microdomains created by protein-protein networks that exclude or trap signaling molecules in T cells. *Cell* 121(6):937-950.
113. Yardimci H, *et al.* (2010) Uncoupling of sister replisomes during eukaryotic DNA replication. *Mol Cell* 40(5):834-840.
114. Tanner NA, *et al.* (2009) Real-time single-molecule observation of rolling-circle DNA replication. *Nucleic Acids Res* 37(4):e27.
115. Adio S, *et al.* (2009) Dissection of kinesin's processivity. *Plos One* 4(2):e4612.
116. Friedman LJ & Gelles J (2012) Mechanism of transcription initiation at an activator-dependent promoter defined by single-molecule observation. *Cell* 148(4):679-689.
117. Sanchez A, *et al.* (2011) Mechanism of transcriptional repression at a bacterial promoter by analysis of single molecules. *Embo J* 30(19):3940-3946.
118. Crawford DJ, *et al.* (2013) Single-molecule colocalization FRET evidence that spliceosome activation precedes stable approach of 5' splice site and branch site. *Proc Natl Acad Sci U S A* 110(17):6783-6788.
119. Hoskins AA, *et al.* (2011) New insights into the spliceosome by single molecule fluorescence microscopy. *Curr Opin Chem Biol* 15(6):864-870.
120. Oberto J, *et al.* (2009) The HU regulon is composed of genes responding to anaerobiosis, acid stress, high osmolarity and SOS induction. *Plos One* 4(2):e4367.
121. Dorman CJ (2007) H-NS, the genome sentinel. *Nat Rev Microbiol* 5(2):157-161.
122. Teramoto J, *et al.* (2010) A novel nucleoid protein of Escherichia coli induced under anaerobiotic growth conditions. *Nucleic Acids Res* 38(11):3605-3618.
123. Zhang AX & Belfort M (1992) Nucleotide-Sequence of a Newly-Identified Escherichia-Coli Gene, Stpa, Encoding an H-Ns-Like Protein. *Nucleic Acids Res* 20(24):6735-6735.
124. Sonden B & Uhlin BE (1996) Coordinated and differential expression of histone-like proteins in Escherichia coli: Regulation and function of the H-NS analog StpA. *Embo J* 15(18):4970-4980.
125. Zhang AX, *et al.* (1996) Escherichia coli protein analogs StpA and H-NS: Regulatory loops, similar and disparate effects on nucleic acid dynamics. *Embo J* 15(6):1340-1349.
126. Gordon BR, *et al.* (2008) Lsr2 of Mycobacterium represents a novel class of H-NS-like proteins. *J Bacteriol* 190(21):7052-7059.
127. Guo FS & Adhya S (2007) Spiral structure of Escherichia coli HU alpha beta provides foundation for DNA supercoiling. *P Natl Acad Sci USA* 104(11):4309-4314.
128. Travers A, *et al.* (2001) DNA supercoiling and transcription in Escherichia coli: The FIS connection. *Biochimie* 83(2):213-217.

129. Shi XL & Bennett GN (1994) Plasmids Bearing Hfq and the Hns-Like Gene Stpa Complement Hns Mutants in Modulating Arginine Decarboxylase Gene-Expression in Escherichia-Coli. *J Bacteriol* 176(21):6769-6775.
130. Free A & Dorman CJ (1997) The Escherichia coli stpA gene is transiently expressed during growth in rich medium and is induced in minimal medium and by stress conditions. *J Bacteriol* 179(3):909-918.
131. Gordon BR, *et al.* (2010) Lsr2 is a nucleoid-associated protein that targets AT-rich sequences and virulence genes in Mycobacterium tuberculosis. *Proc Natl Acad Sci U S A* 107(11):5154-5159.
132. Dame RT, *et al.* (2005) DNA bridging: a property shared among H-NS-like proteins. *J Bacteriol* 187(5):1845-1848.
133. Kim OB, *et al.* (2009) Regulation of tartrate metabolism by TtdR and relation to the DcuS-DcuR-regulatedC(4)-dicarboxylate metabolism of Escherichia coli. *Microbiol-Sgm* 155:3632-3640.
134. Fu H, *et al.* (2011) Transition dynamics and selection of the distinct S-DNA and strand unpeeling modes of double helix overstretching. *Nucleic Acids Res* 39(8):3473-3481.
135. Wang H, *et al.* (2002) Glutaraldehyde modified mica: a new surface for atomic force microscopy of chromatin. *Biophys J* 83(6):3619-3625.
136. Fu H, *et al.* (2011) Atomic force microscope imaging of chromatin assembled in Xenopus laevis egg extract. *Chromosoma*.
137. Rivetti C & Codeluppi S (2001) Accurate length determination of DNA molecules visualized by atomic force microscopy: evidence for a partial B- to A-form transition on mica. *Ultramicroscopy* 87(1-2):55-66.
138. Vossepoel AM & Smeulders AWM (1982) VECTOR CODE PROBABILITY AND METRICATION ERROR IN THE REPRESENTATION OF STRAIGHT-LINES OF FINITE LENGTH. *Computer Graphics and Image Processing* 20(4):347-364.
139. Yan J, *et al.* (2004) Near-field-magnetic-tweezer manipulation of single DNA molecules. *Phys Rev E Stat Nonlin Soft Matter Phys* 70(1 Pt 1):011905.
140. Allemand JF, *et al.* (1996) The elasticity of a single supercoiled DNA molecule (vol 271, pg 1835, 1996). *Science* 272(5263):797-797.
141. Xiao B, *et al.* (2010) Modulation of HU-DNA interactions by salt concentration and applied force. *Nucleic Acids Res* 38(18):6176-6185.
142. Wang HD, *et al.* (2002) Glutaraldehyde modified mica: A new surface for atomic force microscopy of chromatin. *Biophysical Journal* 83(6):3619-3625.
143. Lucchini S, *et al.* (2009) The H-NS-like protein StpA represses the RpoS (sigma 38) regulon during exponential growth of Salmonella Typhimurium. *Mol Microbiol* 74(5):1169-1186.
144. Paymaster NJ (1976) Magnesium-Metabolism - Brief Review. *Ann Roy Coll Surg* 58(4):309-314.
145. Lusk JE, *et al.* (1968) Magnesium and Growth of Escherichia Coli. *J Biol Chem* 243(10):2618-+.
146. Keatch SA, *et al.* (2005) StpA protein from Escherichia coli condenses supercoiled DNA in preference to linear DNA and protects it from digestion by DNase I and EcoKI. *Nucleic Acids Res* 33(20):6540-6546.
147. Johansson J, *et al.* (2001) Heteromeric interactions among nucleoid-associated bacterial proteins: Localization of StpA-stabilizing regions in H-NS of Escherichia coli. *J Bacteriol* 183(7):2343-2347.
148. Badaut C, *et al.* (2002) The degree of oligomerization of the H-NS nucleoid structuring protein is related to specific binding to DNA. *J Biol Chem* 277(44):41657-41666.

149. Wiggins PA, *et al.* (2009) Protein-mediated molecular bridging: a key mechanism in biopolymer organization. *Biophys J* 97(7):1997-2003.
150. de Vries R (2011) Influence of mobile DNA-protein-DNA bridges on DNA configurations: Coarse-grained Monte-Carlo simulations. *J Chem Phys* 135(12):125104.
151. Sonnenfield JM, *et al.* (2001) The nucleoid-associated protein StpA binds curved DNA, has a greater DNA-binding affinity than H-NS and is present in significant levels in hns mutants. *Biochimie* 83(2):243-249.
152. Wolf E, *et al.* (1995) Mutational Analysis of Dnase-I DNA Interactions - Design, Expression and Characterization of a Dnase-I Loop Insertion Mutant with Altered Sequence Selectivity. *Protein Engineering* 8(3):283-291.
153. Ozoline ON & Tsyganov MA (1995) Structure of Open Promoter Complexes with Escherichia-Coli Rna-Polymerase as Revealed by the Dnase-I Footprinting Technique - Compilation Analysis. *Nucleic Acids Res* 23(22):4533-4541.
154. Uyar E, *et al.* (2009) Differential Binding Profiles of StpA in Wild-Type and hns Mutant Cells: a Comparative Analysis of Cooperative Partners by Chromatin Immunoprecipitation-Microarray Analysis. *J Bacteriol* 191(7):2388-2391.
155. Wang W, *et al.* (2011) Chromosome organization by a nucleoid-associated protein in live bacteria. *Science* 333(6048):1445-1449.
156. Qu Y, *et al.* (2013) Mechanism of DNA organization by Mycobacterium tuberculosis protein Lsr2. *Nucleic Acids Res* 41(10):5263-5272.
157. Winardhi RS, *et al.* (2012) Higher order oligomerization is required for H-NS family member MvaT to form gene-silencing nucleoprotein filament. *Nucleic Acids Res*.
158. Lim CJ, *et al.* (2012) The nucleoid-associated protein Dan organizes chromosomal DNA through rigid nucleoprotein filament formation in E. coli during anoxia. *Nucleic Acids Res*.
159. Laurens N, *et al.* (2012) Alba shapes the archaeal genome using a delicate balance of bridging and stiffening the DNA. *Nat Commun* 3:1328.
160. McCauley MJ, *et al.* (2013) Single-molecule kinetics reveal microscopic mechanism by which High-Mobility Group B proteins alter DNA flexibility. *Nucleic Acids Res* 41(1):167-181.
161. Lim CJ, *et al.* (2013) The nucleoid-associated protein Dan organizes chromosomal DNA through rigid nucleoprotein filament formation in E. coli during anoxia. *Nucleic Acids Res* 41(2):746-753.
162. Azam TA, *et al.* (2000) Two types of localization of the DNA-binding proteins within the Escherichia coli nucleoid. *Genes Cells* 5(8):613-626.
163. Niki H, *et al.* (2000) Dynamic organization of chromosomal DNA in Escherichia coli. *Genes Dev* 14(2):212-223.
164. Hulton CS, *et al.* (1990) Histone-like protein H1 (H-NS), DNA supercoiling, and gene expression in bacteria. *Cell* 63(3):631-642.
165. Ueguchi C & Mizuno T (1993) The Escherichia coli nucleoid protein H-NS functions directly as a transcriptional repressor. *Embo J* 12(3):1039-1046.
166. Dame RT, *et al.* (2006) Bacterial chromatin organization by H-NS protein unravelled using dual DNA manipulation. *Nature* 444(7117):387-390.
167. Atlung T & Ingmer H (1997) H-NS: A modulator of environmentally regulated gene expression. *Mol Microbiol* 24(1):7-17.
168. Lim CJ, *et al.* (2011) Gene silencing H-NS paralogue StpA forms a rigid protein filament along DNA that blocks DNA accessibility. *Nucleic Acids Res*.

169. Ueguchi C, *et al.* (1997) Clarification of the dimerization domain and its functional significance for the Escherichia coli nucleoid protein H-NS. *J Mol Biol* 274(2):145-151.
170. Meiners JC & Quake SR (2000) Femtonewton force spectroscopy of single extended DNA molecules. *Phys Rev Lett* 84(21):5014-5017.
171. Wiggins PA, *et al.* (2009) Protein-Mediated Molecular Bridging: A Key Mechanism in Biopolymer Organization. *Biophysical Journal* 97(7):1997-2003.
172. Rimsky S, *et al.* (2001) A molecular mechanism for the repression of transcription by the H-NS protein. *Mol Microbiol* 42(5):1311-1323.
173. Workman JL & Kingston RE (1992) Nucleosome core displacement in vitro via a metastable transcription factor-nucleosome complex. *Science* 258(5089):1780-1784.
174. Adams CC & Workman JL (1993) Nucleosome displacement in transcription. *Cell* 72(3):305-308.
175. Levchenko V, *et al.* (2005) Histone release during transcription: displacement of the two H2A-H2B dimers in the nucleosome is dependent on different levels of transcription-induced positive stress. *Biochemistry* 44(14):5357-5372.
176. Workman JL (2006) Nucleosome displacement in transcription. *Genes Dev* 20(15):2009-2017.
177. Miller WG & Simons RW (1993) Chromosomal supercoiling in Escherichia coli. *Mol Microbiol* 10(3):675-684.
178. Pang ZH, *et al.* (2005) A gyrase mutant with low activity disrupts supercoiling at the replication terminus. *J Bacteriol* 187(22):7773-7783.
179. Baker TA, *et al.* (1986) Extensive Unwinding of the Plasmid Template during Staged Enzymatic Initiation of DNA-Replication from the Origin of the Escherichia-Coli Chromosome. *Cell* 45(1):53-64.
180. Pruss GJ & Drlica K (1989) DNA supercoiling and prokaryotic transcription. *Cell* 56(4):521-523.
181. Wu HY, *et al.* (1988) Transcription generates positively and negatively supercoiled domains in the template. *Cell* 53(3):433-440.
182. Stuger R, *et al.* (2002) DNA supercoiling by gyrase is linked to nucleoid compaction. *Mol Biol Rep* 29(1-2):79-82.
183. Lim CJ, *et al.* (2012) Nucleoprotein filament formation is the structural basis for bacterial protein H-NS gene silencing. *Sci Rep* 2:509.
184. Schlingman DJ, *et al.* (2011) A new method for the covalent attachment of DNA to a surface for single-molecule studies. *Colloid Surface B* 83(1):91-95.
185. Strick TR, *et al.* (1996) The elasticity of a single supercoiled DNA molecule. *Science* 271(5257):1835-1837.
186. Neukirch S (2004) Extracting DNA twist rigidity from experimental supercoiling data. *Physical Review Letters* 93(19).
187. Marko JF & Neukirch S (2012) Competition between curls and plectonemes near the buckling transition of stretched supercoiled DNA. *Phys Rev E* 85(1).
188. Marko JF (2007) Torque and dynamics of linking number relaxation in stretched supercoiled DNA. *Phys Rev E* 76(2).
189. Zhu B, *et al.* (2012) Gene 5.5 protein of bacteriophage T7 in complex with Escherichia coli nucleoid protein H-NS and transfer RNA masks transfer RNA priming in T7 DNA replication. *P Natl Acad Sci USA* 109(21):8050-8055.
190. Fu HX, *et al.* (2013) Force and ATP hydrolysis dependent regulation of RecA nucleoprotein filament by single-stranded DNA binding protein. *Nucleic Acids Res* 41(2):924-932.

191. Schnurr B, *et al.* (2006) Compaction and supercoiling of single, long DNA molecules by HU protein. *Biophysical Reviews and Letters* 01(01):29-44.
192. Winardhi RS, *et al.* (2012) Higher order oligomerization is required for H-NS family member MvaT to form gene-silencing nucleoprotein filament. *Nucleic Acids Res* 40(18):8942-8952.
193. Higgins NP, *et al.* (1978) Purification of Subunits of Escherichia-Coli DNA Gyrase and Reconstitution of Enzymatic-Activity. *P Natl Acad Sci USA* 75(4):1773-1777.
194. Rovinskiy N, *et al.* (2012) Rates of Gyrase Supercoiling and Transcription Elongation Control Supercoil Density in a Bacterial Chromosome. *Plos Genetics* 8(8).
195. Rybenkov VV, *et al.* (1997) Simplification of DNA topology below equilibrium values by type II topoisomerases. *Science* 277(5326):690-693.
196. Yan J, *et al.* (1999) A kinetic proofreading mechanism for disentanglement of DNA by topoisomerases. *Nature* 401(6756):932-935.
197. Yan J, *et al.* (2001) Kinetic proofreading can explain the supression of supercoiling of circular DNA molecules by type-II topoisomerases. *Phys Rev E Stat Nonlin Soft Matter Phys* 63(3 Pt 1):031909.
198. Wang JC (2002) Cellular roles of DNA topoisomerases: A molecular perspective. *Nat Rev Mol Cell Bio* 3(6):430-440.
199. Zechiedrich EL, *et al.* (2000) Roles of topoisomerases in maintaining steady-state DNA supercoiling in Escherichia coli. *J Biol Chem* 275(11):8103-8113.
200. Jensen RB & Shapiro L (1999) The Caulobacter crescentus smc gene is required for cell cycle progression and chromosome segregation. *P Natl Acad Sci USA* 96(19):10661-10666.
201. Cui Y, *et al.* (2008) MukB acts as a macromolecular clamp in DNA condensation. *Nat Struct Mol Biol* 15(4):411-418.
202. Petrushenko ZM, *et al.* (2010) Mechanics of DNA bridging by bacterial condensin MukBEF in vitro and in singulo. *Embo J* 29(6):1126-1135.
203. Broyles SS & Pettijohn DE (1986) Interaction of the Escherichia coli HU protein with DNA. Evidence for formation of nucleosome-like structures with altered DNA helical pitch. *J Mol Biol* 187(1):47-60.
204. Chalmers R, *et al.* (1998) IHF modulation of Tn10 transposition: sensory transduction of supercoiling status via a proposed protein/DNA molecular spring. *Cell* 93(5):897-908.
205. Liu LF & Wang JC (1987) Supercoiling of the DNA template during transcription. *Proc Natl Acad Sci U S A* 84(20):7024-7027.
206. Luijsterburg MS, *et al.* (2008) The Major Architects of Chromatin: Architectural Proteins in Bacteria, Archaea and Eukaryotes. *Crit Rev Biochem Mol* 43(6):393-418.
207. Lucht JM, *et al.* (1994) Interactions of the Nucleoid-Associated DNA-Binding Protein H-Ns with the Regulatory Region of the Osmotically Controlled Prou Operon of Escherichia-Coli. *J Biol Chem* 269(9):6578-6586.
208. May G, *et al.* (1989) Characterization of the osmoregulated Escherichia coli proU promoter and identification of ProV as a membrane-associated protein. *Mol Microbiol* 3(11):1521-1531.
209. Stirling DA, *et al.* (1989) Molecular characterization of the proU loci of Salmonella typhimurium and Escherichia coli encoding osmoregulated glycine betaine transport systems. *Mol Microbiol* 3(8):1025-1038.
210. Fletcher SA & Csonka LN (1995) Fine-structure deletion analysis of the transcriptional silencer of the proU operon of Salmonella typhimurium. *J Bacteriol* 177(15):4508-4513.

211. Revyakin A, *et al.* (2004) Promoter unwinding and promoter clearance by RNA polymerase: detection by single-molecule DNA nanomanipulation. *Proc Natl Acad Sci U S A* 101(14):4776-4780.
212. Revyakin A, *et al.* (2006) Abortive initiation and productive initiation by RNA polymerase involve DNA scrunching. *Science* 314(5802):1139-1143.